AD-A193 864 EFFECTS ON THE RESONANT FREQUENCIES CAUSED BY LOADING A SPHERICAL CAVITY WITH A DIELECTRIC SPHERE(U) HARRY DIAMOND LABS ADELPHI MD L F LIBELO ET AL. APR 88 1/1

UNCLASSIFIED HDL-TR-2130 F/G 20/3 NL

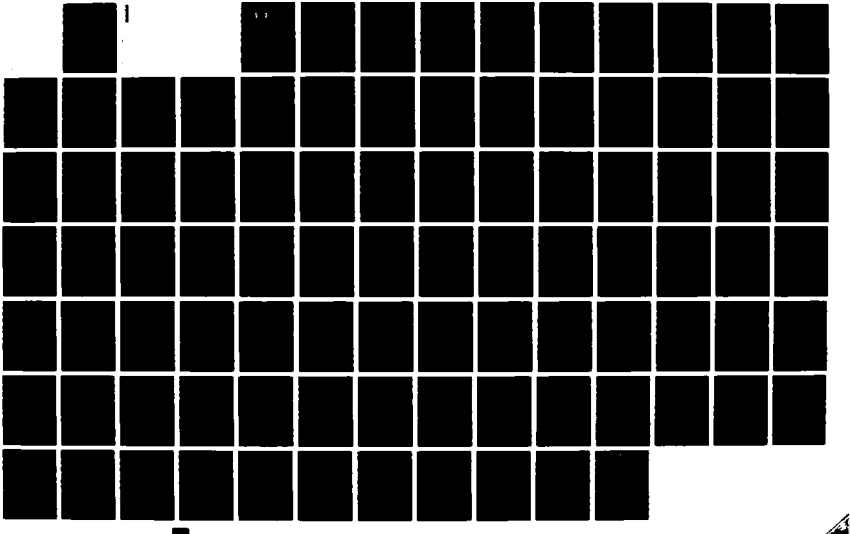

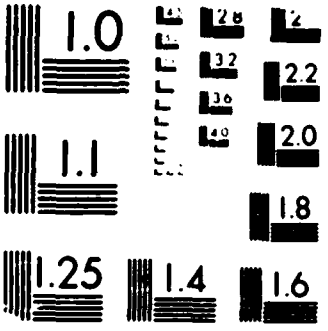

MICROCOPY RESOLUTION TEST CHART

UNCLASSIFIED

SECURITY CLASSIFICATION OF THIS PAGE

DTIC ELECTE MAY 05 1988 H

REPORT DOCUMENTATION PAGE

Form Approved
OMB No. 0704-0188
Exp. Date: Jun 30, 1986

1a REPORT SECURITY CLASSIFICATION: UNCLASSIFIED		1b RESTRICTIVE MARKINGS
2a SECURITY CLASSIFICATION AUTHORITY		3 DISTRIBUTION/AVAILABILITY OF REPORT: Approved for public release; distribution unlimited.
2b DECLASSIFICATION/DOWNGRADING SCHEDULE		
4 PERFORMING ORGANIZATION REPORT NUMBER(S): HDL-TR-2130		5 MONITORING ORGANIZATION REPORT NUMBER(S)
6a NAME OF PERFORMING ORGANIZATION: Harry Diamond Laboratories	6b OFFICE SYMBOL (If applicable): SLCHD-ST-AB	7a NAME OF MONITORING ORGANIZATION
6c ADDRESS (City, State, and ZIP Code): 2800 Powder Mill Road, Adelphi, MD 20783-1197		7b ADDRESS (City, State, and ZIP Code)
8a NAME OF FUNDING/SPONSORING ORGANIZATION: U.S. Army Laboratory Command	8b OFFICE SYMBOL (If applicable): AMC	9 PROCUREMENT INSTRUMENT IDENTIFICATION NUMBER
8c ADDRESS (City, State, and ZIP Code): 2800 Powder Mill Road, Adelphi, MD 20783-1145		10 SOURCE OF FUNDING NUMBERS: PROGRAM ELEMENT NO 61102A; PROJECT NO 1L1611-02AH44; TASK NO; WORK UNIT ACCESSION NO

11 TITLE (Include Security Classification)
Effects on the Resonant Frequencies Caused by Loading a Spherical Cavity with a Dielectric Sphere

12 PERSONAL AUTHOR(S)
Louis F. Libelo, Guy E. Pisane, and Richard Ziolkowski, Lawrence Livermore Laboratories

13a TYPE OF REPORT	13b TIME COVERED	14 DATE OF REPORT (Year, Month, Day)	15 PAGE COUNT
Final	FROM _____ TO _____	April 1988	92

16 SUPPLEMENTARY NOTATION
HDL project: AE1512, AMS code: 611102.H440011

17 COSATI CODES			18 SUBJECT TERMS (Continue on reverse if necessary and identify by block number)
FIELD	GROUP	SUB-GROUP	Resonant frequencies, spherical cavity, dielectric loading

19 ABSTRACT (Continue on reverse if necessary and identify by block number)

An extensive investigation has been carried out of the properties of a conducting spherical cavity filled with a lossless homogeneous dielectric and concentrically loaded with another lossless homogeneous dielectric. This report contains a portion of the results obtained in the course of this investigation. Also presented and discussed are the effects on the cavity system eigenvalues of changing the radius of the dielectric load sphere. This is done for a wide range of relative dielectric strength for the media within the cavity. Specifically, results for relative strengths of 3, 10, and 1/3 are given. The appropriate derivations of the eigenvalue equations are presented. Analysis of the results suggests a broad variety of practical applications. Subsequent reports will contain results of other aspects of the more extensive study.

20 DISTRIBUTION/AVAILABILITY OF ABSTRACT	21 ABSTRACT SECURITY CLASSIFICATION	
☒ UNCLASSIFIED/UNLIMITED ☐ SAME AS RPT ☐ DTIC USERS	UNCLASSIFIED	
22a NAME OF RESPONSIBLE INDIVIDUAL: Louis F. Libelo	22b TELEPHONE (Include Area Code): (202) 394-2290	22c OFFICE SYMBOL: SLCHD-NW-RI

DD FORM 1473, 84 MAR 83 APR edition may be used until exhausted
All other editions are obsolete

SECURITY CLASSIFICATION OF THIS PAGE
UNCLASSIFIED

Contents

Page

1. **Introduction** 7

2. **System Geometry and Formal Developments** 8

   2.1 System Geometry 8
   2.2 Formal Derivation of TE Mode Eigenvalue Relation 9
   2.3 Formal Derivation of TM Mode Eigenvalue Relation 14

3. ***The TE Eigenvalues*** 18

   3.1 Introduction 18
   3.2 The TE Eigenvalues for $\varepsilon_r = 3.00$ 20
   3.3 The TE Eigenvalues for $\varepsilon_r = 10.00$ 27
   3.4 The TE Eigenvalues for $\varepsilon_r = 1/3$ 37

4. **The Transverse Magnetic (TM) Eigenvalues** 47

   4.1 Introduction 47
   4.2 The TM Eigenvalues for $\varepsilon_r = 3.00$ 48
   4.3 The TM Eigenvalues for $\varepsilon_r = 10.00$ 55
   4.4 The TM Eigenvalues for $\varepsilon_r = 1/3$ 64

5. **Summary and Discussion** 74

   5.1 General Summary 74
   5.2 Overview of the TE and TM Eigenvalues for $\varepsilon_r = 3.00$ 75
   5.3 Overview of the TE and TM Eigenvalues for $\varepsilon_r = 10.00$ 79
   5.4 Overview of the TE and TM Eigenvalues for $\varepsilon_r = 1/3$ 84
   5.5 Final Summary and Discussion 88

References 90

Distribution 91

Figures

Page

1. Schematic of conducting spherical cavity containing a concentric spherical dielectric ... 8
2. TE eigenvalues $k_{n1}^{(1)}(R;\varepsilon_r = 3)\,a$ ... 21
3. TE eigenvalues $k_{n2}^{(1)}(R;\varepsilon_r = 3)\,a$ ... 26
4. TE eigenvalues $k_{n3}^{(1)}(R;\varepsilon_r = 3)\,a$ ... 26
5. TE eigenvalues $k_{n4}^{(1)}(R;\varepsilon_r = 3)\,a$ ... 27
6. TE eigenvalues $k_{n1}^{(1)}(R;\varepsilon_r = 10)\,a$ ... 28
7. TE eigenvalues $k_{n2}^{(1)}(R;\varepsilon_r = 10)\,a$ ... 29
8. TE eigenvalues $k_{n3}^{(1)}(R;\varepsilon_r = 10)\,a$ ... 35
9. TE eigenvalues $k_{n4}^{(1)}(R;\varepsilon_r = 10)\,a$ ... 36
10. TE eigenvalues $k_{15}^{(1)}(R;\varepsilon_r = 10)\,a$ ... 37
11. TE eigenvalues $k_{n1}^{(1)}(R;\varepsilon_r = 1/3)\,a$ ... 39
12. TE eigenvalues $k_{n2}^{(1)}(R;\varepsilon_r = 1/3)\,a$ ... 44
13. TE eigenvalues $k_{n3}^{(1)}(R;\varepsilon_r = 1/3)\,a$ ... 44
14. TE eigenvalues $k_{n4}^{(1)}(R;\varepsilon_r = 1/3)\,a$ ... 46
15. TM eigenvalues $k_{n1}^{(2)}(R;\varepsilon_r = 3)\,a$ ... 48
16. TM eigenvalues $k_{n2}^{(2)}(R;\varepsilon_r = 3)\,a$ ... 53
17. TM eigenvalues $k_{n3}^{(2)}(R;\varepsilon_r = 3)\,a$ ... 54
18. TM eigenvalues $k_{n4}^{(2)}(R;\varepsilon_r = 3)\,a$ ... 55
19. TM eigenvalues $k_{n1}^{(2)}(R;\varepsilon_r = 10)\,a$ ... 56
20. TM eigenvalues $k_{n2}^{(2)}(R;\varepsilon_r = 10)\,a$ ... 62
21. TM eigenvalues $k_{n3}^{(2)}(R;\varepsilon_r = 10)\,a$ ... 63
22. TM eigenvalues $k_{n4}^{(2)}(R;\varepsilon_r = 10)\,a$ ... 64
23. TM eigenvalues $k_{n1}^{(2)}(R;\varepsilon_r = 1/3)\,a$ ... 65
24. TM eigenvalues $k_{n2}^{(2)}(R;\varepsilon_r = 1/3)\,a$ ... 71
25. TM eigenvalues $k_{n3}^{(2)}(R;\varepsilon_r = 1/3)\,a$ ... 72
26. TM eigenvalues $k_{n4}^{(2)}(R;\varepsilon_r = 1/3)\,a$ ... 72
27. A composite of the TE eigenvalues $k_{np}^{(1)}(R;\varepsilon_r = 3)\,a$ ... 76
28. A composite of the TM eigenvalues $k_{np}^{(2)}(R;\varepsilon_r = 3)\,a$ ... 79
29. A composite of the TE eigenvalues $k_{np}^{(1)}(R;\varepsilon_r = 10)\,a$ ... 80
30. A composite of the TM eigenvalues $k_{np}^{(2)}(R;\varepsilon_r = 10)\,a$ ... 82
31. A composite of the TE eigenvalues $k_{np}^{(1)}(R;\varepsilon_r = 1/3)\,a$ ... 85
32. A composite of the TM eigenvalues $k_{np}^{(2)}(R;\varepsilon_r = 1/3)\,a$ ... 86

Tables

Page

1. Numerical Values of the TE Eigenvalues $k_n^{(1)}(R;\varepsilon_r = 3)\,a$ 22
2. Numerical Values of the TE Eigenvalues $k_n^{(1)}(r;\varepsilon_r = 10)\,a$ 30
3. Numerical Values of the TE Eigenvalues $k_n^{(1)}(R;\varepsilon_r = 1/3)\,a$ 40
4. Numerical Values of the TM Eigenvalues $k_n^{(2)}(R;\varepsilon_r = 3)\,a$ 49
5. Numerical Values of the TM Eigenvalues $k_n^{(2)}(R;\varepsilon_r = 10)\,a$ 57
6. Numerical Values of the TM Eigenvalues $k_n^{(2)}(R;\varepsilon_r = 1/3)\,a$ 65

1. Introduction

This is the second in a sequence of reports that present results of studies of electromagnetic properties of finite, three-dimensional spherical systems [1]*. Although this particular geometry is an extremely simple idealization, many of the results obtained in the course of the research are quite general. Indeed, they provide considerable insight into the electromagnetic characteristics of real systems of much more complicated geometry and structure which do not readily lend themselves to analytic resolution.

In the study presented here, we investigated one important effect of concentrically enclosing a spherical lossless dielectric within an ideal conducting spherical cavity. This system is clearly of intrinsic importance on its own. In addition, it provides an opportunity to understand, by comparison with a previously reported study [1], how the effect of loading a spherical cavity with a dielectric sphere differs from imbedding a concentric spherical conductor in that cavity. Furthermore, the studies of such systems of very simple geometry will subsequently serve as reliable reference points for studies of systems of successively increasing complexity.

The electromagnetic property we focus on in this report is the set of resonant frequencies of the dielectrically loaded conducting spherical cavity. The dependence of these physical variables on size and dielectric strength will be presented. In section 2 we briefly present the formal development for the eigenvalue problem of the system. In a previous report [1] we gave a more complete formal development. The details of the geometry are given in section 2 also. Transverse-electric (TE) and transverse-magnetic (TM) modes (i.e., relative to the radial direction) are separable and uncoupled for this system. Section 3 contains the resonances for the TE modes of the system as a function of radius of the interior dielectric. Effects of varying the dielectric strength for the eigenvalues of the TE modes are included in this section. Corresponding results for the TM modes are given in section 4. Finally, in section 5 we present a summary discussion of all the results.

References are listed at end of report.

2. System Geometry and Formal Developments

2.1 System Geometry

Figure 1 illustrates the geometry of the system undergoing investigation. It consists of a simple spherical conductor of radius a containing a concentric lossless dielectric sphere of radius b and dielectric constant ε_2.

The remaining volume contains a lossless dielectric of dielectric constant ε_1. The relative dielectric strength is denoted by ε_r, where

$$\varepsilon_r = \varepsilon_2/\varepsilon_1. \tag{1}$$

We shall in this report consider only the case where the magnetic permeability is the same for both dielectrics; i.e., $\mu_1 = \mu_2$.

Quantities related to the region between the outer boundary of the inner dielectric sphere and the conductor will be denoted by the index 1, either as a subscript or superscript. The variables related to the volume occupied by the inner sphere will similarly be denoted by the index 2.

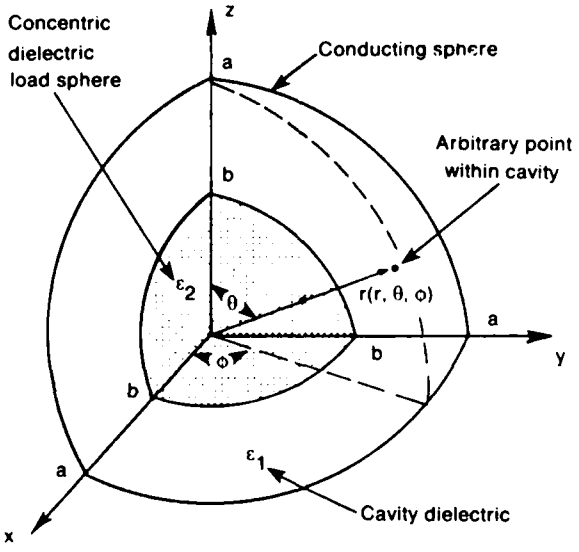

Figure 1. Schematic of the conducting spherical cavity containing a concentric spherical dielectric.

2.2 Formal Derivation of TE Mode Eigenvalue Relation

The Debye potential for the TE mode is of the form

$$\Phi_{nm}(\mathbf{r}) = \begin{cases} Y_{nm}(\theta,\phi)\,\phi_n^{(1)}(r) \;\;, & for\ b \le r \le a \\ Y_{nm}(\theta,\phi)\,\phi_n^{(2)}(r) \;\;, & for\ 0 \le r < b \end{cases} \tag{2}$$

and satisfies

$$\left(\nabla^2 - \gamma_1^2\right)\Phi_{nm}(\mathbf{r}) = 0 \;\;,\; for\ b < r \le a \tag{3a}$$

and

$$\left(\nabla^2 - \gamma_2^2\right)\Phi_{nm}(\mathbf{r}) = 0 \;\;,\; for\ 0 \le r < b \tag{3b}$$

where

$$\gamma_i \equiv j k_i = j\sqrt{\mu_i \varepsilon_i}\;\omega \;. \tag{4}$$

Since the angular part is well-known, we shall only explicitly consider the radially dependent part of equation (2), which is taken in the form

$$\phi_n(r) \equiv \begin{cases} \phi_n^{(1)}(\gamma_1 r) = A_n^{(1)} i_n(\gamma_1 r) + B_n^{(1)} k_n(\gamma_1 r) \;\;, & b \le r \le a \\ \phi_n^{(2)}(\gamma_2 r) = i_n(\gamma_2 r) \;\;, & 0 \le r \le b \end{cases} \tag{5}$$

where we have introduced the modified spherical Bessel functions in equation (5). Note that the coefficient of $\phi_n^{(2)}$ has been chosen as unity for convenience. Applications of the boundary conditions of the fields at $r = a$ and $r = b$ will then determine the coefficients $A_n^{(1)}$ and $B_n^{(1)}$ and establish the eigenvalue relation as a function of a, b, ε_1, and ε_2. The general expressions for the field components in terms of the Debye potential for the TE modes are given by

$$E_{r;nm}(\mathbf{r}) \equiv 0 \tag{6a}$$

$$E_{\phi;nm}(\mathbf{r}) = -\frac{1}{r\sin\theta}\,\frac{\partial}{\partial\phi}\left[r\,\Phi_{nm}(\mathbf{r})\right] \tag{6b}$$

$$E_{\theta;nm}(\mathbf{r}) = \frac{1}{r}\,\frac{\partial}{\partial\theta}\left[r\,\Phi_{nm}(\mathbf{r})\right] \;\;, \tag{6c}$$

$$H_{r;nm}(\mathbf{r}) = \frac{1}{j\omega\mu}\left(\frac{\partial^2}{\partial r^2} - \gamma^2\right)\left[r\Phi_{nm}(\mathbf{r})\right] \ , \tag{6d}$$

$$H_{\theta;nm}(\mathbf{r}) = \frac{1}{j\omega\mu}\ \frac{1}{r}\ \frac{\partial^2}{\partial r\partial\theta}\ \left[r\Phi_{nm}(\mathbf{r})\right] \ . \tag{6e}$$

and

$$H_{\phi;nm}(\mathbf{r}) = \frac{1}{j\omega\mu}\ \frac{1}{r}\ \frac{\partial^2}{\partial r\partial\phi}\ \left[r\Phi_{nm}(\mathbf{r})\right] \ . \tag{6f}$$

Each of these field components is of the form

$$[\ ]_{();nm}(\mathbf{r}) \equiv [\ ]_{();nm}(\theta,\phi)\begin{cases}[\ ]^{(1)}_{();n}(r) & , \ b \le r \le a \\ [\ ]^{(2)}_{();n}(r) & , \ 0 \le r \le b\end{cases} . \tag{7}$$

We then can separate variables and rewrite equations (6) as

$$E_{r;nm}(\mathbf{r}) = 0 \ , \tag{8a}$$

$$E_{\theta;nm}(\mathbf{r}) = E_{\theta;nm}(\theta,\phi)\begin{cases}E^{(1)}_{\theta;n}(r) & , \ b < r \le a \\ E^{(2)}_{\theta;n}(r) & , \ 0 \le r < b\end{cases} , \tag{8b}$$

$$E_{\phi;nm}(\mathbf{r}) = E_{\phi;nm}(\theta,\phi)\begin{cases}E^{(1)}_{\phi;n}(r) & , \ b < r \le a \\ E^{(2)}_{\phi;n}(r) & , \ 0 \le r < b\end{cases} , \tag{8c}$$

$$H_{r;nm}(\mathbf{r}) = H_{r;nm}(\theta,\phi)\begin{cases}H^{(1)}_{r;n}(r) & , \ b \le r \le a \\ H^{(2)}_{r;n}(r) & , \ 0 \le r < b\end{cases} , \tag{8d}$$

$$H_{\theta;nm}(\mathbf{r}) = H_{\theta;nm}(\theta,\phi)\begin{cases}H^{(1)}_{\theta;n}(r) & , \ b < r \le a \\ H^{(2)}_{\theta;n}(r) & , \ 0 \le r < b\end{cases} , \tag{8e}$$

and

$$H_{\phi;nm}(\mathbf{r}) = H_{\phi;nm}(\theta,\phi)\begin{cases} H^{(1)}_{\phi;n}(r) \ , \ b < r \le a \\ H^{(2)}_{\phi;n}(r) \ , \ 0 \le r < b \end{cases} . \tag{8f}$$

Clearly we need only consider the radially dependent factor in all further derivations in this report. Thus we shall write:

$$E_{r;n}(r) \equiv 0 \ . \tag{9a}$$

$$E_{\theta;n}(r) = \begin{cases} E^{(1)}_{\theta;n}(r) = \phi^{(1)}_n(r) \ , \ b < r \le a \\ E^{(2)}_{\theta;n}(r) = \phi^{(2)}_n(r) \ , \ 0 \le r < b \end{cases} , \tag{9b}$$

$$E_{\phi;nm}(\mathbf{r}) = E_{\phi;nm}(\theta,\phi)\begin{cases} E^{(1)}_{\phi;n}(r) \ , \ b < r \le a \\ E^{(2)}_{\phi;n}(r) \ , \ 0 \le r < a \end{cases} , \tag{9c}$$

$$H_{r;nm}(\mathbf{r}) = H_{r;nm}(\theta,\phi)\begin{cases} H^{(1)}_{r,n}(r) \ , \ b < r \le a \\ H^{(2)}_{r;n}(r) \ , \ 0 \le r < b \end{cases} , \tag{9d}$$

$$H_{\theta;nm}(\mathbf{r}) = H_{\theta;nm}(\theta,\phi)\begin{cases} H^{(1)}_{\theta;n}(r) \ , \ b < r \le a \\ H^{(2)}_{\theta;n}(r) \ , \ 0 \le r < b \end{cases} , \tag{9e}$$

and

$$H_{\phi;nm}(\mathbf{r}) = H_{\phi;nm}(\theta,\phi)\begin{cases} H^{(1)}_{\phi;n}(r) \ , \ b < r \le a \\ H^{(2)}_{\phi;n}(r) \ , \ 0 \le r < a \end{cases} . \tag{9f}$$

These can be further expanded to

$$E_{r;n}(r) = 0 \ , \tag{10a}$$

$$E_{\theta;n}(r) = \begin{cases} E^{(1)}_{\theta;n}(r) = \phi^{(1)}_n(r) \ , \ b < r \le a \\ E^{(2)}_{\theta;n}(r) = \phi^{(2)}_n(r) \ , \ 0 \le r < a \end{cases} \tag{10b}$$

$$E_{\phi;n}(r) = E_{\theta;n}(r) \ , \tag{10c}$$

$$H_{r;n}(r) = \begin{cases} H^{(1)}_{r;n}(r) = \sqrt{\dfrac{\varepsilon_1}{\mu_1}} \left[\dfrac{d^2}{d(\gamma_1 r)^2} - 1 \right] \left[\gamma_1 r \phi^{(1)}_n(\gamma_1 r) \right] \\ H^{(2)}_{r;n}(r) = \sqrt{\dfrac{\varepsilon_2}{\mu_2}} \left[\dfrac{d^2}{d(\gamma_2 r)^2} - 1 \right] \left[\gamma_2 r \phi^{(2)}_n(\gamma_2 r) \right] \end{cases} \tag{10d}$$

$$H_{\theta;n}(\mathbf{r}) = \begin{cases} H^{(1)}_{\theta;n}(r) = \sqrt{\dfrac{\varepsilon_1}{\mu_1}} \dfrac{1}{\gamma_1 r} \dfrac{d}{d(\gamma_1 r)} \left[\gamma_1 r \phi^{(1)}_n(\gamma_1 r) \right] \\ \qquad = \sqrt{\dfrac{\varepsilon_1}{\mu_1}} \dfrac{1}{\gamma_1 r} \left[\gamma_1 r \phi^{(1)}_n(\gamma_1 r) \right]' \\ H^{(2)}_{\theta;n}(r) = \sqrt{\dfrac{\varepsilon_2}{\mu_2}} \dfrac{1}{\gamma_2 r} \dfrac{d}{d(\gamma_2 r)} \left[\gamma_2 r \phi^{(2)}_n(\gamma_2 r) \right] \\ \qquad = \sqrt{\dfrac{\varepsilon_2}{\mu_2}} \dfrac{1}{\gamma_2 r} \left[\gamma_2 r \phi^{(2)}_n(\gamma_2 r) \right]' \end{cases} \tag{10e}$$

and

$$H_{o;n}(r) = H_{\theta;n}(r) \quad , \tag{10f}$$

where we have introduced the notation

$$\frac{d}{dx} \left[x\phi(x) \right] \equiv \left[x\phi(x) \right]' \quad .$$

Now let us explicitly consider applying the boundary conditions. At the dielectric interface, both the tangential electric field and the tangential magnetic field are continuous across at $r = b$. From equations (9b) and (e), we obtain then the pair of relations

$$A^{(1)}_n i_n(\gamma_1 b) + B^{(1)}_n k_n(\gamma_1 b) = i_n(\gamma_2 b) \quad , \tag{11}$$

and

$$A_n^{(1)}[\gamma_1 b\, i_n(\gamma_1 b)]' + B_n^{(1)}[\gamma_1 b\, k_n(\gamma_1 b)]' = [\gamma_2 b\, i_n(\gamma_2 b)]' \ . \qquad (12)$$

This pair of equations is readily solved to give

$$A_n^{(1)} = -\gamma_1 b \begin{vmatrix} i_n(\gamma_2 b) & , & k_n(\gamma_1 b) \\ [\gamma_2 b\, i_n(\gamma_2 b)]' & , & [\gamma_1 b\, k_n(\gamma_1 b)]' \end{vmatrix} \qquad (13)$$

and

$$B_n^{(1)} = -\gamma_1 b \begin{vmatrix} i_n(\gamma_1 b) & , & i_n(\gamma_2 b) \\ [\gamma_1 b\, i_n(\gamma_1 b)]' & , & [\gamma_2 b\, i_n(\gamma_2 b)]' \end{vmatrix} \ , \qquad (14)$$

where we have used the Wronskian relation to simplify the results. The coefficients have thus been determined in terms of known quantities.

Next we apply the boundary condition at the conducting surface: namely, the tangential electric field vanishes at $r = a$. This gives us

$$A_n^{(1)} i_n(\gamma_1 a) + B_n^{(1)} k_n(\gamma_1 a) = 0 \ .$$

Upon substituting into this relation from equations (13) and (14) for the coefficients and rearranging, we obtain one form of the eigenvalue relation for the TE modes:

$$i_n(\gamma_2 b)\, \Upsilon_n^{(1)}(a,b) - [\gamma_2 b\, i_n(\gamma_2 b)]'\, \Lambda_n^{(1)}(a,b) = 0 \ . \qquad (15)$$

This is the relation whose roots, $\gamma_l a$, give the system TE eigenvalues. The auxiliary functions introduced in equation (15) are defined as follows:

$$\Lambda_n^{(l)}(a,b) \equiv i_n(\gamma_l a)\, k_n(\gamma_l b) - i_n(\gamma_l b)\, k_n(\gamma_l a) \ . \qquad (16)$$

$$\Upsilon_n^{(l)}(a,b) \equiv i_n(\gamma_l a)\, [\gamma_l b\, k_n(\gamma_l b)]' - k_n(\gamma_l a)\, [\gamma_l b\, i_n(\gamma_l b)]' \ . \qquad (17)$$

In section 3 we shall continue with the considerations of the TE modes.

2.3 Formal Derivation of TM Mode Eigenvalue Relation

For the TM modes, the Debye potential is of the form

$$\Psi_{nm}(\mathbf{r}) = \begin{cases} Y_{nm}(\theta,\phi)\,\psi_n^{(1)}(r) & , \; for\; b < r \le a \;, \\ Y_{nm}(\theta,\phi)\,\psi_n^{(2)}(r) & , \; for\; 0 \le r < b \;, \end{cases} \tag{18}$$

which satisfies the differential equation:

$$\left(\nabla^2 - \gamma_1^2\right)\Psi_{nm}(\mathbf{r}) = 0 \;, \; for\; b < r \le a \tag{19a}$$

and

$$\left(\nabla^2 - \gamma_2^2\right)\Psi_{nm}(\mathbf{r}) = 0 \;, \; for\; 0 \le r < a \;. \tag{19b}$$

Once again we observe that the angular part is well-known. Hence we only explicitly display the radially dependent part. This is

$$\psi_n(r) = \begin{cases} \psi_n^{(1)}(\gamma_1 r) = C_n^{(1)} i_n(\gamma_1 r) + D_n^{(1)} k_n(\gamma_1 r) & , \; for\; b < r \le a \;, \\ \psi_n^{(2)}(\gamma_2 r) = i_n(\gamma_2 r) & , \; for\; 0 \le r < b \;. \end{cases} \tag{20}$$

Again the coefficient of the inner Debye potential has been taken as unity for convenience. Application of the boundary conditions for the fields at the conductor and the dielectric interface will as before explicitly evaluate the coefficient $C_n^{(1)}$ and $D_n^{(1)}$ and generate the eigenvalue relation for the TM modes.

The general formal expressions for the TM mode field components in terms of the Debye potential $\psi_{nm}(\mathbf{r})$ are

$$H_{r;nm}(\mathbf{r}) = 0 \;, \tag{21a}$$

$$H_{\theta;nm}(\mathbf{r}) = \frac{1}{r\sin\theta}\,\frac{\partial}{\partial\phi}\left[r\,\Psi_{nm}(\mathbf{r})\right] \;, \tag{21b}$$

$$H_{\phi;nm}(\mathbf{r}) = -\frac{1}{r}\frac{\partial}{\partial\theta}\left[r\Psi_{nm}(\mathbf{r})\right] \quad , \tag{21c}$$

$$E_{r;nm}(\mathbf{r}) = \frac{1}{j\omega\epsilon}\left(\frac{\partial^2}{\partial r^2} - \gamma^2\right)\left[r\Psi_{nm}(\mathbf{r})\right] \quad , \tag{21d}$$

$$E_{\theta;nm}(\mathbf{r}) = \frac{1}{j\omega\epsilon}\frac{1}{r}\frac{\partial^2}{\partial r\partial\theta}\left[r\Psi_{nm}(\mathbf{r})\right] \quad , \tag{21e}$$

$$E_{\phi;nm}(\mathbf{r}) = \frac{1}{j\omega\epsilon}\frac{1}{r\sin\theta}\frac{\partial^2}{\partial r\partial\phi}\left[r\Psi_{nm}(\mathbf{r})\right] \quad . \tag{21f}$$

Again observe that each of the field components in equations (21) are of the form

$$[\ ]_{();nm}(\mathbf{r}) = [\ ]_{();nm}(\theta,\phi)\begin{cases}[\ ]^{(1)}_{();n}(r) & , \ b < r \le a \\ [\ ]^{(2)}_{();n}(r) & , \ 0 \le r < b\end{cases}$$

and just as we did for the TE components we rewrite equations (21) as follows:

$$H_{r;nm}(\mathbf{r}) = 0 \tag{22a}$$

$$H_{\theta;nm}(\mathbf{r}) = H_{\theta;nm}(\theta,\phi)\begin{cases}H^{(1)}_{\theta;n}(r) & , \ b < r \le a \\ H^{(2)}_{\theta;n}(r) & , \ 0 \le r \le b\end{cases} \tag{22b}$$

$$H_{\phi;nm}(\mathbf{r}) = H_{\phi;nm}(\theta,\phi)\begin{cases}H^{(1)}_{\phi;n}(r) & , \ b < r \le a \\ H^{(2)}_{\phi;n}(r) & , \ 0 \le r \le b\end{cases} \tag{22c}$$

$$E_{r;nm}(\mathbf{r}) = E_{r;nm}(\theta,\phi)\begin{cases}E^{(1)}_{r;n}(r) & , \ b < r \le a \\ E^{(2)}_{r;n}(r) & , \ 0 \le r < b\end{cases} \tag{22d}$$

$$E_{\theta;nm}(\mathbf{r}) = E_{\theta;nm}(\theta,\phi)\begin{cases}E^{(1)}_{\theta;n}(r) & , \ b < r \le a \\ E^{(2)}_{\theta;n}(r) & , \ 0 \le r < b\end{cases} \tag{22e}$$

and

$$E_{\phi;nm}(\mathbf{r}) = E_{\phi;nm}(\theta,\phi)\begin{cases} E^{(1)}_{\phi;n}(r) \ , \ b < r \le a \\ E^{(2)}_{\phi;n}(r) \ , \ 0 \le r < b \end{cases} . \tag{22f}$$

Extracting the radially dependent part we have

$$H_{r;n}(r) = 0 \ , \tag{23a}$$

$$H_{\theta;n}(r) = \begin{cases} H^{(1)}_{\theta;n}(r) = \psi^{(1)}_n(\gamma_1 r) \ , \ b < r \le a \ , \\ H^{(2)}_{\theta;n}(r) = \psi^{(2)}_n(n\gamma_2 r) \ , \ 0 \le r < b \ , \end{cases} \tag{23b}$$

$$H_{\phi;n}(r) = H_{\theta;n}(r) \tag{23c}$$

$$E_{r;n}(r) = \begin{cases} E^{(1)}_{r;n}(r) = \sqrt{\dfrac{\mu_1}{\varepsilon_1}}\left[\dfrac{d^2}{d(\gamma_1 r)^2} - 1\right]\left[\gamma_1 r \psi^{(1)}_n(\gamma_1 r)\right] \ , \ b < r \le a \ , \\ E^{(2)}_{r;n}(r) = \sqrt{\dfrac{\mu_2}{\varepsilon_2}}\left[\dfrac{d^2}{d(\gamma_2 r)^2} - 1\right]\left[\gamma_2 r \psi^{(2)}_n(\gamma_2 r)\right] \ , \ 0 \le r < b \ , \end{cases} \tag{23d}$$

$$E_{\theta;n}(r) = \begin{cases} E^{(1)}_{\theta;n}(r) = \sqrt{\dfrac{\mu_1}{\varepsilon_1}} \ \dfrac{1}{\gamma_1 r}\left[\gamma_1 r \psi^{(1)}_n(\gamma_1 r)\right]' \ , \ b < r < a \ , \\ E^{(2)}_{\theta;n}(r) = \sqrt{\dfrac{\mu_2}{\varepsilon_2}} \ \dfrac{1}{\gamma_2 r}\left[\gamma_2 r \psi^{(2)}_n(\gamma_1 r)\right]' \ , \ 0 \le r < b \ , \end{cases} \tag{23e}$$

$$E_{\phi;n}(r) = E_{\theta;n}(r) \ . \tag{23f}$$

Next we apply the boundary conditions. The tangential components of the electric and magnetic fields are continuous across the dielectric interface at $r = b$. Then from equations (23b) and (23d) we obtain, respectively, the pair of simultaneous equations

$$C^{(1)}_n i_n(\gamma_1 b) + D^{(1)}_n k_n(\gamma_1 b) = i_n(\gamma_2 b) \tag{24}$$

and

$$\frac{1}{\sqrt{\varepsilon_1}} C_n^{(1)} \frac{1}{\gamma_1 b} [\gamma_1 b\, i_n(\gamma_1 b)]' + \frac{1}{\sqrt{\varepsilon_1}} D_n^{(1)} \frac{1}{\gamma_1 b} [\gamma_1 b\, k_n(\gamma_1 b)]' \quad (25)$$

$$= \frac{1}{\sqrt{\varepsilon_2}} \frac{1}{\gamma_2 b} [\gamma_2 b\, i_n(\gamma_2 b)]' .$$

Solving this pair of equations we obtain, after some rearranging and using the Wronskian, the coefficients

$$C_n^{(1)} = -\frac{1}{\gamma_1 b} \begin{vmatrix} i_n(\gamma_2 b) & , & k_n(\gamma_1 b) \\ \frac{\varepsilon_1}{\varepsilon_2} \gamma_2 b\, i_n(\gamma_2 b) & , & [\gamma_1 b\, k_n(\gamma_1 b)]' \end{vmatrix} , \quad (26)$$

$$D_n^{(1)} = -\frac{1}{\gamma_1 b} \begin{vmatrix} i_n(\gamma_1 b) & , & i_n(\gamma_2 b) \\ \gamma_1 b\, i_n(\gamma_1 b) & , & \frac{\varepsilon_1}{\varepsilon_2} [\gamma_2 b\, i_n(\gamma_2 b)]' \end{vmatrix} . \quad (27)$$

At the conducting surface $r = a$, the tangential components of the electric field vanish. This gives us the relation

$$C_n^{(1)} [\gamma_1 a\, i_n(\gamma_1 a)]' + D_n^{(1)} [\gamma_1 a\, k_n(\gamma_1 a)]' = 0 . \quad (28)$$

If we substitute into this the expressions for the coefficients from equations (26) and (27), we obtain, after some rearranging, one form of the eigenvalue relation for the TM modes of the system:

$$\varepsilon_r i_n(\gamma_2 b) T_n^{(1)}(a,b) + [\gamma_2 b\, i_n(\gamma_2 b)]' T_n^{(1)}(b,a) = 0 . \quad (29)$$

In equation (29) we introduced the additional auxiliary function

$$\begin{aligned} T_n^{(l)}(a,b) \equiv\ & [\gamma_l a\, i_n(\gamma_l a)]' [\gamma_l b\, k_n(\gamma_l b)]' \\ & - [\gamma_l b\, i_n(\gamma_l b)]' [\gamma_l a\, k_n(\gamma_l a)]' . \end{aligned} \quad (30)$$

The TM eigenvalues were found by solving equation (29) for its roots $\gamma_l a$. We shall continue the discussion of the TM modes in section 4.

3. The TE Eigenvalues

3.1 Introduction

Before presenting the TE eigenvalues, we must first establish some conventions.

We introduce the notation

$$R \equiv b/a \ . \tag{31}$$

Using the identities

$$\gamma_2 b \equiv \frac{\gamma_2}{\gamma_1}\,\frac{b}{a}\,\gamma_1 a = \sqrt{\varepsilon_r}\, R\,\gamma_1 a \ ,$$

and

$$\gamma_1 b \equiv \frac{b}{a}\,\gamma_1 a = R\,\gamma_1 a \ ,$$

we rewrite equations (15) through (17) as follows:

$$i_n\left(\sqrt{\varepsilon_r}\, R\,\gamma_1 a\right)\,\Upsilon_n^{(1)}(a,Ra) - \varepsilon_r R\,\gamma_1 a\, i_n\left(\sqrt{\varepsilon_r}\, R\,\gamma_1 a\right)\,\Lambda_n^{(1)}(a,Ra) = 0 \ , \tag{32}$$

where

$$\Lambda_n^{(1)}(a,b) = \Lambda_n^{(1)}(a,Ra) = i_n(\gamma_1 a)\,k_n(R\,\gamma_1 a) - i_n(R\,\gamma_1 a)\,k_n(\gamma_1 a) \ , \tag{33}$$

and

$$\begin{aligned}\Upsilon_n^{(1)}(a,b) &= \Upsilon_n^{(1)}(a,Ra) \\ &= i_n(\gamma_1 a)\,[R\,\gamma_1 a\,k_n(R\,\gamma_1 a)]' - k_n(\gamma_1 a)\,[R\,\gamma_1 a\,i_n(R\,\gamma_1 a)]' \ .\end{aligned} \tag{34}$$

Clearly, for fixed values of ε_r and R we can consider $\gamma_1 a$ as the variable in equation (32) and solve for those values of the variable that satisfy equation (32). These values we call the "eigenvalues" for the TE modes. Since the dielectrics within the cavity are lossless and the outer cavity wall is a perfect conductor, all the roots of equation (32) are purely im-

aginary. Thus, the TE eigenvalue spectrum for each value of n will be a doubly infinite discrete set of ordered real numbers, each of which we denote by $k_{np}^{(1)} a$ where $j k_{np}^{(1)}(a)$ is a root of equation (32) for fixed n (by allowing $\gamma_{np}^2 = -k_{np}^2$), and

$$k_{np}^{(1)} a < k_{np'}^{(1)}(a) \quad for \quad p < p', \; p \; and \; p' = 1, 2, \ldots .$$

Further each value $k_{np}^{(1)} a$ is a function of the relative dielectric strength, ε_r, and of the ratio of inner dielectric radius to outer cavity radius, R:

$$k_{np}^{(1)} a \equiv k_{np}^{(1)}(\varepsilon_r ; R)\, a \quad . \tag{35}$$

First we consider two limiting cases:

- The inner dielectric has $b \equiv 0$. In this limit the eigenvalues are exactly the same as those for the well-known spherical cavity [2], filled homogeneously with dielectric ε_1. Thus, for each n the $k_{np}^{(1)} a$ are found from the roots of $i_n\left(\gamma_1^{(1)} a\right) = 0$.

- The inner dielectric, ε_2, fills the entire cavity, so that $b = a$ (or R = 1). In this limit we find the eigenvalues $\gamma_1^{(1)} a$ by merely taking those already obtained for the cavity filled with dielectric of strength ε_1 and dividing by $\sqrt{\varepsilon_r}$. That is to say,

$$k_{np}^{(1)}(R=0)\, a = 1/\sqrt{\varepsilon_r}\, k_{np}^{(1)}(R=1)\, a .$$

Clearly, no more effort is required to obtain the TE eigenvalues when the inner dielectric sphere has zero radius than in the other limit when the inner dielectric has expanded to fill the cavity completely.

We note that if $\varepsilon_r > 1$ (i.e., the inner dielectric constant exceeds the outer, surrounding, dielectric constant), the eigenvalues, in general, shift downward as the inner sphere fills the cavity.

This is of course to be expected. (However, it still remains to be seen how the TE eigenvalues behave in between these limits.) In the situations where $\varepsilon_r < 1$ (i.e., the dielectric constant of the inner sphere is less than that of the surrounding dielectric in the cavity), the reverse behavior

is of course to be expected. That is, when the inner sphere fills the cavity, the TE eigenvalues $\gamma_2^{(1)} a$ take on the values that are well-known for the cavity with a homogeneous dielectric in its interior. As the inner sphere shrinks in radius, the TE eigenvalues reduce to this latter set multiplied by the factor $1/\sqrt{\epsilon_r} > 1$. Hence, we now observe that in the absence of the inner dielectric sphere, all the TE resonance frequencies are shifted to lower values. (Again, we have yet to see the behavior in the intermediate region.)

We now proceed to examine the behavior of the TE eigenvalues as a function of the radius of the concentric dielectric sphere in the cavity for several representative choices of dielectric strength. Though other representations can be construed, we choose to keep the relative dielectric strength, ϵ_2/ϵ_1, fixed, and we solve equation (32) for the eigenvalues, $\gamma_1 a$, while varying the normalized inner radius, b/a. The solutions in this representation group themselves naturally into families of curves in accordance with the second subscript, p. We shall present the solutions so grouped into these families.

3.2 The TE Eigenvalues for $\epsilon_r = 3.00$

The first detailed case we shall consider is that for which the inner dielectric sphere has a dielectric constant of $\epsilon_2 = 3.00\epsilon_1$. Note that ϵ_1 is assumed to be the dielectric constant in the cavity in the absence of the concentric dielectric sphere.

In figure 2 the results obtained from equation (32) for $k_{np}^{(1)}(R;\epsilon_r=3.00)\,a$ are shown plotted against R for the family $p = 1$ and n ranging from 1 to 5. Table 1(a) contains numerical values for these eigenvalues. Examination of these $k_{n1}^{(1)}(R;\epsilon_r)\,a$ curves shows the following behavior between the limiting cases discussed above. For a given value of the index n, the eigenvalues at first decrease in value slowly as the normalized inner sphere radius, R, grows. The greater the index n, the slower this decrease in eigenvalue becomes and the larger the range in R over which this initial behavior persists. Immediately following this characteristic initial behavior with increasing radius b (or equivalently R), a speed-up in the rate of change of $k_{n1}^{(1)} a$ occurs. This increase in the rate at which the eigenvalue decreases becomes more marked as n increases. There is a clearly defined knee in the $k_{n1}^{(1)} a$ eigenvalue trajectories for $n > 1$ marking where the curve departs from the slowly varying to the quickly varying

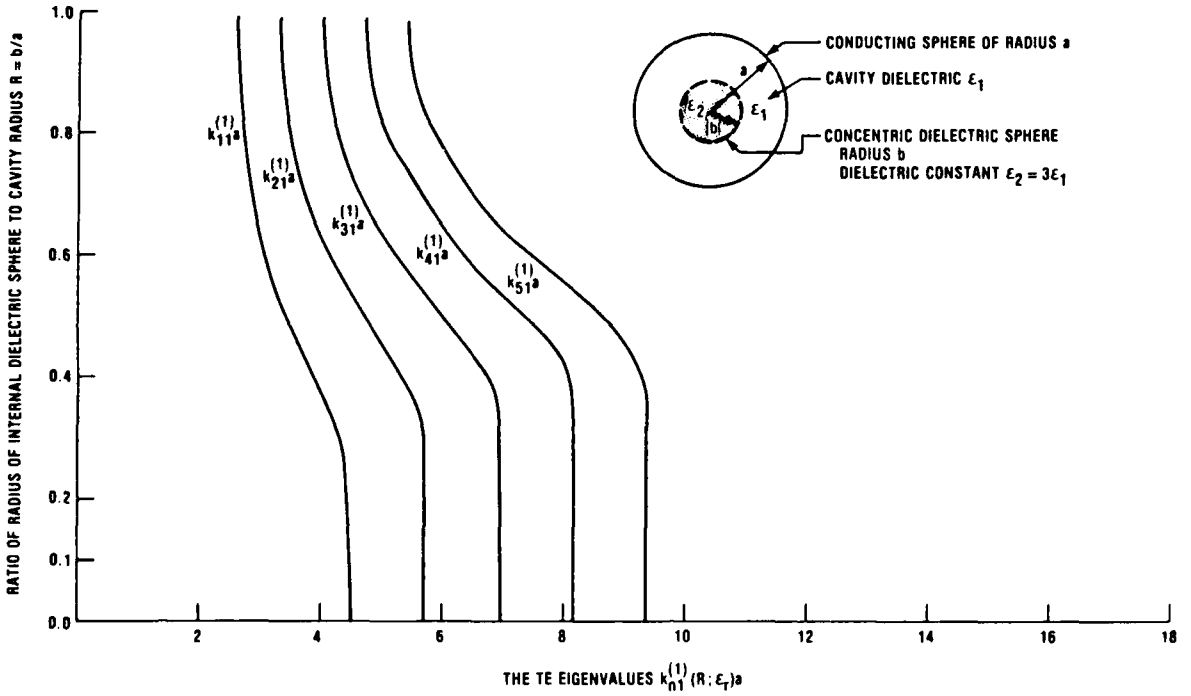

Figure 2. TE eigenvalues $k_{n1}^{(1)}(R;\varepsilon_r = 3)a$ for the spherical cavity of radius *a* filled with dielectric ε_1 internally loaded with a concentric dielectric sphere of radius *b* and strength $\varepsilon_2 = 3\varepsilon_1$.

behavior. For large n this knee becomes quite a sharp bend. Following these noteworthy characteristics the $k_{n1}^{(1)}a$ trajectories show a slowing up in the rate of decrease of the eigenvalues as the inner sphere continues to grow. For large R values, corresponding to a high factor of filling of the cavity by the inner dielectric sphere, we again observe a very slow change in the eigenvalues as R grows further towards unity. As R reaches unity, the eigenvalues reach their limiting values of $1/\sqrt{3}$ times their initial values. Clearly, three distinct regimes are evident from the $k_{n1}^{(1)}(R;\varepsilon_r=3)a$ trajectories. These correspond to the presence of a small, intermediate, or large concentric inner dielectric sphere.

The set of TE eigenvalue trajectories, $k_{n1}^{(1)}(R;\varepsilon_r)$, raises two questions. First, why does the eigenvalue remain nearly constant for the higher n values over such a substantial range of R? Second, why does it then change so rapidly with increase in size of the dielectric sphere in the interior? Clearly this behavior will be even more pronounced for even higher values of n. The answers to these questions can be found in an examination of the corresponding spatial distribution of the field components within the dielectrically loaded cavity. This subject will be taken up in

Table 1a. Numerical Values of the TE Eigenvalues $k_{n1}^{(1)}(R;\varepsilon_r = 3)\,a$ for the Spherical Cavity Loaded Internally with a Dielectric Sphere

R=b/a	n=1	n=2	n=3	n=4	n=5
0.05	4.49338	5.76346	6.98793	8.18256	9.35581
0.10	4.49254	5.76343	6.98793	8.18256	9.35581
0.20	4.46441	5.75970	6.98749	8.18251	9.35581
0.30	4.27463	5.69606	6.97091	8.17856	9.35491
0.40	3.83541	5.31497	6.74779	8.07928	9.31677
0.50	3.38457	4.66134	5.97362	7.30555	8.64409
0.60	3.04328	4.10949	5.19990	6.30710	7.42375
0.70	2.81017	3.71817	4.63497	5.56076	6.49309
0.80	2.66886	3.46968	4.26308	5.05552	5.84923
0.90	2.60509	3.34950	4.07203	4.78186	5.48385
0.95	2.59570	3.33051	4.03971	4.73248	5.41376

Table 1b. Numerical Values of the TE Eigenvalues $k_{n2}^{(1)}(R;\varepsilon_r = 3)\,a$ for the Spherical Cavity Loaded Internally with a Dielectric Sphere

R=b/a	n=1	n=2	n=3	n=4	n=5
0.05	7.72486	9.09501	10.41712	11.70491	12.96653
0.10	7.71219	9.09434	10.41709	11.70491	12.96653
0.15	7.61736	9.08326	10.41601	11.70481	12.96652
0.20	7.26888	8.99890	10.40211	11.70273	12.96623
0.25	6.70702	8.61623	10.29108	11.67880	12.96135
0.30	6.25514	7.91051	9.74735	11.46473	12.90377
0.35	6.01878	7.32347	8.88154	10.59698	12.34333
0.40	5.94320	7.01957	8.24572	9.64212	11.17173
0.45	5.93663	6.93209	7.97131	9,08310	10.28875
0.50	5.90684	6.92584	7.92209	8.93074	9.96407
0.55	5.78584	6.87104	7.90644	8.92085	9.93401
0.60	5.58018	6.69032	7.76864	8.82638	9.87332
0.65	5.34200	6.42117	7.48287	8.53538	9.58448
0.70	5.10996	6.13349	7.14235	8.14328	9.14047
0.80	4.72953	5.63503	6.52371	7.40152	8.27184
0.90	4.50832	5.32483	6.11855	6.89681	7.66396
0.95	4.46713	5.26212	6.03067	6.78049	7.51630

Table 1c. Numerical Values of the TE Eigenvalues $k_{n3}^{(1)}(R;\varepsilon_r = 3)\,a$ for the Spherical Cavity Loaded Internally with a Dielectric Sphere

R=b/a	n=1	n=2	n=3	n=4
0.05	10.90192	12.32290	13.69802	15.0397
0.10	10.82516	12.31732	13.69769	15.03965
0.15	10.26354	12.21370	13.68510	15.03826
0.20	9.43374	11.46032	13.48429	15.00451
0.25	9.15424	10.48578	12.33261	14.44791
0.30	9.13449	10.21737	11.43087	12.94811
0.35	9.01077	10.20009	11.29319	12.41148
0.40	8.61039	9.99714	11.24205	12.38336
0.45	8.14505	9.49576	10.84570	12.14966
0.50	7.82181	8.99353	10.23540	11.50694
0.55	7.70064	8.68985	9.75206	10.87014
0.60	7.69066	8.61488	9.54641	10.50728
0.65	7.60805	8.59006	9.52819	10.44599
0.70	7.38682	8.40977	9.39927	10.36375
0.75	7.10426	8.10593	9.08477	10.04735
0.80	6.82694	7.78215	8.71681	9.63658
0.90	6.41015	7.26823	8.10480	8.92541
0.95	6.31397	7.14057	7.94314	8.72761
0.99	6.29566	7.11489	7.90888	8.68359

Table 1d. Numerical Values of the TE Eigenvalues $k_{n4}^{(1)}(R;\varepsilon_r = 3)\,a$ for the Spherical Cavity Loaded Internally with a Dielectric Sphere

R=b/a	n=1	n=2	n=3
0.05	14.05819	15.51439	16.92362
0.10	13.74719	15.48531	16.92143
0.15	12.59739	14.86023	16.82536
0.20	12.30726	13.57811	15.49753
0.25	12.23821	13.41956	14.58338
0.30	11.66648	13.23988	14.53831
0.35	11.04040	12.48532	14.04369
0.40	10.87308	11.92911	13.18152
0.45	10.82319	11.85081	12.84483
0.50	10.46800	11.69153	12.80069
0.55	9.97096	11.19225	12.39661
0.60	9.60650	10.68693	11.80285
0.65	9.49097	10.41708	11.38032
0.70	9.46447	10.38642	11.28030
0.75	9.26066	10.24452	11.19505
0.80	8.93346	9.90793	10.85978
0.90	8.32657	9.21190	10.07710
0.95	8.15809	9.00530	9.83100
0.99	8.12147	8.95783	9.77147

detail in a forthcoming report giving the fields in the cavity for the TE eigenmodes.

Continuing, we show in figure 3 the results obtained for the eigenvalues $k_{n2}^{(1)}(R;\varepsilon_r = 3)\,a$ from equation (32). Table 1(b) contains numerical values for these eigenvalues. Examination of figure 3 reveals that for a given index value n the initial behavior of the eigenvalues is similar to that of figure 2. That is, at first, as R increases, the eigenvalue only very slowly decreases from the initial value when the inner sphere is not present. This slow variation persists over a larger range of size of the inner sphere as the index n increases. Now, however, for each value of n the $k_{n2}^{(1)}a$ trajectory begins to change rapidly with R noticeably earlier than the $k_{n1}^{(1)}a$ trajectory. For the higher values the $k_{n2}^{(1)}a$ trajectories show a faster variation with increasing R.

A new feature can be seen in the curves in figure 3. After the initial knee in the curve, the eigenvalues again display a very slow decrease in value with increasing inner sphere radius. As n increases, this behavior persists for a decreasing range of R, after starting at a larger value of R for higher n. Again, as R increases further, we observe another rapid decrease in $k_{n2}^{(1)}a$, which is more pronounced as n increases. This behavior gradually tapers to a slow decrease in eigenvalue with R from about $R = 0.8$, thus enabling the trajectories to go over to the known limiting values. Note that figure 3 clearly indicates two knees in each of the $k_{n2}^{(1)}a$ eigenvalue trajectories. Roughly speaking, we can still distinguish between the three regimes—small, intermediate, and large inner dielectric spheres. This method of classification now seems less clear in some ways than earlier.

Figure 4 shows the eigenvalue trajectories for the modes $k_{n3}^{(1)}(R;\varepsilon_r = 3)\,a$ for $n = 1,2,3,4$. The corresponding numerical values of these eigenvalues are given in table 1(c). Upon examination of figure 4 we observe behavior very similar to what we previously described for the $k_{n2}^{(1)}a$ in figure 3. The new feature present in figure 4 is another knee in each of the trajectories as an addition to a behavior similar to figure 3. Once again we indicate that we shall be able to better understand the structure of the trajectories for the $k_{n3}^{(1)}a$ eigenvalues only by resorting to an investigation of the distribution of the field components for each eigenmode. This will be done in a subsequent report.

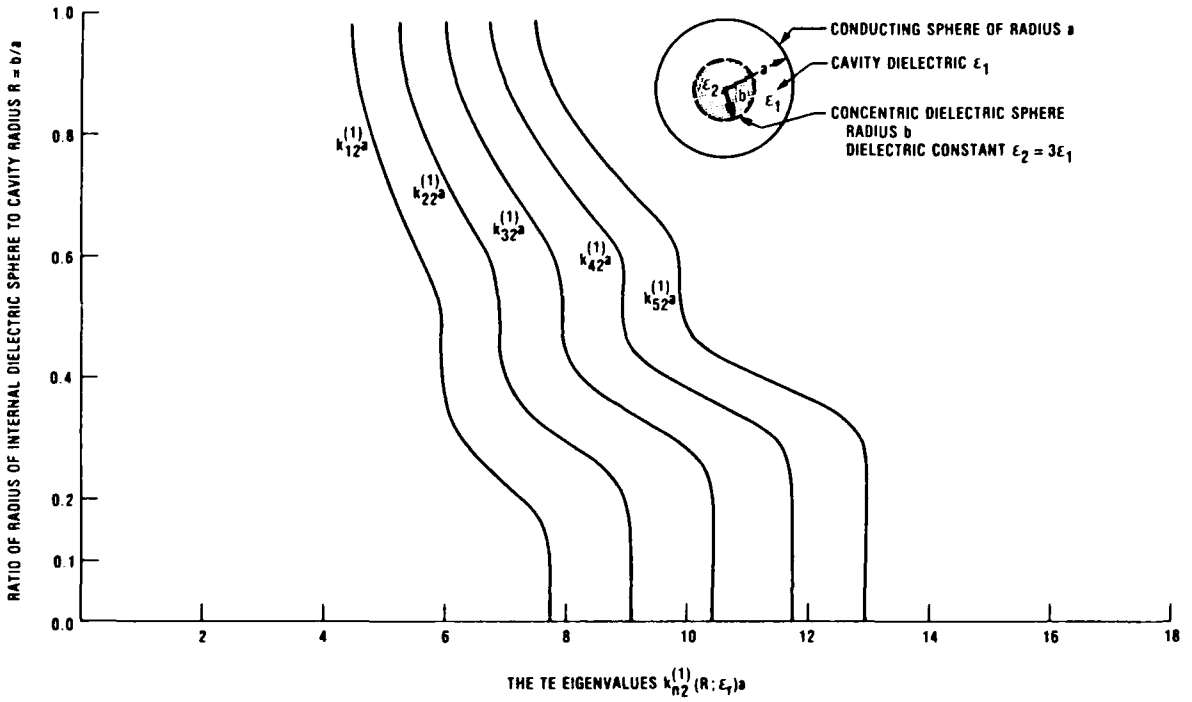

Figure 3. TE eigenvalues $k_{n2}^{(1)}(R;\varepsilon_r = 3)\,a$ for the spherical cavity of radius a filled with dielectric ε_1 internally loaded with a concentric dielectric sphere of radius b and strength $\varepsilon_2 = 3\varepsilon_1$.

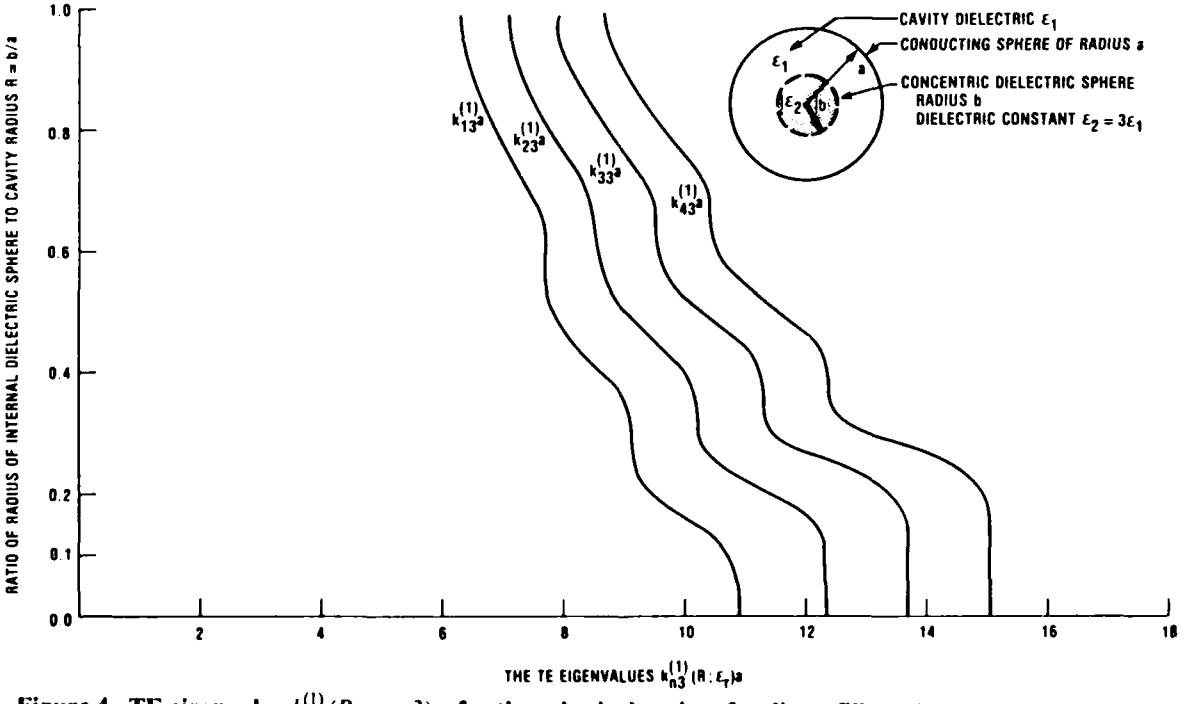

Figure 4. TE eigenvalue $k_{n3}^{(1)}(R;\varepsilon_r = 3)\,a$ for the spherical cavity of radius a filled with dielectric ε_1 internally loaded with a concentric dielectric sphere of radius b and strength $\varepsilon_2 = 3\varepsilon_1$.

In figure 5 we present the final set of TE eigenvalues, for $k_{n4}^{(1)}(R;\varepsilon_r)\,a$, to be included in this report. Table 1(d) gives the corresponding numerical values for these eigenvalues. Again we can readily note from examination of figure 5 that the trajectories for the $k_{n4}^{(1)}\,a$ demonstrate the same kind of behavior with R, the size of the inner sphere, as the previous set. Again that behavior is emphasized more strongly. Once again the predominantly new feature appearing is the occurrence of an additional knee in the curves.

At this stage of the report, we can readily conclude that a further increase in the index p beyond 4 will result in the same behavior with R that we have already seen occurring. Indeed we can, with reasonable accuracy, predict from the data in figures 2 through 4 the trajectories of the higher order mode eigenvalues. With the aid of the tables we can extrapolate to find their numerical values with some degree of accuracy.

3.3 The TE Eigenvalues for $\varepsilon_r = 10.00$

We consider next the results of concentrically loading the conducting spherical cavity with a dielectric sphere of large relative dielectric

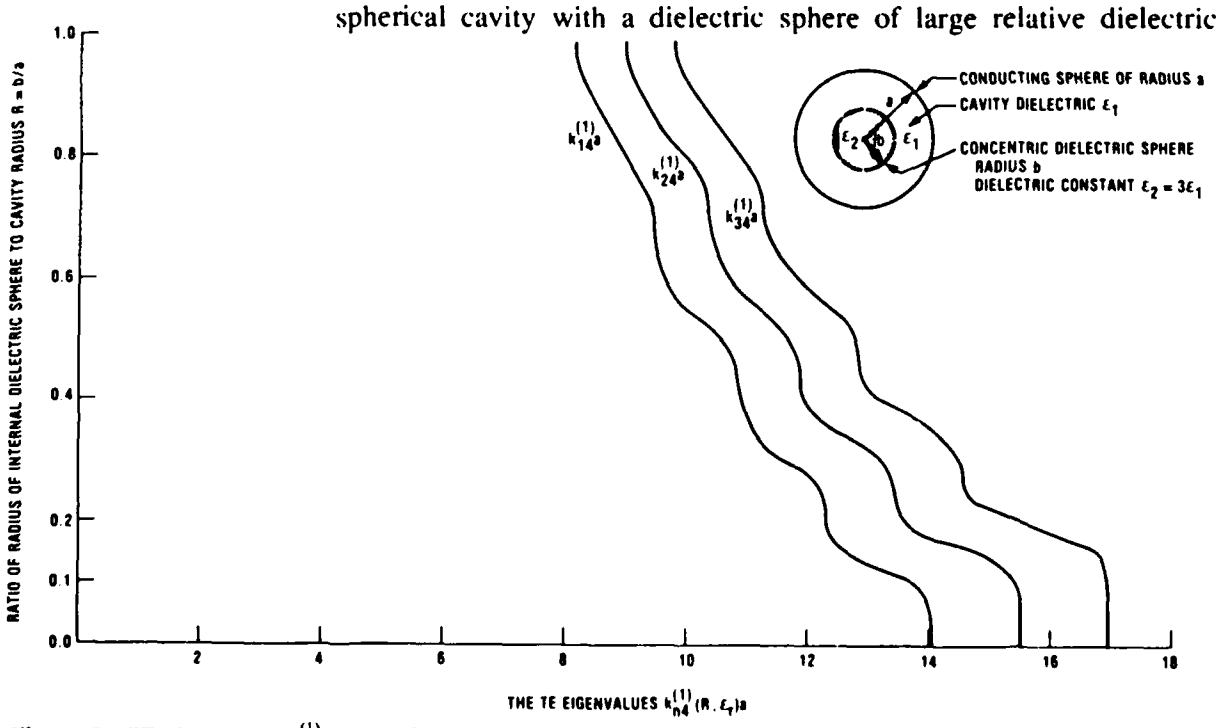

Figure 5. TE eigenvalue $k_{n4}^{(1)}(R;\varepsilon_r = 3)\,a$ for the spherical cavity of radius a filled with dielectric ε_1 internally loaded with a concentric dielectric sphere of radius b and strength $\varepsilon_2 = 3\varepsilon_1$.

constant, namely, $\varepsilon_2 = 10.00\ \varepsilon_1$. Figure 6 shows results calculated from equation (32) for $p = 1$ and n ranging from 1 to 6. Table 2(a) contains numerical values for the $k_{n1}^{(1)}(R;\varepsilon_r = 10)\,a$ eigenvalues plotted in figure 6. Inspection of figure 6 immediately reveals that the trajectories of the eigenvalues behave much like those shown in figure 2 for $p = 1$ and $\varepsilon_2 = 3\varepsilon_1$. Each trajectory still starts, for $R << 1$, at the same value, decreases slowly at first with increasing R, then at an accelerated rate with further increase in R, and gradually slows its rate of decrease as R approaches unity. In this limit the value of the eigenvalues $k_{n1}^{(1)}(R = 1;\ \varepsilon_r = 10)\,a$ are given explicitly by the quantities

$$\sqrt{1/\varepsilon_r}\ k_n^{(1)}(R = 0;\ \varepsilon_r)\,a\ = 1/\sqrt{10}\ k_n^{(1)}(R = 0;\ \varepsilon_r = 10)\,a.$$

We thus observe that for $\varepsilon_r = 10$ the trajectories start for $R << 1$ at the same values as for $\varepsilon_r = 3$, but decrease to values for $R \approx 1$ that are considerably lower than for $\varepsilon_r = 3$. The net result is that, compared to the $\varepsilon_r = 3$ case, for $\varepsilon_r = 10$ the trajectories also display a very slow decrease for increasing R initially. This behavior persists for a larger range of R as n increases. A clearly defined knee is immediately evident in each eigenvalue trajectory, but appears earlier with R for $\varepsilon_r = 10$ compared to what

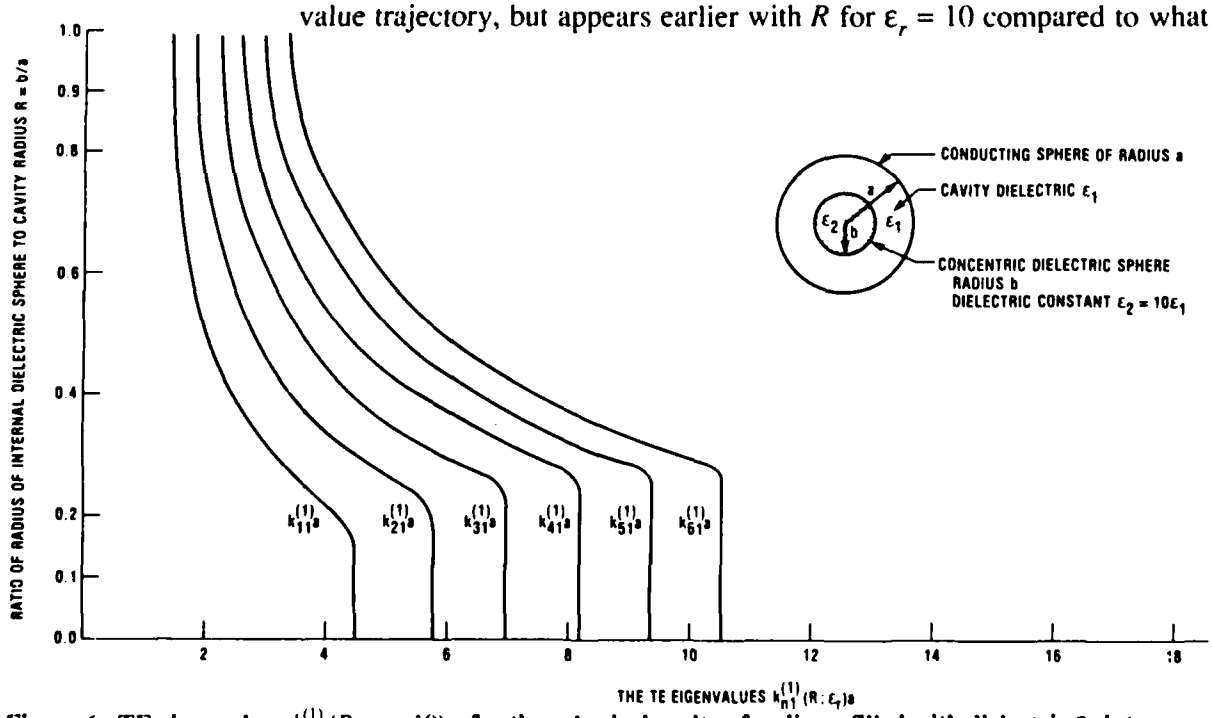

Figure 6. TE eigenvalues $k_{n1}^{(1)}(R;\varepsilon_r = 10)\,a$ for the spherical cavity of radius a filled with dielectric ε_1 internally loaded with a concentric dielectric sphere of radius b and strength $\varepsilon_r = 10\varepsilon_1$.

is observed in figure 2 for $\varepsilon_r = 3$. The $k_{n1}^{(1)}(R; \varepsilon_r = 10)\,a$ values then exhibit a rapid decrease over a much larger range in R than is seen in figure 2 for $\varepsilon_r = 3$. This range is larger the larger the index n is. We note in figure 6 that this rate of decrease in $k_{n1}^{(1)}\,a$ gradually slows as R increases. Finally, as R increases further, the rate at which the eigenvalues decrease becomes nearly imperceptible. This latter behavior can be seen to persist for a shorter range of R as the index n increases. Again we can discern three quite distinct regimes in the eigenvalue trajectories of figure 6, namely those of a small inner sphere, an intermediate size inner sphere, and a large size inner sphere.

Results obtained from equation (32) for $p = 2$ are displayed in figure 7 for $n = 1$ to $n = 5$. Again we note that these eigenvalue trajectories start at $R = 0$ exactly where the corresponding trajectories for $\varepsilon_r = 3$ start, but they end, at $R = 1$, at values $\sqrt{3}/\sqrt{10}$ times those for $\varepsilon_r = 3$. There is a considerable amount of similarity in both sets. Examination of table 2(b), which gives numerical values for the $k_{n2}^{(1)}(R;\varepsilon_r = 10)\,a$, will also show the behavior of these eigenvalue trajectories.

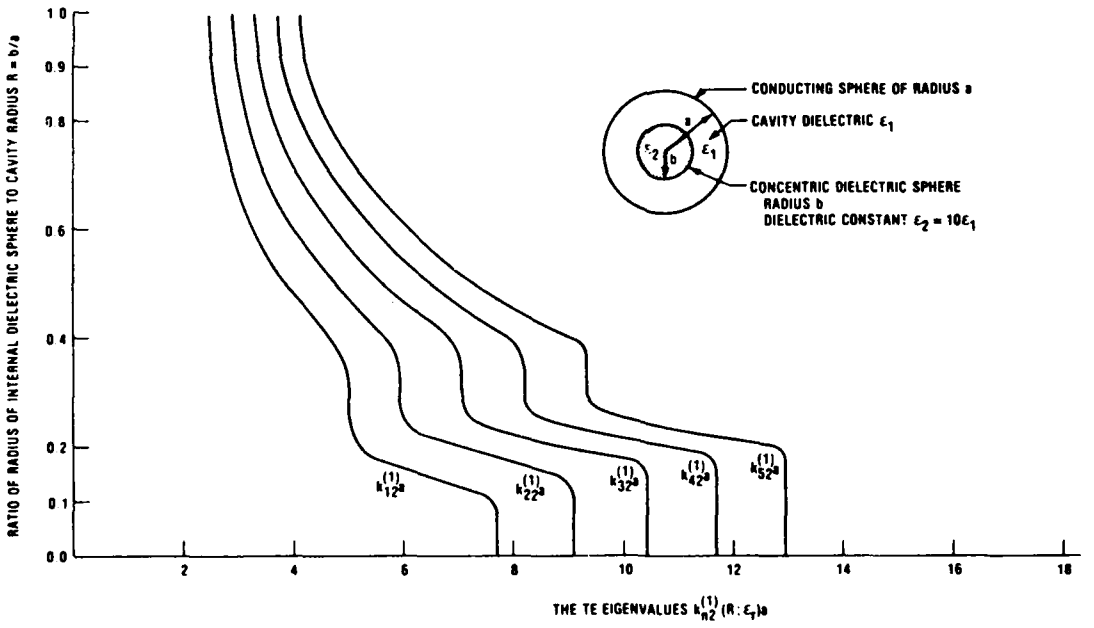

Figure 7. TE eigenvalues $k_{n2}^{(1)}(R;\varepsilon_r = 10)\,a$ for the spherical cavity of radius a filled with dielectric ε_1 internally loaded with a concentric dielectric sphere of radius b and strength $\varepsilon_2 = 10\varepsilon_1$.

Table 2a. Numerical Values of the TE Eigenvalues $k_{n1}^{(1)}(R;\varepsilon_r = 10)\,a$ for the Spherical Cavity Loaded Internally with a Dielectric Sphere

R=b/a	n=1	n=2	n=3	n=4	n=5	n=6
0.05	4.49328	5.76346	6.98793	8.18256	9.35581	10.51284
0.10	4.48885	5.76331	6.98793	8.18256	9.35581	10.51284
0.15	4.44690	5.76035	6.98773	8.18255	9.35581	10.51284
0.20	4.19332	5.72477	6.98410	8.18218	9.35577	10.51283
0.22	3.98261	5.65198	6.97555	8.18118	9.35565	10.51282
0.25	3.63193	5.30554	6.87027	8.16964	9.35428	10.51264
0.27	3.41190	4.98023	6.51613	7.98705	9.33367	10.51108
0.30	3.11966	4.52433	5.90075	7.22583	8.50653	9.75569
0.40	2.42757	3.44379	4.44930	5.42871	6.38311	7.31778
0.50	2.00997	2.79284	3.57706	4.35019	5.10919	5.85518
0.60	1.74458	2.37268	3.00662	3.63843	4.26405	4.88225
0.70	1.57502	2.09576	2.62051	3.14684	3.67224	4.19504
0.80	1.47448	1.92305	2.36881	2.81429	3.25991	3.70540
0.90	1.42884	1.83849	2.23677	2.62865	3.01669	3.40233
0.95	1.42199	1.82475	2.21361	2.59360	2.96743	3.33677
0.99	1.42095	1.82258	2.20981	2.58760	2.95864	3.32456

Table 2b. Numerical Values of the TE Eigenvalues $k_{n2}^{(1)}(R;\varepsilon_r = 10)\,a$ for the Spherical Cavity Loaded Internally with a Dielectric Sphere

R=b/a	n=1	n=2	n=3	n=4	n=5
0.01	7.72525	9.09501	10.41712	11.70491	12.96653
0.05	7.72328	9.09499	10.41712	11.70491	12.96653
0.10	7.60820	9.09059	10.41694	11.70490	12.96653
0.12	7.26468	9.07331	10.41605	11.70485	12.96653
0.15	6.28435	8.76617	10.40257	11.70402	12.96647
0.17	5.73488	7.97978	10.22983	11.69839	12.96609
0.19	5.35232	7.22448	9.32264	11.38203	12.96086
0.20	5.22407	6.90371	8.87423	10.83897	12.74741
0.22	5.07038	6.39234	8.09527	9.86524	11.60250
0.25	4.98980	6.03912	7.25222	8.70091	10.21430
0.27	4.97848	5.98749	7.09258	8.24502	9.47997
0.30	4.97672	5.97476	7.06823	8.20943	9.36395
0.35	4.90201	5.94765	7.05511	8.20232	9.36035
0.37	4.81017	5.88405	7.00951	8.17039	9.34000

Table 2b. (cont'd) Numerical Values of the TE Eigenvalues $k_{n2}^{(1)}(R;\varepsilon_r = 10)\,a$ for the Spherical Cavity Loaded Internally with a Dielectric Sphere

R=b/a	n=1	n=2	n=3	n=4	n=5
0.40	4.61003	5.68039	6.79150	7.92259	9.03553
0.50	3.86827	4.73848	5.60393	6.45592	7.28853
0.60	3.30421	4.01465	4.71619	5.40802	6.08893
0.70	2.90437	3.50044	4.08755	4.66730	5.24019
0.80	2.63149	3.14215	3.64355	4.13843	4.62817
0.90	2.47744	2.92854	3.36759	3.79849	4.22351
0.95	2.44803	2.88419	3.30604	3.71778	4.12201
0.99	2.44298	2.87617	3.29429	3.70157	4.10058

Table 2c. Numerical Values of the TE Eigenvalues $k_{n3}^{(1)}(R;\varepsilon_r = 10)\,a$ for the Spherical Cavity Loaded Internally with a Dielectric Sphere

R=b/a	n=1	n=2	n=3	n=4	n=5
0.01	10.90412	12.32294	13.69802	15.03966	16.35471
0.05	10.89124	12.32272	13.69802	15.03966	16.35471
0.07	10.79431	12.32009	13.69795	15.03966	16.35471
0.10	9.44433	12.24105	13.69526	15.03955	16.35470
0.12	8.52775	11.29151	13.66549	15.03840	16.35464
0.14	8.24860	9.93125	12.65103	15.01216	16.35385
0.15	8.21188	9.52894	11.84970	14.44290	16.35000
0.17	8.19600	9.31562	10.66391	12.77442	15.01515
0.19	8.19058	9.29530	10.49781	11.75659	13.44347
0.20	8.17245	9.29504	10.49196	11.73292	12.98646
0.22	8.04956	9.28069	10.49068	11.72901	12.97369
0.25	7.55990	9.04977	10.42793	11.71673	12.97161
0.27	7.15361	8.63818	10.13765	11.59456	12.94049
0.30	6.60346	7.93799	9.32125	10.72313	12.11663
0.35	5.98979	7.02022	8.13281	9.27935	10.43389
0.39	5.81796	6.65264	7.57634	8.54937	9.55434
0.40	5.80722	6.61699	7.51797	8.48018	9.49624
0.45	5.78991	6.58340	7.46212	8.42822	9.46678
0.48	5.70555	6.53506	7.42170	8.37745	9.38868
0.50	5.59773	6.43978	7.32087	8.24660	9.19462
0.60	4.87694	5.61702	6.35145	7.07965	7.79857
0.70	4.26651	4.89482	5.51222	6.12089	6.72171

Table 2c. (cont'd) Numerical Values of the TE Eigenvalues $k_{n3}^{(1)}(R;\varepsilon_r = 10)\,a$ for the Spherical Cavity Loaded Internally with a Dielectric Sphere

R=b/a	n=1	n=2	n=3	n=4	n=5
0.80	3.81758	4.35949	4.89019	5.41234	5.92759
0.90	3.52889	4.00412	4.46778	4.92280	5.37109
0.95	3.46157	3.91555	4.35652	4.78772	5.21127
0.99	3.44831	3.89703	4.33194	4.75628	5.17222

Table 2d. Numerical Values of the TE Eigenvalues $k_{n4}^{(1)}(R;\varepsilon_r = 10)\,a$ for the Spherical Cavity Loaded Internally with a Dielectric Sphere

R=b/a	n=1	n=2	n=3	n=4
0.01	14.06618	15.51460	16.92362	18.30126
0.05	14.00421	15.51336	16.92360	18.30126
0.10	11.43270	13.72226	16.86368	18.29972
0.12	11.37161	12.58012	14.83143	18.01644
0.14	11.36031	12.52015	13.78803	15.53453
0.15	11.31392	12.51957	13.77198	15.07830
0.18	10.59372	12.36687	13.75764	15.06262
0.20	9.86784	11.72783	13.54654	15.03454
0.22	9.32661	10.90445	12.69866	14.54095
0.25	9.02345	10.06308	11.41212	12.96304
0.27	9.00406	9.89851	10.96020	12.18163
0.29	8.99128	9.87796	10.86449	11.94701
0.30	8.95668	9.87656	10.85977	11.93240
0.34	8.47016	9.61876	10.74045	11.87308
0.35	8.29660	9.45505	10.60593	11.77077
0.40	7.47526	8.51649	9.56963	10.62991
0.45	6.90635	7.76619	8.66383	9.57430
0.49	6.73440	7.44741	8.22620	9.04498
0.50	6.72620	7.41735	8.17691	8.98707
0.55	6.68379	7.38512	8.12963	8.93470
0.57	6.59710	7.32354	8.07623	8.87086
0.60	6.39671	7.12858	7.86922	8.62393
0.70	5.63633	6.28050	6.91513	7.54230
0.80	5.02010	5.57962	6.12794	6.66742

Table 2d. (cont'd) Numerical Values of the TE Eigenvalues $k_{n4}^{(1)}(R;\varepsilon_r = 10)\,a$ for the Spherical Cavity Loaded Internally with a Dielectric Sphere

R=b/a	n=1	n=2	n=3	n=4
0.90	4.59071	5.08176	5.56186	6.03332
0.95	4.47463	4.94037	5.39444	5.83934
0.99	4.44838	4.90650	5.35217	5.78794

Table 2e. Numerical Values of the TE Eigenvalues $k_{n5}^{(1)}(R;\varepsilon_r = 10)\,a$ for the Spherical Cavity Loaded Internally with a Dielectric Sphere

R=b/a	n=1	R=b/a	n=1
0.01	17.22072	0.33	9.92883
0.03	17.21129	0.35	9.91307
0.04	17.16672	0.37	9.88331
0.05	16.90815	0.40	9.59286
0.07	15.75413	0.45	8.78128
0.08	14.57621	0.50	8.08606
0.10	14.53178	0.52	7.88497
0.12	14.44114	0.54	7.75027
0.15	13.10915	0.55	7.71145
0.17	12.35053	0.60	7.66990
0.18	12.22112	0.62	7.60734
0.20	12.17430	0.65	7.41396
0.22	12.13745	0.70	6.99874
0.23	12.03661	0.80	6.23063
0.25	11.56566	0.90	5.66142
0.30	10.21668	0.95	5.49014
0.32	9.97392	0.99	5.44616

For $\varepsilon_r = 10$, we can plainly see the presence of a second knee in the curves. Now, however, we find all the characteristics are strongly accentuated. We see in figure 7 a very slow decrease in $k_{n2}^{(1)}(R; \varepsilon_r = 10)\,a$ as R increases from zero. This behavior persists for a larger range in R as n increases. Now the first knee appears for $\varepsilon_r = 10$, earlier than for $\varepsilon_r = 3$. Thus, for example, the knee appears for $k_{52}^{(1)}(R; \varepsilon_r = 10)\,a$ at $R \approx 0.2$, whereas for $k_{52}^{(1)}(R; \varepsilon_r = 3)\,a$, it is at $R \cong 0.3$. The region immediately following the first knee shows a much more rapid decrease as R increases for $\varepsilon_r = 10$ than for $\varepsilon_r = 3$, taking place over a smaller range of R. As n increases, this behavior is accentuated further. As we can see in figure 7, this is followed by a region of quite slow decrease in the eigenvalue as R increases and then the appearance of a second knee which is sharper for $\varepsilon_r = 10$ than for $\varepsilon_r = 3$. Furthermore, this second knee occurs at lower R values for the larger ε_r. Figure 7 shows that the second knee appears at slightly higher values of R for larger values of n. After rounding the second knee the eigenvalue decreases rapidly at first and then ever more slowly thereafter as R increases. The larger the value of n, the more pronounced this behavior is. Finally, as R approaches the limit unity the trajectories continue to decrease as R increases, but very slowly. The range of this latter behavior is smaller, but the rate of decrease is slower with increasing value of the index n.

The existence of three regimes is again quite evident in figure 7. For the initial range of R for which the eigenvalues $k_{n2}^{(1)}\,a$ change very slowly as R increases, we have a small interior sphere. For the upper range of R for which the eigenvalues again change slowly with R, we have a large dielectric sphere loading the cavity. The remainder of the range of R from the onset of the first knee then corresponds to an intermediate interior dielectric sphere. For the intermediate sphere, as R increases, a variety of behaviorial aspects are displayed by the system eigenvalues.

As expected, going from $p = 2$ to $p = 3$ causes a third knee to appear in the eigenvalue trajectories for $\varepsilon_r = 10$, just as we saw happen for $\varepsilon_r = 3$. Figure 8 shows $k_{n3}^{(1)}(R; \varepsilon_r = 10)\,a$ for $n = 1$ to $n = 5$. Table 2(c) gives numerical values for these eigenvalues. Again we observe a sharpening up of the characteristics of the trajectories. Starting at the empty cavity resonances for $R = 0$, we note that as R increases the $k_{n3}^{(1)}(R; \varepsilon_r = 10)\,a$ values decrease at a rate slower than for the $k_{n2}^{(1)}(R; \varepsilon_r = 10)\,a$ values, but for a

shorter range of R now. The first knee occurs earlier for $p = 3$ than for $p = 2$ and is followed by a sharper turn and a shorter region in which $k_{n3}^{(1)} a$ changes more rapidly with R than we saw for $k_{n2}^{(1)} a$. The higher the value of the index n, the more this behavior is emphasized. Figure 8 shows a second knee followed by a range in R over which a rapid decrease in $k_{n3}^{(1)} a$ occurs. This region ends in the third knee, after which we see in the figure the usual behavior as R increases. Notice that the trajectories in figure 8 are flatter in the region between the first and second knees than in the region between the second and third knees. The higher the value of n, the more emphasized this is. Again there are three distinguishable regions, with the intermediate regime displaying richer variation with R than we saw in figure 7 for $p = 2$.

In going from $p = 3$ to $p = 4$, we observe another knee and shoulder impressed on the trajectories. The same pattern of changes in the trajectories is evident in figure 9, which contains the eigenvalues $k_{n4}^{(1)}(R; \varepsilon_r = 10)\, a$ with the sharpening of the features over the $p = 3$ case for $\varepsilon_r = 10$ and the $p = 4$ case for $\varepsilon_r = 3$. Table 2(d) contains numerical values for the $k_{n4}^{(1)} a$ of figure 9.

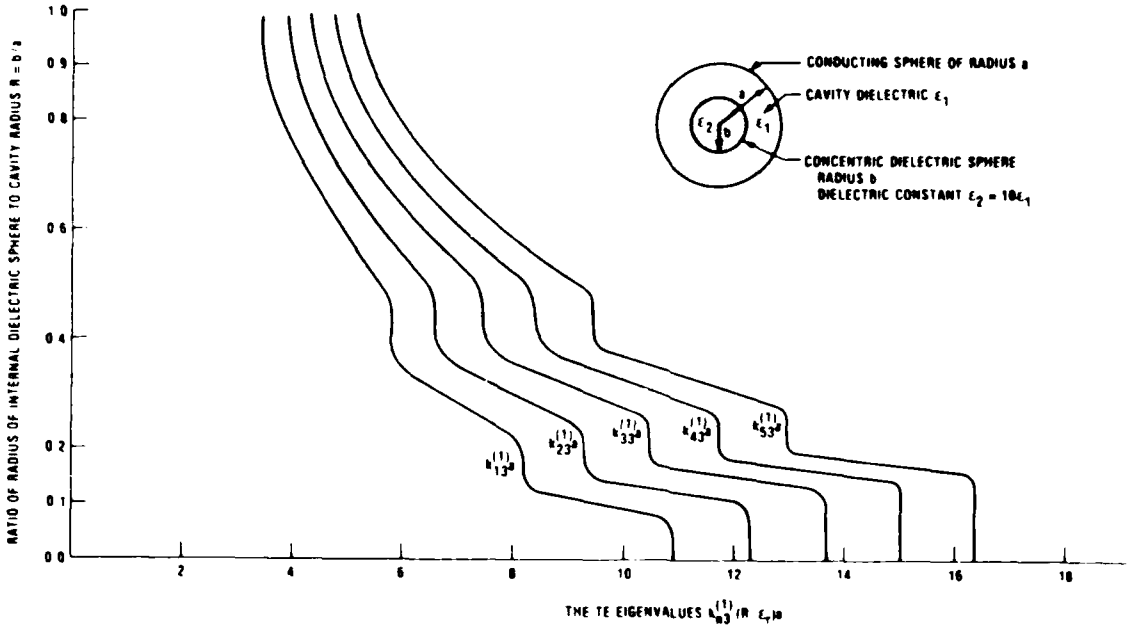

Figure 8. TE eigenvalues $k_{n3}^{(1)}(R; \varepsilon_r = 10)\, a$ for the spherical cavity of radius a filled with dielectric ε_1 internally loaded with a concentric dielectric sphere of radius b and strength $\varepsilon_2 = 10\varepsilon_1$.

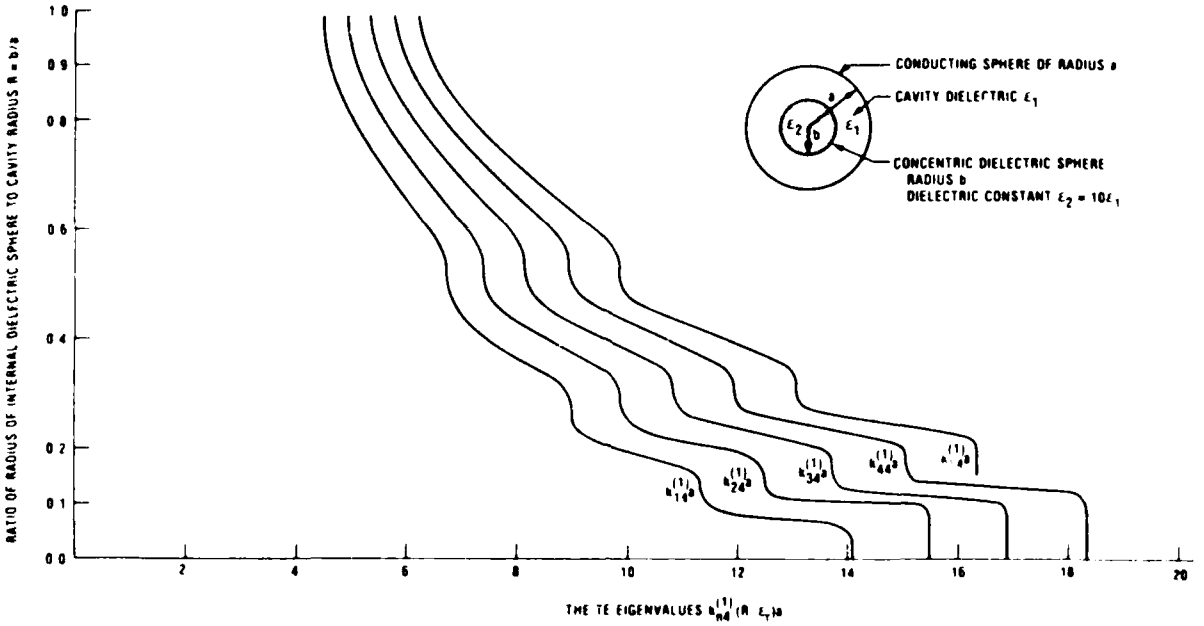

Figure 9. TE eigenvalues $k_{n,1}^{(1)}(R\,\varepsilon_r = 10)\,a$ for the spherical cavity of radius a filled with dielectric ε_1 internally loaded with a concentric dielectric sphere of radius b and strength $\varepsilon_2 = 10\varepsilon_1$.

The pattern of changes induced as the index p increases by unity is now evident. Thus, in figure 10 we show only the $n = 1$, $p = 5$ trajectory with an additional knee and shoulder and further emphasis of the detailed behavior as R increases. Table 2(e) gives numerical values for the $k_{1,5}^{(1)}(R; \varepsilon_r = 10)$ a trajectory shown in figure 9.

It should be quite evident what one would expect the trajectories for higher order eigenvalues to look like after examining the given sets in detail. It is a relatively simple exercise to locate with good accuracy the limiting values for R ≈ 1, for $n = 1$ and p greater than 5. Thus, for $p = 5 + q$, say, $k_{1,5+q}^{(1)}(R; \varepsilon_r = 10)\,a \cong (5 + q) + 0.45$. This result can be deduced from inspection of figures 6 through 10. Similar predictions for the other values of n can be made in the same way, which means we can find these eigenvalues (approximately) without directly resorting to solving equation (32).

To summarize, some very intriguing characteristics are exhibited by the eigenvalue trajectories. Nevertheless, we shall have to defer the explanation of these to a subsequent report giving the detailed behavior of the corresponding spatial distribution of the field components in the

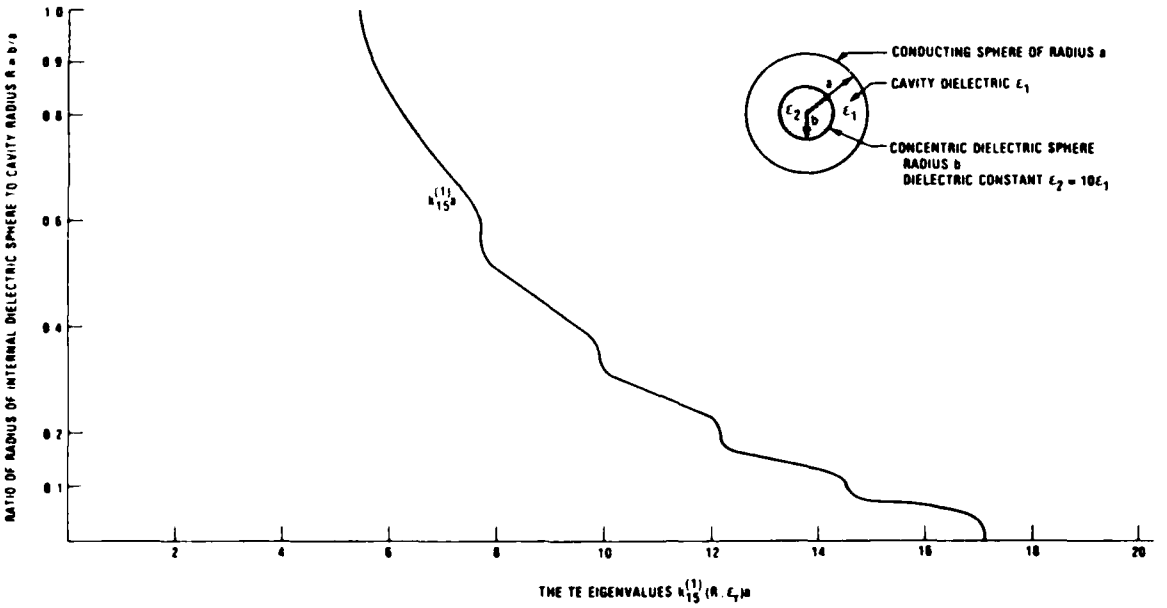

Figure 10. TE eigenvalues $k_{15}^{(1)}(R;\epsilon_r = 10)\,a$ for the spherical cavity of radius a filled with dielectric ϵ_1 internally loaded with a concentric dielectric sphere of radius b and strength $\epsilon_2 = 10\epsilon_1$.

dielectric loaded cavity. We shall have to be content here with merely noting the rich variety of interesting characteristics displayed by the eigenvalue trajectories.

3.4 The TE Eigenvalues for $\epsilon_r = 1/3$

We have thus far examined effects on the eigenvalues induced by loading the interior of the cavity with a dielectric sphere whose dielectric constant is larger than that of the cavity, i.e., $\epsilon_r = \epsilon_2/\epsilon_1 > 1$. For that situation we considered representative values of ϵ_r that covered a substantial range. In an attempt at completeness, we next consider effects on eigenvalues of the spherical cavity that result when the cavity is concentrically loaded with a dielectric sphere whose relative dielectric constant is less than unity. Many of the essential characteristics can be seen in the results for $\epsilon_r = \epsilon_2/\epsilon_1 = 1/3$. Therefore, we limit ourselves to considering only this one case. Now, when $R = 0$, the eigenvalues $\gamma_1 a$ are once again the same as for the empty spherical cavity. But, in the other limit, as R approaches unity, the eigenvalues are multiplied, rather than divided, by $\sqrt{3}$, since $\sqrt{\epsilon_r} = \sqrt{1/3}$.

In the previous two cases of dielectric loading, we solved for the eigenvalue, $\gamma_1 a$, knowing that we would be able to find the corresponding wavenumber in the denser dielectric region by means of the equation

$$\gamma_2 = \sqrt{\frac{\varepsilon_2}{\varepsilon_1}}\ \gamma_1 \ .$$

If we wish to be consistent in defining our eigenvalue as the one in the region of smaller dielectric constant, we should be solving for $\gamma_2 a$, rather than $\gamma_1 a$. This formulation is usually desirable when the medium of lesser dielectric strength is air, for example. But $\gamma_2 a$ is equivalent to $\gamma_1 a$ multiplied by the square root of the relative dielectric constant. Please note that it is this "normalized" $\gamma_1 a$ or, equivalently, ka, that is listed in the tables and plotted in the figures which relate to this section. The "true" values of ka are achieved by multiplying the tabled values by $\sqrt{1/3}$.

Some very interesting behavior manifests itself immediately in figure 11, which displays the eigenvalue trajectories $k_{n1}^{(1)}(R; \varepsilon_r = 1/3)\, a$ for $p = 1$ and $n = 1$ to $n = 6$. We clearly observe that there is a considerable range over R for which the eigenvalues increase with R, but at an astonishingly slow rate. This behavior clearly becomes even more pronounced as n increases. Thus, the total change for $n = 1$ as R goes from zero to 0.3 is only about 0.1, whereas, for $n = 6$ as R goes from 0 to 0.55, the same total change is incurred. That is, for $n = 6$, about twice the range in R results in the same total change. Considered from the point of view of the filling factor of the cavity, it is quite remarkable to note that substantial filling of the cavity by the dielectric load hardly affects the eigenvalues $k_{n1}^{(1)} a$, and this effect persists to larger R as n increases. Thus, the higher modes $n > 1$ appear to change even more reluctantly as the load increases in size.

Following this range of slow variation the eigenvalue $k_{11}^{(1)} a$ increases more rapidly with R at first and then exhibits a moderately slow rate of increase with R. Then for large R at about $R = 0.9$, the eigenvalue $k_{11}^{(1)} a$ again resumes a very slow rate of increase as R increases to unity where the load has expanded to homogeneously fill the cavity. These characteristics are more enhanced as n increases. Indeed, as n increases a larger range of variation in $k_{n1}^{(1)} a$ can be seen in the intermediate region and a

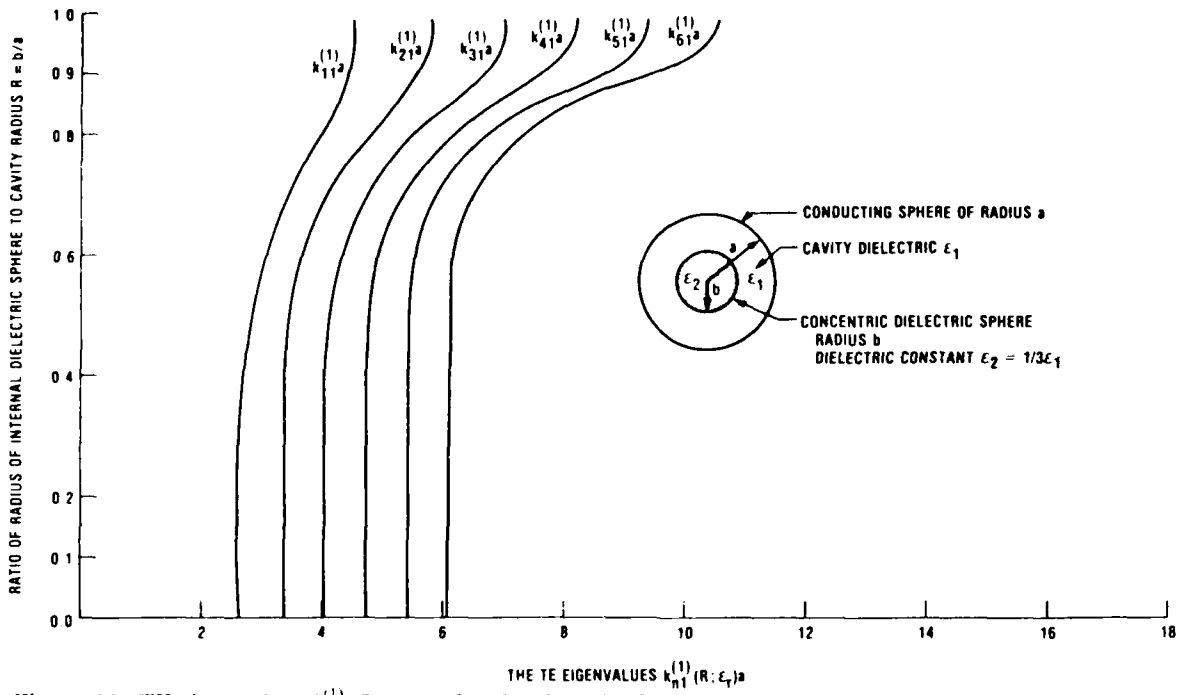

Figure 11. TE eigenvalues $k_{n1}^{(1)}(R;\varepsilon_r = 1/3)\,a$ for the spherical cavity of radius a filled with dielectric ε_1 internally loaded with a concentric dielectric sphere of radius b and strength $\varepsilon_2 = 1/3\varepsilon_1$.

shorter range in the final slowly varying region as R approaches unity. Table 3(a) contains numerical values for the $k_{n1}^{(1)}a$ eigenvalues of figure 11.

Before continuing on to $p = 2$, let us compare the eigenvalue trajectories for $p = 1$, $\varepsilon_r = 3$, and $p = 1$, $\varepsilon_r = 1/3$; i.e., the curves in figures 2 and 11. Clearly they are all monotonic. For $p = 1$ and fixed n the trajectories for $\varepsilon_r = 1/3$ display increasing values of the eigenvalues with increasing R, whereas those for $\varepsilon_r = 3$ show decreasing values as R increases. Both sets suggest three size regimes for the inner dielectric sphere—small, intermediate, and large. The small inner sphere regime appears to cover a larger range of sizes for $\varepsilon_r = 1/3$ than for $\varepsilon_r = 3$. The opposite is true for the large inner sphere regime. The intermediate regimes are about the same. Now let us proceed to $p = 2$ for $\varepsilon_r = 1/3$.

Figure 12 shows the $p = 2$ eigenvalue trajectories for $n = 1$ to $n = 5$ and table 3(b) contains numerical values for the corresponding eigenvalues $k_{n1}^{(1)}(R;\varepsilon_r = 1/3)\,a$. For $R = 0$, they start out where expected, then show a very slow increase with increasing R at first. This behavior persists for a smaller range of R than we saw in figure 11 for $p = 1$ for each value n.

Table 3a. Numerical Values of the TE Eigenvalues $k_{n1}^{(1)}(R;\varepsilon_r = 1/3)\,a$ for the Spherical Cavity Loaded Internally with a Dielectric Sphere

R=b/a	n=1	n=2	n=3	n=4	n=5	n=6
0.05	2.59428	3.32753	4.03448	4.72420	5.40158	6.06959
0.10	2.59443	3.32754	4.03448	4.72420	5.40158	6.06959
0.20	2.59872	3.32813	4.03456	4.72421	5.40158	6.06959
0.30	2.62210	3.33555	4.03660	4.72473	5.40170	6.06962
0.40	2.68788	3.37083	4.05340	4.73207	5.40471	6.07079
0.50	2.82307	3.47099	4.12148	4.77548	5.43102	6.08608
0.60	3.06229	3.68799	4.30495	4.92383	5.54699	6.17424
0.70	3.45372	4.10280	4.70920	5.30154	5.89075	6.48127
0.80	4.00972	4.83103	5.52816	6.15939	6.75615	7.33493
0.85	4.26971	5.28293	6.14535	6.89590	7.57135	8.19897
0.90	4.42804	5.61867	6.71618	7.72475	8.64548	9.48357
0.95	4.48565	5.74678	6.95753	8.13244	9.27855	10.39934
0.99	4.49335	5.76333	6.98770	8.18219	9.35526	10.51206

Table 3b. Numerical Values of the TE Eigenvalues $k_{n2}^{(1)}(R;\varepsilon_r = 1/3)\,a$ for the Spherical Cavity Loaded Internally with a Dielectric Sphere

R=b/a	n=1	n=2	n=3	n=4	n=5
0.05	4.46025	5.25101	6.01433	6.75783	7.48623
0.10	4.46228	5.25112	6.01433	6.75783	7.48623
0.20	4.50698	5.26123	6.01619	6.75813	7.48627
0.30	4.67880	5.34694	6.05175	6.77099	7.49046
0.40	5.02509	5.61047	6.22883	6.87885	7.55093
0.50	5.55227	6.12289	6.67413	7.24173	7.83216
0.60	6.13356	6.90351	7.48865	8.02226	8.54929
0.65	6.29287	7.31436	8.03667	8.61560	9.14461
0.70	6.32829	7.56756	8.56799	9.32160	9.92728
0.75	6.33922	7.61942	8.83647	9.91024	10.78773
0.80	6.45504	7.64411	8.86344	10.07269	11.23393
0.85	6.81283	7.88007	8.97735	10.11151	11.26856
0.90	7.37109	8.51928	9.58584	10.61248	11.63328
0.95	7.68393	9.02563	10.30954	11.54703	12.74418
0.99	7.72494	9.09451	10.41636	11.70383	12.96506

Table 3c. Numerical Values of the TE Eigenvalues $k_{n3}^{(1)}(R;\varepsilon_r = 1/3)\,a$ for the Spherical Cavity Loaded Internally with a Dielectric Sphere

R=b/a	n=1	n=2	n=3	n=4	n=5
0.05	6.29589	7.11466	7.90856	8.68315	9.44240
0.10	6.30579	7.11552	7.90861	8.68316	9.44240
0.20	6.46361	7.16979	7.92311	8.68637	9.44302
0.30	6.89422	7.46634	8.09436	8.77173	9.48058
0.40	7.55005	8.09855	8.62558	9.18115	9.77332
0.50	8.10967	8.99227	9.57439	10.08155	10.58411
0.55	8.15397	9.35481	10.15639	10.72741	11.22935
0.60	8.19431	9.45837	10.61068	11.43380	12.03077
0.65	8.45088	9.49536	10.71575	11.89237	12.83231
0.70	8.95862	9.82443	10.80233	11.94343	13.13739
0.75	9.42703	10.48337	11.35852	12.23209	13.22150
0.80	9.54680	10.89733	12.10373	13.13389	14.02286
0.85	9.58831	10.93208	12.25989	13.55397	14.79674
0.90	10.04004	11.23666	12.43592	13.64711	14.86768
0.95	10.78049	12.13873	13.43716	14.68489	15.88868
0.99	10.90325	12.32168	13.69629	15.03737	16.35175

Table 3d. Numerical Values of the TE Eigenvalues $k_{n4}^{(1)}(R;\varepsilon_r = 1/3)\,a$ for the Spherical Cavity Loaded Internally with a Dielectric Sphere

R=b/a	n=1	n=2	n=3	n=4
0.05	8.12245	8.95740	9.77086	10.56624
0.10	8.15202	8.96111	9.77119	10.56626
0.20	8.49046	9.12083	9.83003	10.58388
0.30	9.19020	9.71212	10.25741	10.85562
0.40	9.90277	10.66974	11.19390	11.68674
0.45	9.97521	11.12443	11.80829	12.31948
0.50	10.04684	11.28868	12.36939	13.05365
0.55	10.41778	11.34393	12.55668	13.66935
0.60	10.98816	11.77403	12.65503	13.79198
0.65	11.34156	12.45693	13.27072	14.06253
0.70	11.37485	12.75106	13.98707	14.95315
0.75	11.68947	12.82383	14.09741	15.39889
0.80	12.46143	13.52556	14.51208	15.56183
0.85	12.72179	14.12917	15.44163	16.63609
0.90	12.84194	14.19586	15.54383	16.87999
0.95	13.78510	15.12991	16.41936	17.66522
0.99	14.06432	15.51208	16.92034	18.29709

At the upper limit of R, a short range of R is shown also for which the eigenvalues increase very slowly with R. This range decreases very rapidly as n increases. The region between these two limits reveals the presence of an indentation towards lower ka values. The range in R covered by this "dent" decreases with increasing values of n. It also produces an intermediate region in which the rate of change of $k_{n2}^{(1)}(R;\varepsilon_r = 1/3)\,a$ changes from fast to slow to fast as R increases. Although the region of slow variation covers a smaller range in R as n increases, it simultaneously results in a much slower rate of change with R.

Compared with the $k_{n2}^{(1)}a$ trajectories for $\varepsilon_r = 3$ in figure 3, where we note that the eigenvalues are monotonic and decreasing with increasing R, the eigenvalues for $\varepsilon_r = 1/3$ are monotonic and increasing with increasing R. The curves of figure 12 for $\varepsilon_r = 1/3$ do not display the sharp characteristics of those of figure 3 for $\varepsilon_r = 3$. They do, however, retain many of the other features of the trajectories of figure 3.

Figure 13 displays the eigenvalue trajectories for $p = 3$ and for $n = 1$ to $n = 5$. Numerical values for these $k_{n3}^{(1)}(R;\varepsilon_r = 1/3)\,a$ curves are given in table 3(c). We shall first consider these curves with regard to how they vary as R and n vary. Next we compare them to the $p = 2$ curves. Then we shall make some comparisons with the case $\varepsilon_r = 3$, i.e., for the situation in which the dielectrics in the cavity are interchanged. Initially, we observe that the values start at the known values for a cavity homogeneously filled with dielectric. Since we have the stronger dielectric filling the cavity, these $R = 0$ values for each n are reduced by the factor $\sqrt{1/\varepsilon_r} = \sqrt{3}$, as we discussed earlier. As R increases, the eigenvalue for $n = 1$ very slowly increases with R up to about $R = 0.1$. Further increase in R causes the eigenvalue to increase at a more rapid rate until about $R = 0.5$, where again it dramatically slows its rate of increase until R has increased to about $R = 0.6$. This is followed again by a more rapid increase in $k_{13}^{(1)}(R;\varepsilon_r = 1/3)\,a$ with R and a tapering off from this rate of increase with further increase in R, starting at about $R = 0.7$. We observe that over approximately the range $0.5 \leq R \leq 0.7$ there is present in the $k_{13}^{(1)}a$ trajectory an indentation.

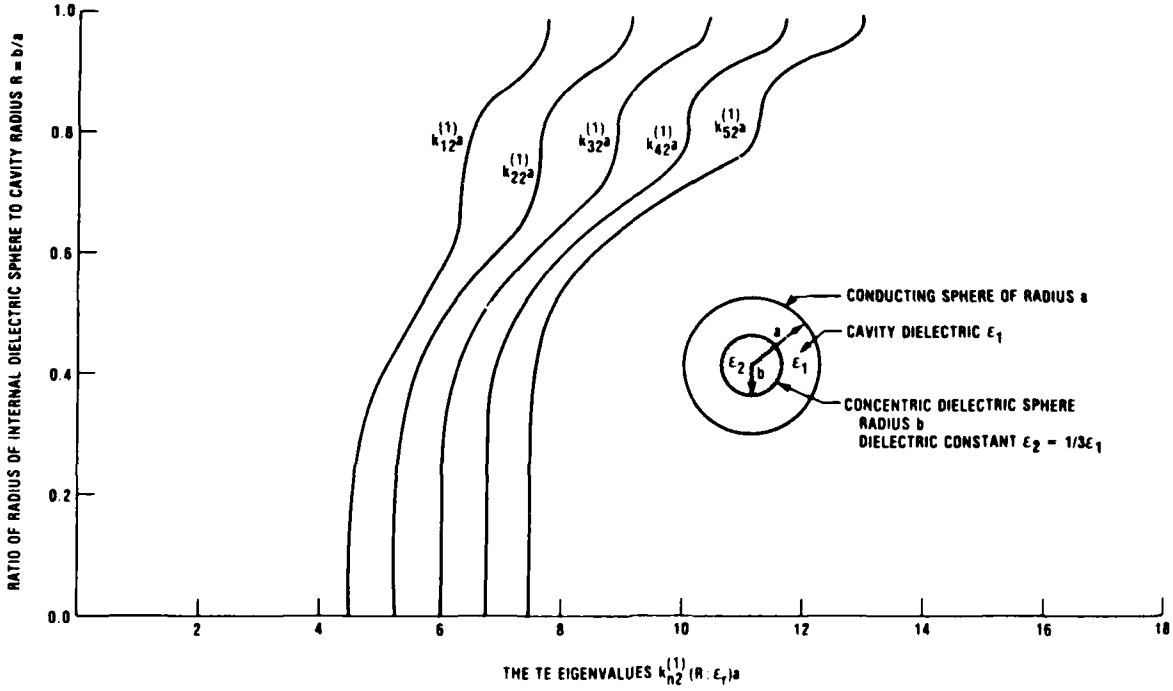

Figure 12. TE eigenvalues $k_{n2}^{(1)}(R;\varepsilon_r = 1/3)\,a$ for the spherical cavity of radius *a* filled with dielectric ε_1 internally loaded with a concentric dielectric sphere of radius *b* and strength $\varepsilon_2 = 1/3\varepsilon_1$.

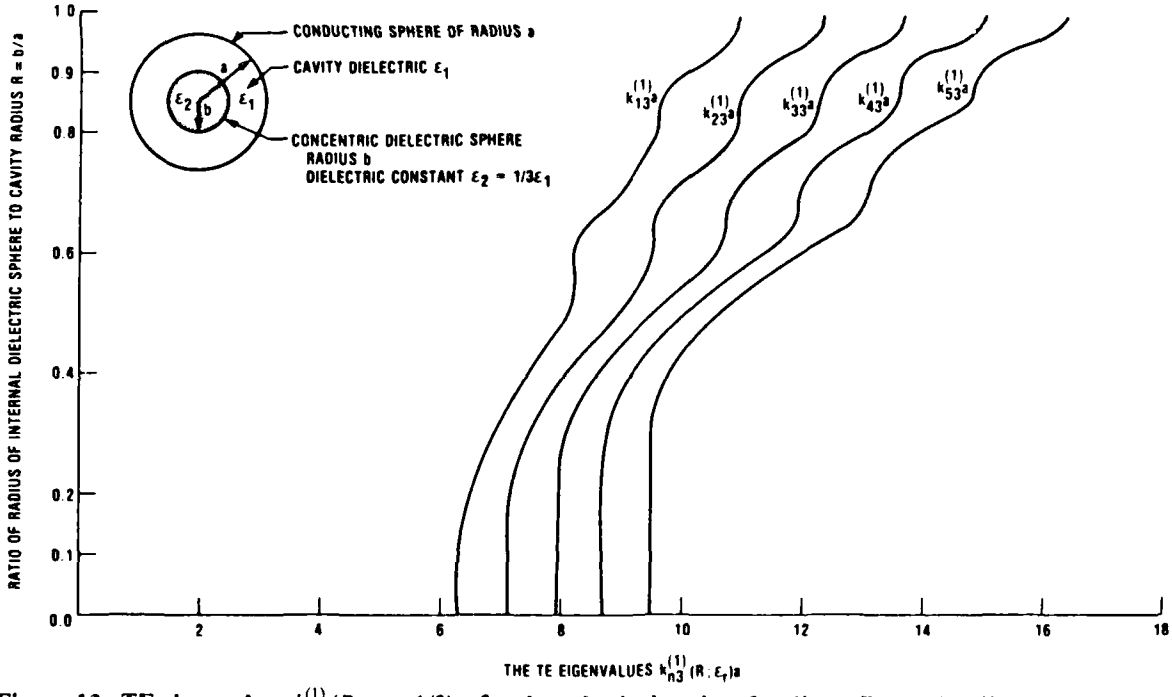

Figure 13. TE eigenvalues $k_{n3}^{(1)}(R;\varepsilon_r = 1/3)\,a$ for the spherical cavity of radius *a* filled with dielectric ε_1 internally loaded with a concentric dielectric sphere of radius *b* and strength $\varepsilon_2 = 1/3\varepsilon_1$.

Immediately beyond this range in R, we can clearly see another identation over which the same sort of behavior in $k_{13}^{(1)}a$ is clearly visible. Just after this second indentation in the trajectory there is a rapid return, as R approaches unity, to the limiting eigenvalue for the cavity homogeneously filled with dielectric.

As we let n increase, the slowness of the very early increase in $k_{n3}^{(1)}a$ as R increases from $R = 0$ becomes even more pronounced and persists for a larger range of R. Thus, at $n = 5$ this behavior is quite obvious in figure 13 up to about $R = 0.3$. Clearly, as n increases further, this would be even more enhanced for a larger range in R. Also, the rapid variation with R that follows this initial behavior increases further, as n increases, over a slowly increasing range of R. This behavior as R increases is then followed by a short range of R over which $k_{n3}^{(1)}a$ increases with R, but slowly. As n increases, this region of the trajectory becomes shorter until at $n = 5$, it almost is undetectable in figure 13.

Following this behavior, we find that $k_{n3}^{(1)}a$ increases more rapidly with R through an indented region. We note in figure 13 as n increases this range of increase with R grows more rapid. Thereafter, we observe the effects of a second indentation in the trajectories and a repeat in the behavior of the $k_{n3}^{(1)}a$ values as R increases through the range corresponding to the identation up to the limit at $R = 1$.

The $p = 3$ case of figure 13 primarily differs from the $p = 2$ case of figure 12 by the addition of one more identation in the trajectories and the resultant characteristics. If we compare the $p = 3$ case for $\varepsilon_r = 1/3$ of figure 13 with the $p = 3$ case for $\varepsilon_r = 3$ of figure 8, we observe the former is monotonically increasing with R, whereas the latter is monotonically decreasing as R increases. The $k_{n3}^{(1)}(R;\varepsilon_r = 1/3)a$ curves are considerably smoother than the $k_{n3}^{(1)}(R;\varepsilon_r = 3)a$ curves, although both have the same number of indentations in the same sense relative to ka. Thus, interchanging the dielectrics in the cavity results in some very remarkable differences in the corresponding eigenvalue trajectories.

The trends in the TE eigenvalue trajectories as p is increased further are now clearly apparent. We see in figure 14 pretty much what we now expect to for $p = 4$. This is also evident in table 3(d) for the $k_{n4}^{(1)}(R;\varepsilon_r = 1/3)a$ numerical values. Clearly, another indentation, the

third one now, is present in the $k_{n4}^{(1)} a$ trajectories, and the expected behavior is exhibited over the consecutive ranges of R as we go from $R = 0$ to $R = 1$.

We have just completed examining a large number of sets of TE $k_{np}^{(1)}(R;\varepsilon_r)\,a$ trajectories for each value of p and for a substantial range of relative dielectric strength ε_r. Next, we proceed to consideration of the corresponding sets of TM eigenvalues.

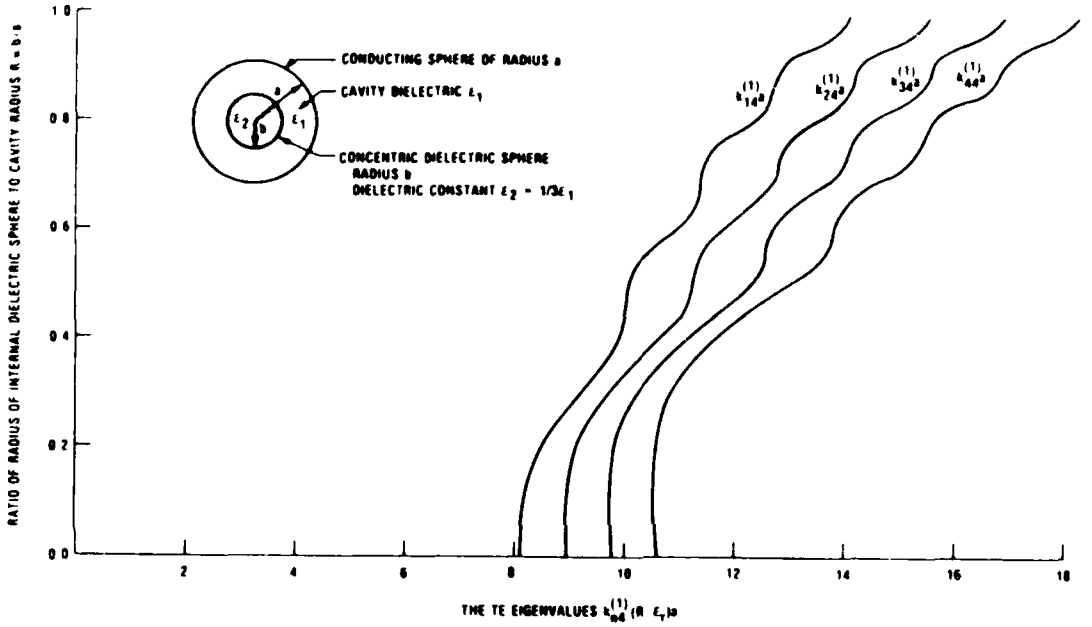

Figure 14. TE eigenvalues $k_{n4}^{(1)}(R;\varepsilon_r = 1/3)\,a$ for the spherical cavity of radius a filled with dielectric ε_1 internally loaded with a concentric dielectric sphere of radius b and strength $\varepsilon_2 = 1/3\varepsilon_1$.

4. The Transverse Magnetic (TM) Eigenvalues

4.1 Introduction

Just as we did in section 3.1 earlier for the TE eigenvalues, we now introduce some notation conventions for the TM eigenvalues. Using the identities just preceding equation (32), we rewrite equations (29) and (30), respectively, as follows:

$$\begin{aligned} &\varepsilon_r i_n\left(\sqrt{\varepsilon_r} R\gamma_1 a\right) T_n^{(1)}(a,Ra) \\ &+\left[\sqrt{\varepsilon_r} R\gamma_1 a\, i_n\left(\sqrt{\varepsilon_r} R\gamma_1 a\right)\right]' \Upsilon_n^{(1)}(Ra,a) = 0 \ , \end{aligned} \tag{36}$$

where

$$\begin{aligned} &T_n^{(1)}(a,b) \equiv T_n^{(1)}(a,Ra) \\ &\equiv \left[\gamma_1 a\, i_n(\gamma_1 a)\right]'\left[R\gamma_1 a\, k_n(R\gamma_1 a)\right]' - \left[R\gamma_1 a\, i_n(R\gamma_1 a)\right]'\left[\gamma_1 a\, k_n(\gamma_1 a)\right]' . \end{aligned} \tag{37}$$

For fixed values of R and ε_r we consider $\gamma_1 a$ the variable in equation (36) (just as in the TE case). The values $\gamma_1 a$ that satisfy this equation are the eigenvalues for the TM modes. Again we note that since the dielectrics within the cavity are lossless, and the outer cavity wall is a perfect conductor, all the roots of equation (36) are purely imaginary. Then, as for the TE eigenvalues, for each value of the index n, the TM eigenvalue spectrum will be a doubly infinite discrete set of ordered real numbers, each of which we denote by $k_{np}^{(2)} a$ where $jk_{np}^{(2)} a$ is a root of equation (36). For fixed n we thus have $k_{np'}^{(2)} a > k_{np}^{(2)} a$ for $p' > p$ where $p,p' = 1,2,3...$

Each value of $k_{np}^{(2)} a$ is a function of the relative dielectric strength, ε_r, and of R, the ratio of the radius of the inner dielectric radius b, to the cavity radius a. Thus $k_{np}^{(2)} a = k_{np}^{(2)}(R;\varepsilon_r) a$. For the TM case, we shall use the same convention for the dielectrics as in the TE case at the limits $R = 0$ and $R = 1$, or equivalently, $b = 0$ and $b = a$, which correspond, respectively, to the absence of the inner dielectric sphere that loads the cavity, and to the inner dielectric load sphere completely filling the cavity. Thus, we can immediately obtain the TM eigenvalues from the well-known cavity eigenvalues in these limits. As before, for $\varepsilon_r > 1$, the eigenvalues $k_{np}^{(2)} a$ for $R = 0$ are the usual ones for the spherical cavity, which vary with R until $R = 1$, whereupon they are just those for $R = 0$ reduced by the factor $\sqrt{\varepsilon_r}$. For ε_r

< 1 they start at $R = 0$ as the reduced normalized values, and go over at $R = 1$ to the unreduced values. The eigenvalues between these limits must be computed using equation (36) to obtain the entire picture. This has been done, and we now proceed to consider the results so obtained for the same range of dielectric properties as in the TE case.

4.2 The TM Eigenvalues for $\varepsilon_r = 3.00$

We shall first consider the details of the results obtained for $\varepsilon_r = 3$. Here we recall that the inner dielectric sphere of radius b has a dielectric constant ε_2, which is three times that of the dielectric constant ε_1 of the cavity dielectric in the absence of the inner load.

In figure 15, we find the TM eigenvalue trajectories $k_{n1}^{(2)}(R;\varepsilon_r = 3)a$ for $p = 1$ and with n going from $n = 1$ to $n = 8$. Table 4(a) contains numerical values for these eigenvalues.

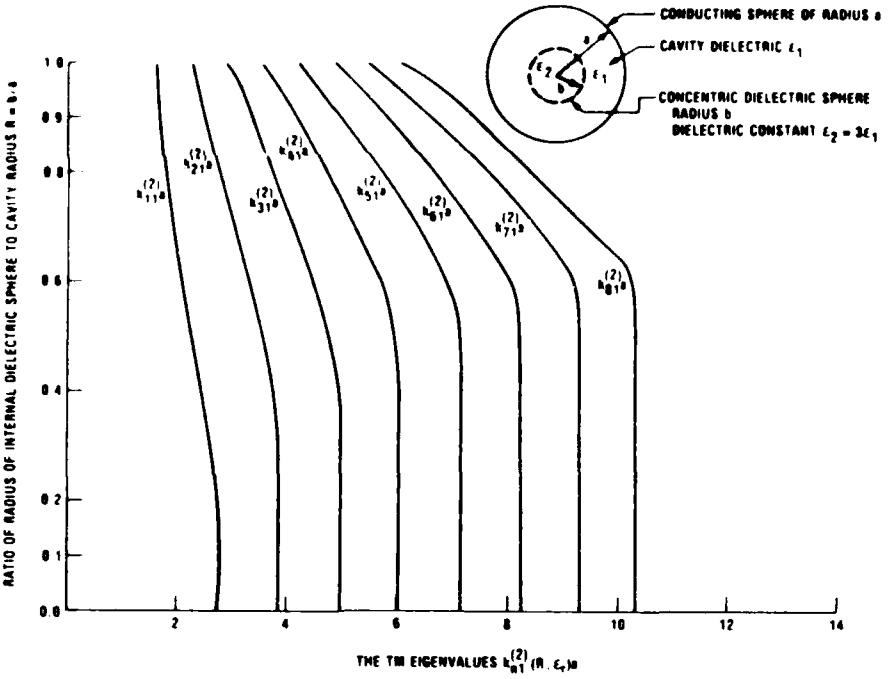

Figure 15. TM eigenvalues $k_{n1}^{(2)}(R;\varepsilon_r = 3)a$ for the spherical cavity of radius a filled with dielectric ε_1 internally loaded with a concentric dielectric sphere of radius b and strength $\varepsilon_2 = 3\varepsilon_1$.

Table 4a. Numerical Values of the TM Eigenvalues $k_{n1}^{(2)}(R;\varepsilon_r = 3)\,a$ for the Spherical Cavity Loaded Internally with a Dielectric Sphere

R=b/a	n=1	n=2	n=3	n=4	n=5
0.05	2.74288	3.87023	4.97342	6.06195	7.14023
0.10	2.73706	3.87007	4.97342	6.06195	7.14023
0.20	2.69190	3.86492	4.97291	6.06190	7.14022
0.30	2.58539	3.83249	4.96545	6.06035	7.13991
0.40	2.43108	3.73200	4.92125	6.04385	7.13420
0.50	2.26204	3.54208	4.77545	5.95374	7.08509
0.55	2.17964	3.42198	4.64826	5.84425	7.00431
0.60	2.10058	3.29330	4.48936	5.67699	6.84888
0.65	2.02536	3.16109	4.30924	5.45979	6.60725
0.70	1.95399	3.02859	4.11815	5.21204	6.30396
0.80	1.82162	2.76782	3.72715	4.68780	5.64199
0.90	1.69988	2.50972	3.32898	4.15081	4.97012
0.95	1.64157	2.37657	3.11535	3.85667	4.59870
0.99	1.59555	2.26400	2.92417	3.58021	4.23397

Table 4a. (cont'd) Numerical Values of the TM Eigenvalues $k_{n1}^{(2)}(R;\varepsilon_r = 3)\,a$ for the Spherical Cavity Loaded Internally with a Dielectric Sphere

R=b/a	n=6	n=7	n=8
0.05	8.21084	9.27546	10.33524
0.10	8.21084	9.27546	10.33524
0.20	8.21084	9.27546	10.33524
0.30	8.21078	9.27545	10.33524
0.40	8.20888	9.27484	10.33504
0.50	8.18396	9.26270	10.32929
0.55	8.13056	9.22989	10.31005
0.60	8.00051	9.13009	10.23846
0.65	7.74811	8.88003	10.00150
0.70	7.38917	8.46338	9.52239
0.80	6.58395	7.50955	8.41636
0.90	5.78326	6.58770	7.38191
0.95	5.33969	6.07819	6.81306
0.99	4.88643	5.53809	6.18923

Table 4b. Numerical Values of the TM Eigenvalues $k_{n2}^{(2)}(R;\varepsilon_r = 3)\,a$ for the Spherical Cavity Loaded Internally with a Dielectric Sphere

R=b/a	n=1	n=2	n=3	n=4	n=5
0.05	6.10886	7.44298	8.72175	9.96755	11.18898
0.10	6.05385	7.43963	8.72160	9.96754	11.18898
0.20	5.71699	7.34454	8.70488	9.96504	11.18864
0.30	5.33241	6.92317	8.49585	9.89331	11.16763
0.35	5.18844	6.62768	8.19692	9.71259	11.08859
0.40	5.05083	6.34388	7.79200	9.31550	10.81376
0.45	4.89193	6.08469	7.37505	8.76706	10.22011
0.50	4.70492	5.83982	7.00053	8.22779	9.51894
0.55	4.50438	5.60029	6.67709	7.77279	8.90497
0.60	4.30845	5.36815	6.39444	7.40906	8.42805
0.65	4.12893	5.15080	6.14206	7.11422	8.07612
0.70	3.97157	4.95453	5.91497	6.86154	7.80095
0.80	3.73125	4.63748	5.53332	6.42664	7.32360
0.90	3.59128	4.42487	5.24643	6.06267	6.87761
0.95	3.55456	4.35349	5.13403	5.90342	6.66576
0.99	3.53556	4.30780	5.05449	5.78389	6.50075

Table 4c. Numerical Values of the TM Eigenvalues $k_{n2}^{(2)}(R;\varepsilon_r = 3)\,a$ for the Spherical Cavity Loaded Internally with a Dielectric Sphere

R=b/a	n=1	n=2	n=3	n=4
0.05	9.28897	10.71235	12.06358	13.38012
0.10	9.10628	10.69302	12.06224	13.38005
0.15	8.77250	10.57386	12.04292	13.37761
0.20	8.48286	10.24119	11.92761	13.35179
0.25	8.24336	9.77384	11.54281	13.19856
0.30	7.90934	9.33457	10.89296	12.63995
0.35	7.49142	8.90388	10.27771	11.76078
0.40	7.13785	8.47827	9.78701	11.07181
0.45	6.92502	8.13346	9.38185	10.61430
0.50	6.83769	7.91323	9.06659	10.25283
0.55	6.79459	7.79473	8.84867	9.95403
0.60	6.69222	7.69193	8.68765	9.71039
0.70	6.24923	7.25848	8.23221	9.18334

Table 4c. (cont'd) Numerical Values of the TM Eigenvalues $k_{n3}^{(2)}(R;\varepsilon_r = 3)\,a$ for the Spherical Cavity Loaded Internally with a Dielectric Sphere

R=b/a	n=1	n=2	n=3	n=4
0.80	5.78179	6.71995	7.63368	8.52910
0.90	5.47244	6.33328	7.17548	8.00447
0.95	5.40210	6.23206	7.04158	7.83653
0.99	5.38160	6.19214	6.97764	7.74468

Table 4d. Numerical Values of the TM Eigenvalues $k_{n4}^{(2)}(R;\varepsilon_r = 3)\,a$ for the Spherical Cavity Loaded Internally with a Dielectric Sphere

R=b/a	n=1	n=2	n=3	n=4
0.05	12.41947	13.91814	15.31350	16.67415
0.10	12.04265	13.84993	15.30689	16.67365
0.15	11.62708	13.48050	15.21499	16.65837
0.20	11.24562	12.84136	14.72384	16.49682
0.25	10.61792	12.22503	13.81468	15.66128
0.30	10.15323	11.59708	13.07775	14.54327
0.35	10.01586	11.19032	12.52571	13.90196
0.40	9.91200	11.02213	12.18209	13.44077
0.45	9.56698	10.80230	11.94798	13.09572
0.50	9.10805	10.36373	11.56787	12.72224
0.55	8.75829	9.90507	11.06709	12.21408
0.60	8.61046	9.60926	10.65945	11.73258
0.70	8.45130	9.41560	10.34744	11.26968
0.80	7.87959	8.84116	9.77566	10.68876
0.90	7.37383	8.25694	9.12024	9.96792
0.95	7.24289	8.09214	8.92173	9.73616
0.99	7.21087	8.04246	8.85120	9.64218

It is important to notice, at the outset, that the TM eigenvalues $k_{11}^{(2)}a$ are the lowest-lying set for $\varepsilon_r = 3$. Furthermore, to cover the same frequency range shown in figure 2 for the TE values $k_{n1}^{(1)}a$, we require TM eigenvalues $k_{n1}^{(2)}a$ to higher order (i.e., to $n = 7$ compared with $n = 5$ for the TE range). This circumstance will be seen to hold true for higher p values.

We now make one comparison, i.e., the behavior of the TM trajectories relative to the TE trajectories as R increases from zero to unity or as the dielectric load increases in size until it fills the cavity completely. Note then that, in general, the TM eigenvalue trajectories are concave downward for the entire range of R, whereas, in the TE case, for $p = 1$, the trajectories change over at about $R = 0.5$ from concave down to concave upward.

The TM eigenvalue trajectories $k_{n1}^{(2)}a$ are monotonic, decreasing as R increases. Initially, this is a quite slow decrease with increasing R, for a range of R that grows with increasing value of the order index n. Indeed, we can observe in figure 15 that for $n = 1$, this holds up to about $R = 0.1$ and increases so that at $n = 8$ it holds up to about $R = 0.6$. Clearly, this range continues to grow with further increase in n. Following this initial behavior the eigenvalues $k_{n1}^{(2)}a$ decrease more rapidly with increasing R and continue in this manner almost to $R = 1$ itself. Note in figure 15 that, as n increases, the eigenvalue trajectory shows a more rapid rate of decrease as R increases. For the $p = 1$ case, we cannot clearly discern three distinct regimes corresponding to a small-sized inner dielectric, an intermediate one, and a large one.

Before continuing to higher p values, we pause to focus on a very remarkable feature exhibited in figure 15. Notice that for $n = 8$, we find that $k_{81}^{(2)}a$ changes by less than one percent (compare table 4(a)), as R increases to $R = 0.6$. This tells us that we have an inner dielectric sphere whose radius can vary from zero to 0.6 times the radius of the entire cavity, with very little change in the eigenvalue, $k_{81}^{(2)}a$. A small increase in the size of the inner sphere from this point on, then, causes a rather substantial increase in the eigenvalue. To understand this interesting property requires a detailed study of the corresponding spatial distributions of the field components. We defer this discussion to a subsequent report.

Next consider the results for $p = 2$ shown in figure 16, where $k_{n2}^{(2)}a$ is plotted for $n = 1$ to $n = 5$. Table 4(b) gives numerical values for these eigenvalues. Another quite notable feature shows up. The $k_{n2}^{(1)}(R{:}\varepsilon_r = 3)\,a$ trajectories very closely resemble the TE trajectories for $p = 1$, $k_{n1}^{(1)}(R{:}\varepsilon_r = 3)\,a$. The TM curves seem merely to be shifted to higher values in $\gamma_1 a$ than the TE curves.

For $p = 2$, the TM curves are still monotonically decreasing as R increases and display the now familiar feature of a single knee in each curve. Unlike the $p = 1$ family, we note that once again three size regimes are suggested for the load sphere.

We show in figure 17 the TM eigenvalue trajectories for $p = 3$ where n goes from $n = 1$ to $n = 4$. Numerical values for these $k_{n3}^{(2)}(R{:}\varepsilon_r = 3)\,a$ are given in table 4(c). Comparison of figure 17 and figure 3 for the TE eigenvalues for $p = 2$, i.e., $k_{n2}^{(1)}(R{:}\varepsilon_r = 3)\,a$, show that the corresponding trajectories are quite similar. They are not as much alike as we just noted

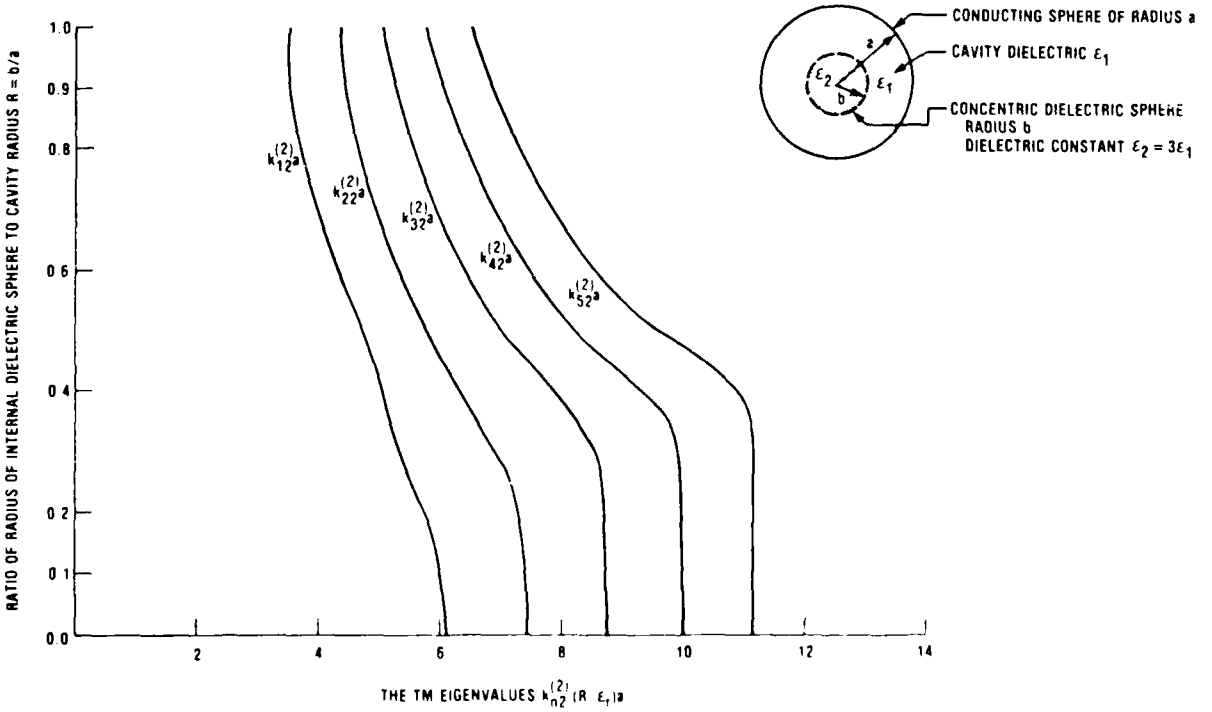

Figure 16. TM eigenvalues $k_{n2}^{(2)}(R{:}\varepsilon_r = 3)\,a$ for the spherical cavity of radius a filled with dielectric ε_1 internally loaded with a concentric dielectric sphere of radius b and strength $\varepsilon_2 = 3\varepsilon_1$.

for the TM $p = 2$ and TE $p = 1$ trajectories. There are two knees present in each set. The TM eigenvalues $k_{n3}^{(2)} a$ show smaller ranges in R, for which we have a very slow decrease in $\gamma_1 a$ with increasing R, than we found for the TE case of $k_{n2}^{(1)} a$. The TM trajectories then reveal a succeeding range over which $k_{n3}^{(2)} a$ decreases more rapidly as R increases, with the rate increasing with n. This rate of variation with R is much slower than we observed in figure 3 for the TE trajectories for $k_{n2}^{(1)} a$. The next range in R shows that $k_{n3}^{(2)} a$ changes slowly with increasing R, but not nearly as slowly as the TE trajectories did for $k_{n2}^{(1)} a$. For the remainder of the range of R, both $k_{n3}^{(2)} a$ and $k_{n2}^{(1)} a$ behave about the same. The TM trajectories, $k_{n3}^{(2)} (R; \varepsilon_r = 3)\, a$, still can be thought of as displaying three distinctly sized regimes for the size of the loading dielectric sphere.

Figure 18 gives the calculated set of TM eigenvalue trajectories for $p = 4$. Here we show results for $n = 1$ to $n = 4$. Numerical values of $k_{n4}^{(2)} (R; \varepsilon_r = 3)\, a$ are presented in table 4(d). The same trend we saw for the TM $p = 3$ and TE $p = 2$ eigenvalues continues here. As anticipated, an

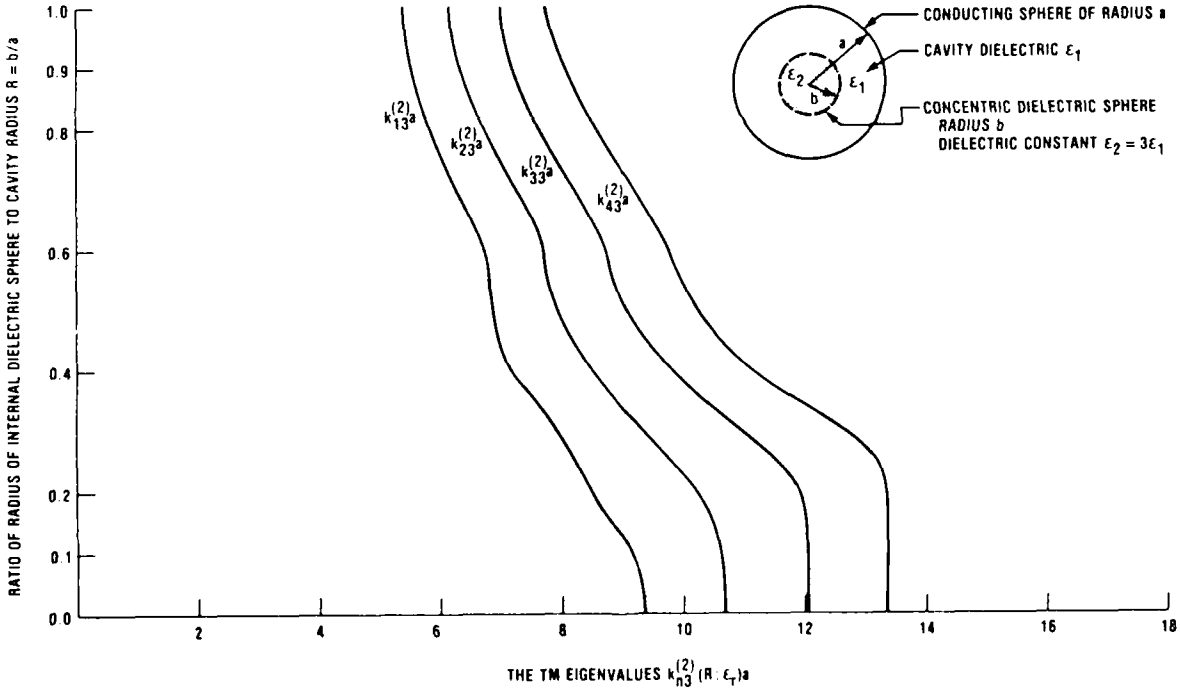

Figure 17. TM eigenvalues $k_{n3}^{(2)} (R; \varepsilon_r = 3)\, a$ for the spherical cavity of radius a filled with dielectric ε_1 internally loaded with a concentric dielectric sphere of radius b and strength $\varepsilon_2 = 3\varepsilon_1$.

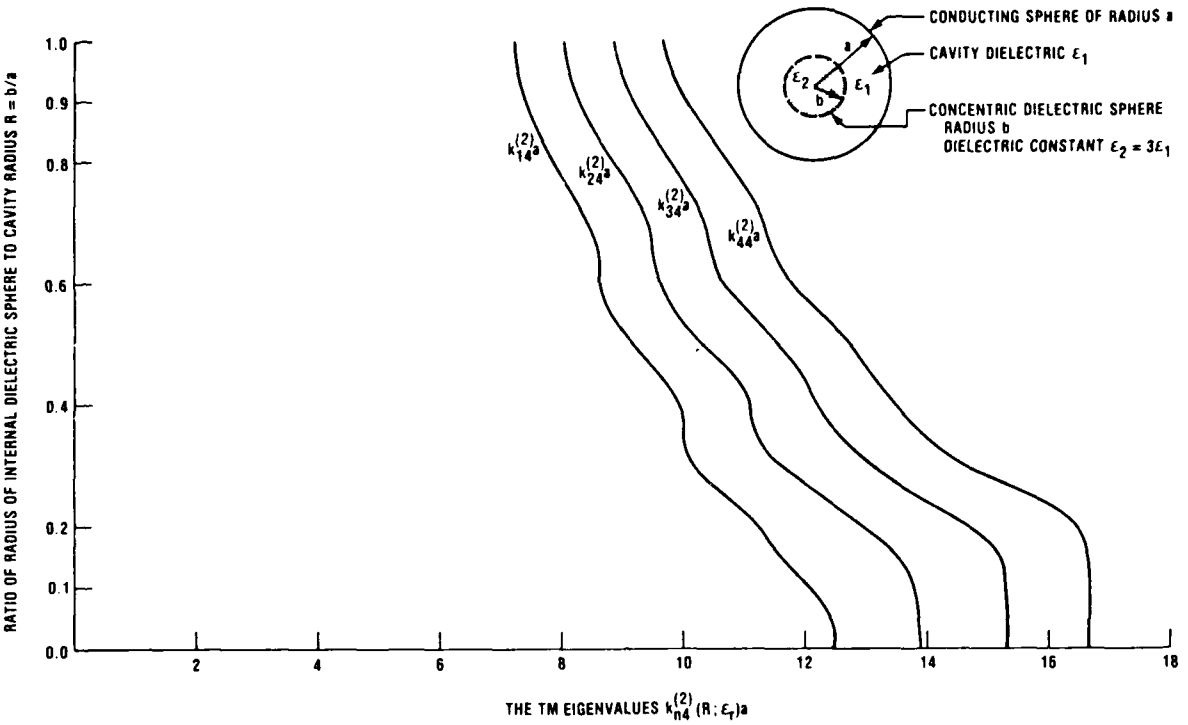

Figure 18. TM eigenvalues $k_{n4}^{(2)}(R;\varepsilon_r = 3)\,a$ for the spherical cavity of radius a filled with dielectric ε_1 internally loaded with a concentric dielectric sphere of radius b and strength $\varepsilon_2 = 3\varepsilon_1$.

additional knee appears in the curves for the $k_{n4}^{(2)}a$. The $k_{n4}^{(2)}a$ and $k_{n3}^{(1)}a$ eigenvalue trajectories again are quite similar, with the TM trajectories showing much less pronounced emphasis of the features over the successive ranges of R. Of course, the TM eigenvalue trajectories for $k_{n4}^{(2)}a$ are at larger ka values than the TE trajectories for $k_{n3}^{(1)}a$.

4.3 The TM Eigenvalues for $\varepsilon_r = 10.00$

We will now consider the TM eigenvalues for the inner sphere of a larger dielectric constant of $\varepsilon_2 = 10\varepsilon_1$. First we examine the results obtained from equation (36) for $p = 1$ and $n = 1$ to $n = 8$. These results are the trajectories plotted in figure 19 and whose numerical values of $k_{n1}^{(2)}(R;\varepsilon_r = 10)\,a$ are given in table 5(a). Again we begin by pointing out that for all R, the TM eigenvalues $k_{11}^{(2)}(R;\varepsilon_r = 10)\,a$ lie lower than the TE eigenvalue $k_{11}^{(1)}(R;\varepsilon_r = 10)\,a$.

In fact, the TM $k_{11}^{(2)}a$ are the lowest-lying eigenvalues for $\varepsilon_r = 10$. This can be seen by simply comparing the curves of figures 6 and 19.

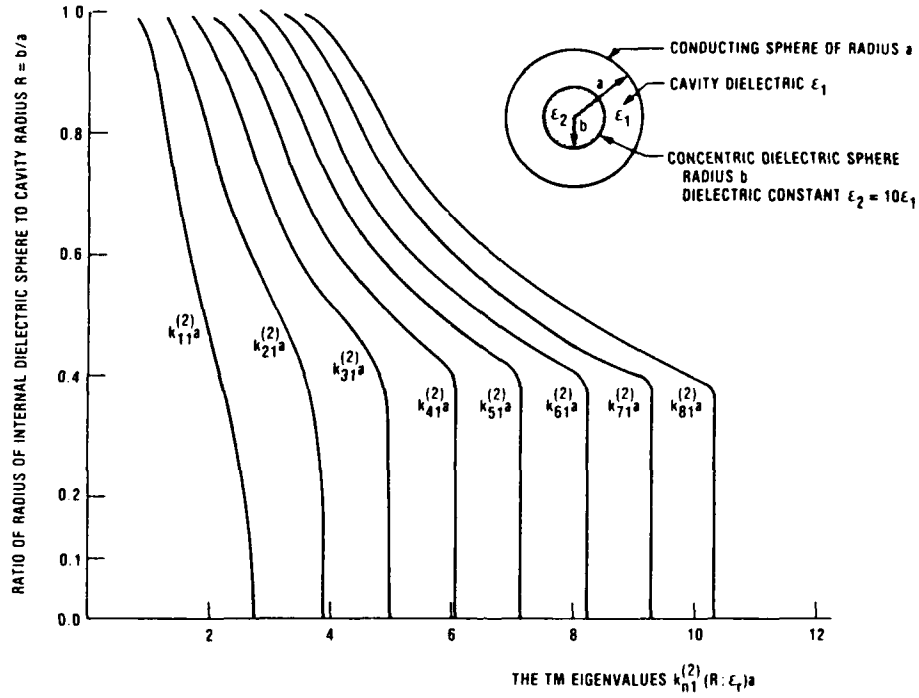

Figure 19. TM eigenvalues $k_{n1}^{(2)}(R;\varepsilon_r = 10)\,a$ for the spherical cavity of radius a filled with dielectric $_1$ internally loaded with a concentric dielectric sphere of radius b and strength $\varepsilon_2 = 10\varepsilon_1$.

We have a rather involved situation, in which there are a fairly large number of parameters in relation to which the different eigenvalues can be compared; i.e., TM compared with TE, $\varepsilon_r = 10$ relative to $\varepsilon_r = 3$, and, for given ε_r, the TM eigenvalues for given n can be compared for different p values, or for different n values all other parameters kept fixed. In spite of this complexity we shall try to carry through the comparisons where they appear significant.

Continuing, we compare the $k_{n1}^{(2)}(R;\varepsilon_r = 10)\,a$ trajectories of figure 19 with the $k_{n1}^{(2)}(R;\varepsilon_r = 3)\,a$ trajectories of figure 15. For $n = 1$, we see they both begin at the same value at $R = 0$. As R increases, they both decrease slowly at first and then more rapidly, with $k_{11}^{(2)}(R;\varepsilon_r = 10)\,a$ having its rate of change somewhat higher, so that at $R = 1$, we have the ratio

$$\frac{k_{11}^{(2)}(R=1;\varepsilon_r=10)\,a}{k_{11}^{(2)}(R=1;\varepsilon_r=3)\,a} = \sqrt{\frac{3}{10}} \quad .$$

Table 5a. Numerical Values of the TM Eigenvalues $k_{n1}^{(2)}(R{:}\varepsilon_r = 10)\,a$ for the Spherical Cavity Loaded Internally with a Dielectric Sphere

R=b/a	n=1	n=2	n=3	n=4
0.05	2.74214	3.87023	4.97342	6.06195
0.10	2.73105	3.86993	4.97341	6.06195
0.20	2.64339	3.86052	4.97252	6.06187
0.30	2.44378	3.79690	4.95825	6.05896
0.35	2.31574	3.71345	4.92707	6.04950
0.375	2.24897	3.65122	4.89390	6.03630
0.40	2.18174	3.57298	4.83418	5.99852
0.45	2.04872	3.37092	4.54925	5.53510
0.50	1.92058	3.13335	4.14872	4.99242
0.60	1.68455	2.67539	3.47315	4.16142
0.70	1.47479	2.29613	2.96820	3.55954
0.80	1.28336	1.97686	2.56689	3.09291
0.90	1.09462	1.67147	2.19867	2.68187
0.925	1.04438	1.58649	2.09550	2.56951
0.95	0.99112	1.49106	1.97528	2.43705
0.975	0.93313	1.37652	1.81883	2.25449
0.99	0.89498	1.29160	1.68879	2.08593

Table 5a. (cont'd) Numerical Values of the TM Eigenvalues $k_{n1}^{(2)}(R{:}\varepsilon_r = 10)\,a$ for the Spherical Cavity Loaded Internally with a Dielectric Sphere

R=b/a	n=5	n=6	n=7	n=8
0.05	7.14023	8.21084	9.27546	10.33524
0.10	7.14023	8.21084	9.27546	10.33524
0.20	7.14022	8.21084	9.27546	10.33524
0.30	7.13965	8.21073	9.27544	10.33524
0.35	7.13700	8.21002	9.27526	10.33519
0.375	7.13233	8.20844	9.27472	10.33501
0.40	7.10384	8.13416	9.06122	9.96681
0.45	6.40689	7.23980	8.05514	8.85948
0.50	5.76783	6.51605	7.24965	7.97353
0.60	4.80582	5.42951	6.04110	6.64448
0.70	4.11466	4.65122	5.17663	5.69448
0.80	3.58569	4.06005	4.52305	4.97835
0.90	3.13486	3.56829	3.98876	4.40023

Table 5a. Numerical Values of the TM Eigenvalues $k_{n1}^{(2)}(R;\varepsilon_r = 10)\,a$ for the Spherical Cavity Loaded Internally with a Dielectric Sphere

R=b/a	n=5	n=6	n=7	n=8
0.925	3.01614	3.44341	3.85718	4.26132
0.95	2.87747	3.30045	3.71001	4.10939
0.975	2.68072	3.09676	3.50308	3.90070
0.99	2.48199	2.87605	3.26741	3.65560

Table 5b. Numerical Values of the TM Eigenvalues $k_{n2}^{(2)}(R;\varepsilon_r = 10)\,a$ for the Spherical Cavity Loaded Internally with a Dielectric Sphere

R=b/a	n=1	n=2	n=3	n=4	n=5
0.05	6.10160	7.44289	8.72175	9.96755	11.18898
0.10	5.98960	7.43678	8.72148	9.96754	11.18898
0.15	5.69933	7.39369	8.71724	9.96717	11.18896
0.20	5.26552	7.20470	8.68543	9.96260	11.18834
0.225	5.02341	6.94597	8.61675	9.95149	11.18654
0.23	4.97386	6.87218	8.58611	9.94672	11.18578
0.24	4.87396	6.70551	8.47633	9.92863	11.18322
0.25	4.77340	6.52213	8.27290	9.85558	11.17612
0.26	4.67267	6.33255	8.01299	9.58447	11.06590
0.30	4.27969	5.62072	7.00767	8.33831	9.61651
0.35	3.84258	4.92412	6.04519	7.15857	8.24588
0.39	3.54785	4.50996	5.47705	6.44758	7.41018
0.40	3.48151	4.42358	5.36332	6.30471	7.24398
0.41	3.41790	4.34339	5.26305	6.18938	7.16024
0.42	3.35693	4.26900	5.17761	6.11654	7.14239
0.45	3.18869	4.07635	5.00409	6.03773	7.12132
0.50	2.95091	3.82869	4.83290	5.94295	7.06296
0.53	2.82963	3.70623	4.73435	5.85696	6.98214
0.55	2.75633	3.63099	4.66392	5.78179	6.88751
0.60	2.59564	3.45729	4.47009	5.52795	6.48720
0.65	2.46170	3.29754	4.25768	5.21219	6.02879
0.70	2.34909	3.14768	4.03744	4.88694	5.60866
0.80	2.17202	2.86919	3.60328	4.28918	4.89480
0.90	2.03996	2.60861	3.18883	3.75198	4.28117
0.95	1.98493	2.48136	2.98009	3.47497	3.95896
0.99	1.94417	2.37939	2.80409	3.22212	3.63549

Table 5c. Numerical Values of the TM Eigenvalues $k_{n3}^{(2)}(R;\varepsilon_r = 10)\,a$ for the Spherical Cavity Loaded Internally with a Dielectric Sphere

R=b/a	n=1	n=2	n=3	n=4	n=5
0.01	9.31621	10.71301	12.06359	13.38012	14.67012
0.05	9.26192	10.71183	12.06357	13.38012	14.67012
0.10	8.85483	10.67402	12.06114	13.37999	14.60711
0.12	8.55316	10.60966	12.05479	13.37946	14.67007
0.14	8.18958	10.45346	12.03635	13.37748	14.66988
0.15	7.98515	10.29326	12.01612	13.37513	14.66961
0.17	7.54113	9.67286	11.87103	13.36210	14.66807
0.18	7.31408	9.27880	11.53410	13.33712	14.66588
0.19	7.09348	8.89665	11.01897	13.09883	14.65905
0.20	6.88492	8.54797	10.50791	12.49429	14.40867
0.24	6.21966	7.62350	8.97068	10.45512	12.02533
0.25	6.09741	7.49808	8.81040	10.10740	11.55074
0.30	5.69648	7.06652	8.51199	9.88585	11.16333
0.32	5.60586	6.92199	8.37712	9.80510	11.12933
0.34	5.53769	6.78319	8.20939	9.66465	11.04770
0.35	5.50855	6.71509	8.11276	9.55969	10.95706
0.40	5.35337	6.36755	7.53202	8.73223	9.87265
0.45	5.08304	5.96893	6.91103	7.87507	8.82188
0.50	4.73153	5.54339	6.35694	7.17504	7.98944
0.55	4.38900	5.14612	5.89083	6.63380	7.39158
0.60	4.08514	4.79742	5.50468	6.23711	7.07480
0.65	3.82306	4.49806	5.18430	5.93650	6.83130
0.70	3.59977	4.24355	4.91516	5.67488	6.55191
0.80	3.25674	3.84884	4.48193	5.18153	5.91635
0.90	3.04264	3.57702	4.13069	4.70382	5.28066
0.95	2.98287	3.47554	3.97044	4.46826	4.96624
0.97	2.96632	3.43930	3.90782	4.37386	4.83778
0.99	2.95251	3.40466	3.84574	4.27893	4.70625

Table 5d. Numerical Values of the TM Eigenvalues $k_{n4}^{(2)}(R;\varepsilon_r = 10)\,a$ for the Spherical Cavity Loaded Internally with a Dielectric Sphere

R=b/a	n=1	n=2	n=3	n=4
0.01	12.48495	13.92052	15.31356	16.67415
0.05	12.34864	13.91620	15.31346	16.67415
0.09	11.66566	13.83091	15.30744	16.67380
0.10	11.39210	13.75563	15.30059	16.67324
0.11	11.07169	13.61101	15.28721	16.67202
0.12	10.70612	13.30020	15.25973	16.66941
0.13	10.32192	12.73787	15.18674	16.66379
0.14	9.95744	12.08968	14.81789	16.64928
0.15	9.64061	11.52244	13.99140	16.51772
0.16	9.38302	11.10856	13.18860	15.62409
0.18	9.03329	10.66961	12.17109	13.93284
0.20	8.83911	10.40660	11.97936	13.37331
0.22	8.72520	10.17569	11.82085	13.31414
0.25	8.56776	9.83956	11.43985	13.10634
0.27	8.37583	9.58818	11.05765	12.71313
0.28	8.23946	9.44241	10.83503	12.41234
0.30	7.91356	9.10830	10.36626	11.75247
0.35	7.09866	8.22480	9.32598	10.41587
0.40	6.54310	7.56107	8.64055	9.79060
0.45	6.32088	7.20096	8.21410	9.33433
0.50	6.23596	7.00887	7.88291	8.83148
0.55	5.99439	6.73500	7.49604	8.28084
0.60	5.63298	6.34331	7.04389	7.74185
0.70	4.95085	5.58490	6.20868	6.83158
0.80	4.42896	4.99928	5.57003	6.15672
0.90	4.07959	4.59918	5.12427	5.66306
0.95	3.98594	4.47725	4.96790	5.46056
0.99	3.95318	4.41489	4.86623	5.30972

Thus, all the $k_{n1}^{(2)}(R;\varepsilon_r = 10)\,a$ and $k_{n1}^{(2)}(R;\varepsilon_r = 3)\,a$ will have the same ratio at $R = 1$ for each n.

For $n = 1$, both trajectories look pretty much alike for $\varepsilon_r = 10$ and $\varepsilon_r = 3$. However, we have already noted that as R increases the $k_{n1}^{(2)}a$ values decrease faster for $\varepsilon_r = 10$ than for $\varepsilon_r = 3$. There are some other dissimilarities that arise when we compare figure 19 with figure 15. Clearly, for $\varepsilon_r = 10$, the trajectories decrease slowly with increasing R; the rate decreases as n increases. This was also true of the eigenvalue trajectories $k_{n1}^{(2)}(R;\varepsilon_r = 3)\,a$. However, at the knee we observe a much sharper turning for the $\varepsilon_r = 10$ trajectories relative to those for $\varepsilon_r = 3$. One new feature is that as n increases, for $\varepsilon_r = 10$, we have a decreasing initial range of R over which this very slow changing of $k_{n1}^{(2)}a$ occurs. In addition to this behavior, we observe that the $k_{n1}^{(2)}(R;\varepsilon_r = 10)\,a$ trajectories in figure 19, just beyond the knee, are clearly concave upward. This behavior persists for a large range of R and is immediately followed by a region of rapid decrease in $k_{n1}^{(2)}a$, as R goes to unity. In figure 15, there is only a hint of this concavity in the $k_{n1}^{(2)}a$ trajectories for $\varepsilon_r = 3$. Note that the $k_{n1}^{(2)}(R;\varepsilon_r = 10)\,a$ trajectories somewhat resemble the $k_{n1}^{(1)}(R;\varepsilon_r = 10)\,a$ trajectories (compare fig. 6 and 19), except near $R = 1$.

In summary, then, our considerations thus far have been to compare the TM $k_{n1}^{(2)}(R;\varepsilon_r = 10)\,a$ to the TE $k_{n1}^{(1)}(R;\varepsilon_r = 10)\,a$ and also to compare the TM $k_{n1}^{(2)}(R;\varepsilon_r = 10)\,a$ to the TM $k_{n1}^{(2)}(R;\varepsilon_r = 3)\,a$.

Next, we examine the characteristics of the TM eigenvalue trajectories for $p = 2$, $k_{n2}^{(2)}(R;\varepsilon_r = 10)\,a$, when n goes from 1 to 5. The $k_{n2}^{(2)}a$ curves are shown in figure 20, and numerical values are given in table 5(b). Comparing figure 20 with figure 7, we see that there are two knees in all the TE trajectories $k_{n2}^{(1)}a$, whereas only for $n \geq 4$ do we see two clearly defined knees in the TM eigenvalue curves for $k_{n2}^{(2)}(R;\varepsilon_r = 10)\,a$. For $n \geq 4$, the TE and TM trajectories are similar, except for values of large R. For $n < 3$, the $k_{n2}^{(2)}(R;\varepsilon_r = 10)\,a$ trajectories resemble more closely the TE eigenvalue trajectories $k_{n1}^{(1)}(R;\varepsilon_r = 10)\,a$. There now appears to be a transition of some sort occurring in the inflection characteristics of the curves as we vary n.

Going to higher order in p, we can follow the development of this transition. Thus, we consider next the $p = 3$ TM eigenvalues $k_{n3}^{(2)}a$. The

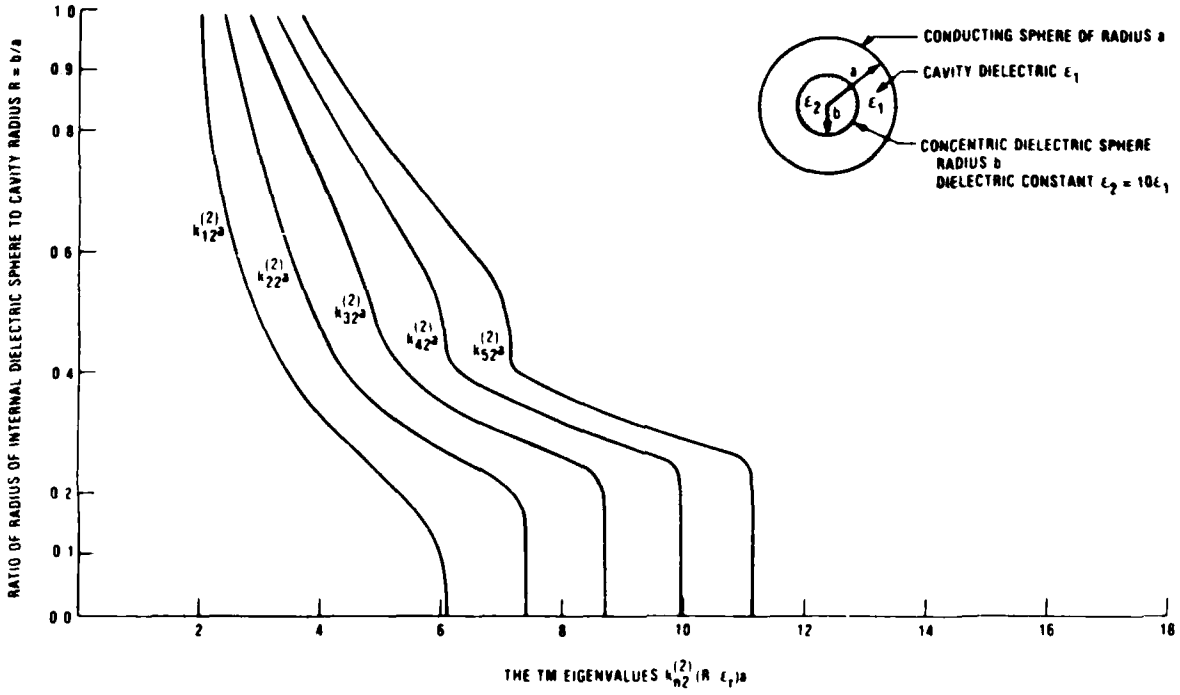

Figure 20. TM eigenvalues $k_{n2}^{(2)}(R{:}\varepsilon_r = 10)\,a$ for the spherical cavity of radius a filled with dielectric ε_1 internally loaded with a concentric dielectric sphere of radius b and strength $\varepsilon_2 = 10\varepsilon_1$.

trajectories are shown in figure 21 for $n = 1$ to $n = 5$, and in table 5(c) are corresponding numerical values. We first compare the TE trajectories $k_{n3}^{(1)}(R{:}\varepsilon_r = 10)\,a$ and the TM trajectories $k_{n3}^{(2)}(R{:}\varepsilon_r = 10)\,a$. All the TE trajectories, as can be seen in figure 8, have increased the number of knees to three for all values of n. Figure 21 reveals two well-defined knees occuring in the TM trajectories for values of $n \leq 4$. The $n = 5$ TM trajectory, $k_{53}^{(2)}(R{:}\varepsilon_r = 10)\,a$, shows just a vestige of a third knee, but at a rather large value of R.

Perhaps as n increases much further, the $k_{n3}^{(2)}a$ will display a clearly defined third knee. If we compare the $k_{n3}^{(2)}a$ trajectories with the TE trajectories $k_{n2}^{(1)}(R{:}\varepsilon_r = 10)\,a$ of figure 7, we observe that for $n = 1$, 2, and 3 the TM trajectories appear to more or less resemble the corresponding TE trajectories. Considerable differences are obvious. Again, we appear to find that a transition in the TM trajectory characteristics is taking place.

Comparing figure 17 for the $k_{n3}^{(2)}(R{:}\varepsilon_r = 3)\,a$ with figure 21 for the $k_{n3}^{(2)}(R{:}\varepsilon_r = 10)\,a$, we see that for $n = 1$ and $n = 2$, the trajectories are similar. For the larger values of n this is no longer the case.

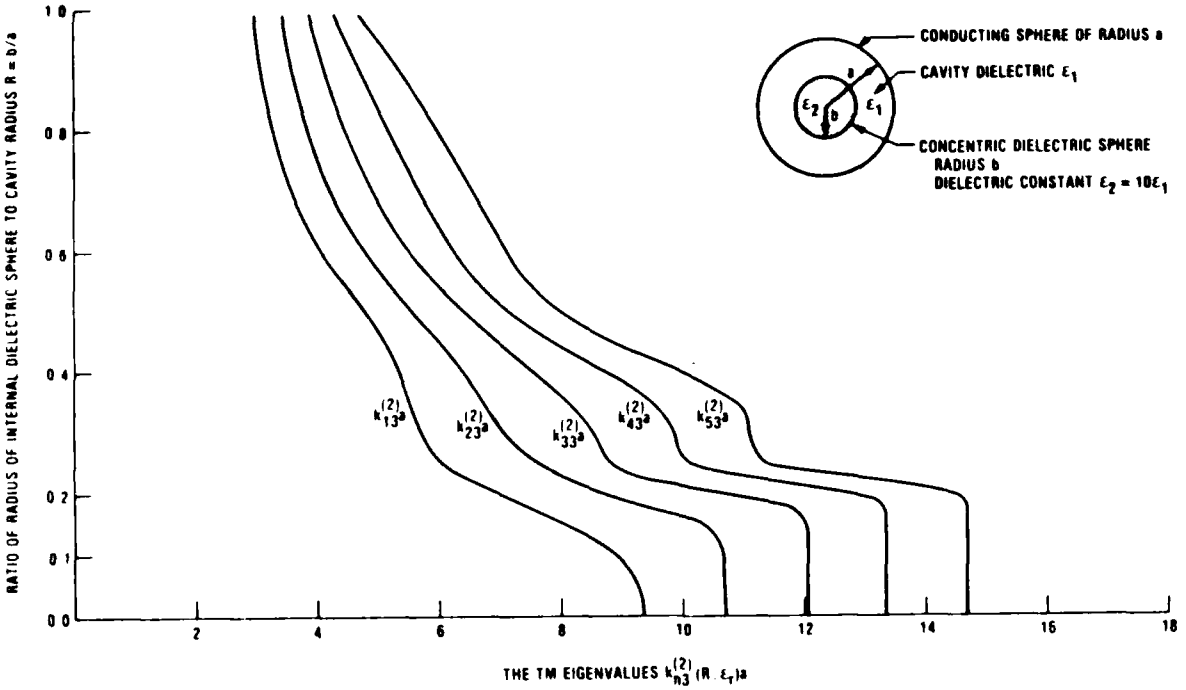

Figure 21. TM eigenvalues $k_{n1}^{(2)}(R:\varepsilon_r = 10)\,a$ for the spherical cavity of radius a filled with dielectric ε_1 internally loaded with a concentric dielectric sphere of radius b and strength $\varepsilon_2 = 10\varepsilon_1$.

For $p = 4$, we find that the same trends continue for the TM trajectories $k_{n4}^{(2)}(R:\varepsilon_r = 10)\,a$. Figure 22 shows these trajectories for n from $n = 1$ to $n = 5$. Table 5(d) contains corresponding numerical values for the eigenvalues $k_{n4}^{(2)}(R:\varepsilon_r = 10)\,a$. Let us start by first making the observation from figure 22 that, for R from about 0.5 up to unity, all the TM trajectories manifest the more familiar behavior as R increases that we had become accustomed to. Furthermore, there are three distinct knees in each curve. In fact, all the familiar features are present in each trajectory. At this value of p, it seems that the transitioning in the behavior of the eigenvalue trajectories has pretty much been completed. Once again we notice upon comparing figure 22 with figure 8 that for the same ε_r the TM eigenvalues for the index p are very similar to the TE eigenvalues belonging to the index one lower in value.

Although we have not calculated $k_{np}^{(2)}(R:\varepsilon_r = 10)\,a$ for $p > 4$, we anticipate that the trend will continue, and the familiar pattern of behavior will result.

We have now seen TM eigenvalues for a substantial range of $\varepsilon_r > 1$ and the corresponding effects due to the strength of the dielectric load.

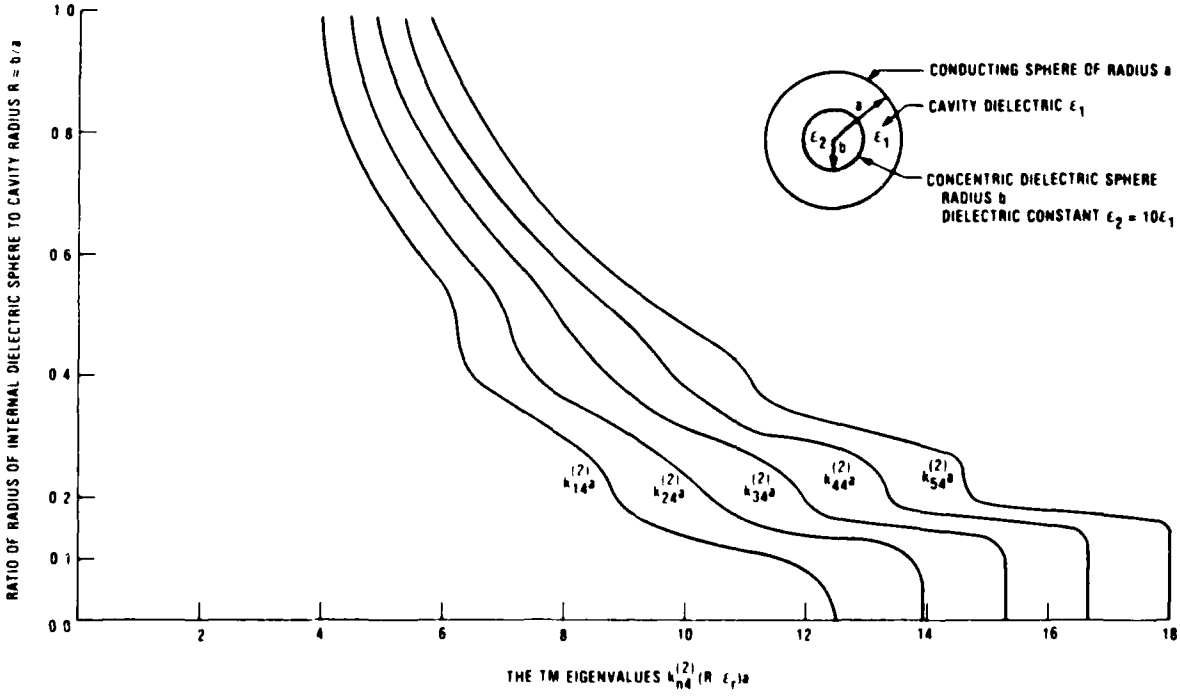

Figure 22. TM eigenvalues $k_{n4}^{(2)}(R;\varepsilon_r = 10)\,a$ for the spherical cavity of radius a filled with dielectric ε_1 internally loaded with a concentric dielectric sphere of radius b and strength $\varepsilon_2 = 10\varepsilon_1$.

4.4 The TM Eigenvalues for $\varepsilon_r = 1/3$

The final TM eigenvalue trajectories we shall consider are those for which we interchange the dielectric strengths within the cavity. We now have the case of $\varepsilon_r = 1/3$. Figure 23 shows the first set of these eigenvalue trajectories corresponding to $p = 1$, namely, the $k_{n1}^{(2)}(R;\varepsilon_r = 1/3)\,a$ for $n = 1$ to $n = 9$. Table 6(a) contains corresponding numerical values.

Note first that for all values of R the TM eigenvalues $k_{n1}^{(2)}(R;\varepsilon_r = 1/3)\,a$ lie lower than the lowest TE eigenvalues for $\varepsilon_r = 1/3$, which are the $k_{11}^{(1)}(R;\varepsilon_r = 1/3)\,a$.

Just as for the TE trajectories $k_{n1}^{(1)}(R;\varepsilon_r = 1/3)\,a$ (compare fig. 11), the TM trajectories of figure 23, $k_{n1}^{(2)}(R;\varepsilon_r = 1/3)\,a$, display the very remarkable feature of increasing very slowly at first as R increases from $R = 0$, and changing even more slowly with R as n increases, for an increasing range of R. Thus, for example, for $n = 9$, $k_{01}^{(2)}\,a$ changes by considerably less than one percent as R changes from $R = 0$ to about $R = 0.65$. This is indeed a very noteworthy feature: the radius of the inner sphere increases to about

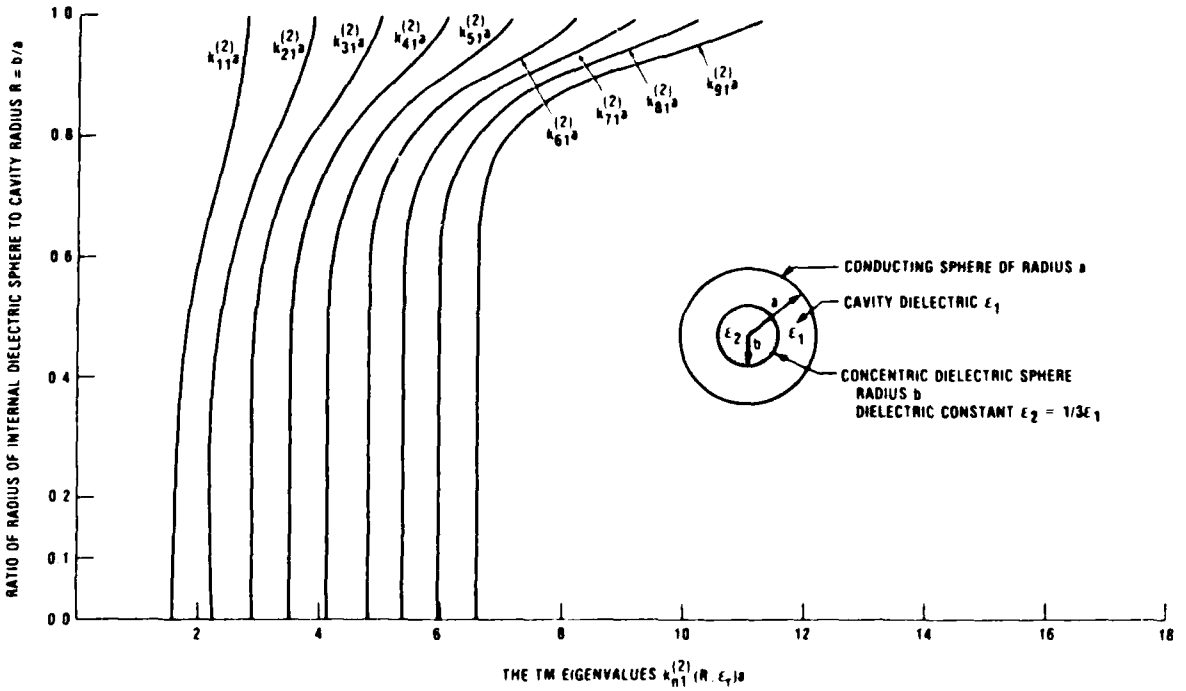

Figure 23. TM eigenvalues $k_{n1}^{(2)}(R{:}\varepsilon_r = 1/3)\,a$ for the spherical cavity of radius a filled with dielectric ε_1 internally loaded with a concentric dielectric sphere of radius b and strength $\varepsilon_2 = 1/3\varepsilon_1$.

Table 6a. Numerical Values of the TM Eigenvalues $k_{n1}^{(2)}(R{:}\varepsilon_r = 1/3)\,a$ for the Spherical Cavity Loaded Internally with a Dielectric Sphere

R=b/a	n=1	n=2	n=3	n=4	n=5
0.05	1.58442	2.23449	2.87141	3.49987	4.12241
0.10	1.58674	2.23456	2.87141	3.49987	4.12241
0.20	1.60414	2.23682	2.87165	3.49989	4.12241
0.30	1.64733	2.24998	2.87488	3.50060	4.12256
0.40	1.72508	2.28995	2.89205	3.50723	4.12494
0.50	1.84634	2.37795	2.94671	3.53842	4.14174
0.60	2.01985	2.54163	3.07754	3.63556	4.21074
0.70	2.24474	2.81645	3.34626	3.87599	4.41647
0.80	2.48256	3.21933	3.84044	4.40321	4.94112

Table 6a. (cont'd) Numerical Values of the TM Eigenvalues $k_{n1}^{(2)}(R;\varepsilon_r = 1/3)\,a$ for the Spherical Cavity Loaded Internally with a Dielectric Sphere

R=b/a	n=1	n=2	n=3	n=4	n=5
0.85	2.58072	3.43959	4.17773	4.82901	5.42371
0.90	2.65484	3.63064	4.51880	5.32948	6.07207
0.95	2.70661	3.77138	4.78887	5.76744	6.71068
0.99	2.73699	3.85265	4.94139	6.01218	7.06961

Table 6a. (cont'd) Numerical Values of the TM Eigenvalues $k_{n1}^{(2)}(R;e_r = 1/3)\,a$ for the Spherical Cavity Loaded Internally with a Dielectric Sphere

R=b/a	n=6	n=7	n=8	n=9
0.05	4.74053	5.35519	5.96705	6.57660
0.10	4.74053	5.35519	5.96705	6.57660
0.20	4.74053	5.35519	5.96705	6.57660
0.30	4.74056	5.35520	5.96706	6.57660
0.40	4.74138	5.35547	5.96714	6.57663
0.50	4.75004	5.35979	5.96924	6.57763
0.60	4.79751	5.39163	5.99017	6.59115
0.70	4.96892	5.53187	6.10334	6.68145
0.80	5.47133	6.00201	6.53679	7.07704
0.85	5.98466	6.52711	7.06061	7.59089
0.90	6.75734	7.39678	8.00117	8.57980
0.95	7.62019	8.49677	9.34098	10.15346
0.99	8.11636	9.15419	10.18427	11.20746

Table 6b. Numerical Values of the TM Eigenvalues $k_{n2}^{(2)}(R;\varepsilon_r = 1/3)\,a$ for the Spherical Cavity Loaded Internally with a Dielectric Sphere

R=b/a	n=1	n=2	n=3	n=4	n=5
0.05	3.53464	4.29732	5.03551	5.75477	6.45996
0.10	3.55430	4.29879	5.03558	5.75477	6.45996
0.20	3.67302	4.33247	5.04234	5.75588	6.46012
0.30	3.89707	4.46871	5.10415	5.77899	6.46766
0.40	4.19283	4.74932	5.30765	5.90625	6.53899
0.50	4.46870	5.16215	5.71318	6.24962	6.80624

Table 6b. (cont'd) Numerical Values of the TM Eigenvalues $k_{n2}^{(2)}(R;\varepsilon_r = 1/3)\,a$ for the Spherical Cavity Loaded Internally with a Dielectric Sphere

R=b/a	n=1	n=2	n=3	n=4	n=5
0.60	4.61418	5.58355	6.30254	6.88120	7.41095
0.70	4.74989	5.83512	6.83170	7.67987	8.38242
0.75	4.91025	5.96067	7.00539	7.98584	8.86366
0.80	5.18611	6.18401	7.20685	8.22912	9.22090
0.85	5.57252	6.58177	7.57069	8.56728	9.57072
0.90	5.92529	7.08509	8.16141	9.18788	10.18974
0.95	6.08487	7.37546	8.60637	9.79266	10.94311
0.99	6.11428	7.43672	8.71029	9.94994	11.16424

Table 6c. Numerical Values of the TM Eigenvalues $k_{n3}^{(2)}(R;\varepsilon_r = 1/3)\,a$ for the Spherical Cavity Loaded Internally with a Dielectric Sphere

R=b/a	n=6	n=7	n=8
0.05	7.15422	7.83968	8.51786
0.10	7.15422	7.83968	8.51786
0.20	7.15424	7.83968	8.51786
0.30	7.15647	7.84029	8.51802
0.40	7.19311	7.85784	8.52595
0.50	7.38866	7.99383	8.61649
0.60	7.93396	8.46664	9.01445
0.70	8.98304	9.52724	10.04568
0.75	9.62647	10.28862	10.87838
0.80	10.15707	11.01921	11.79863
0.85	10.57054	11.55457	12.51114
0.90	11.18270	12.17409	13.16565
0.95	12.06366	13.15887	14.23260
0.99	12.35869	13.53702	14.70191

Table 6c. (cont'd) Numerical Values of the TM Eigenvalues $k_{n3}^{(2)}(R;\varepsilon_r = 1/3)\,a$ for the Spherical Cavity Loaded Internally with a Dielectric Sphere

R=b/a	n=1	n=2	n=3	n=4
0.05	5.38931	6.18546	6.96492	7.72502
0.10	5.44748	6.19321	6.96554	7.72506
0.20	5.72571	6.32290	7.00705	7.73533

Table 6c. (cont'd) Numerical Values of the TM Eigenvalues $k_{n3}^{(2)}(R;\varepsilon_r = 1/3)\,a$ for the Spherical Cavity Loaded Internally with a Dielectric Sphere

R=b/a	n=1	n=2	n=3	n=4
0.30	6.11831	6.68514	7.24937	7.86803
0.40	6.40685	7.20440	7.77256	8.30556
0.45	6.47571	7.44291	8.11120	8.65427
0.50	6.56969	7.61158	8.44730	9.06910
0.55	6.76217	7.74247	8.71475	9.49613
0.60	7.08112	7.94254	8.91417	9.84700
0.65	7.48305	8.30227	9.17317	10.11814
0.70	7.81542	8.79397	9.62997	10.48509
0.75	7.93460	9.17657	10.21325	11.10187
0.80	7.96052	9.28267	10.53328	11.67875
0.85	8.14174	9.37617	10.61980	11.85040
0.90	8.71535	9.87300	11.00993	12.14933
0.95	9.23482	10.57775	11.86018	13.09449
0.99	9.31459	10.70821	12.05511	13.36718

Table 6c. (cont'd) Numerical Values of the TM Eigenvalues $k_{n3}^{(2)}(R;\varepsilon_r = 1/3)\,a$ for the Spherical Cavity Loaded Internally with a Dielectric Sphere

R=b/a	n=5	n=6	n=7
0.05	8.46980	9.20221	9.92439
0.10	8.46980	9.20221	9.92439
0.20	8.47191	9.20259	9.92446
0.30	8.53397	9.22811	9.93390
0.40	8.86157	9.45259	10.07624
0.45	9.17901	9.72119	10.29060
0.50	9.60272	10.11856	10.64437
0.55	10.11024	10.64454	11.15398
0.60	10.62833	11.26444	11.81449
0.65	11.04319	11.86359	12.55689
0.70	11.39681	12.32197	13.19962
0.75	11.94870	12.81932	13.72198
0.80	12.70426	13.63031	14.50499
0.85	13.05176	14.21104	15.31727
0.90	13.29621	14.44773	15.59905
0.95	14.28938	15.45194	16.58848
0.99	14.65198	15.91469	17.15903

Table 6d. Numerical Values of the TM Eigenvalues $k_{n4}^{(2)}(R;\varepsilon_r = 1/3)\,a$ for the Spherical Cavity Loaded Internally with a Dielectric Sphere

R=b/a	n=1	n=2	n=3	n=4	n=5	n=6
0.05	7.23212	8.03807	8.84132	9.62683	10.39723	11.15508
0.10	7.34737	8.06208	8.84414	9.62706	10.39725	11.15508
0.20	7.79088	8.35000	8.97442	9.67251	10.41008	11.15814
0.30	8.20645	8.93072	9.47653	10.02946	10.62925	11.27669
0.35	8.29921	9.22891	9.84606	10.37672	10.91752	11.49413
0.40	8.42530	9.44257	10.23331	10.81339	11.33429	11.85969
0.45	8.69580	9.60117	10.55160	11.28459	11.85562	12.37088
0.50	9.10309	9.86534	10.78236	11.68733	12.41425	12.99682
0.55	9.52710	10.31643	11.09718	11.99178	12.88249	13.64077
0.60	9.74453	10.83041	11.63100	12.40714	13.26524	14.15221
0.65	9.78081	11.09210	12.20129	13.06583	13.84316	14.65510
0.70	10.00693	11.16375	12.41521	13.59417	14.60022	15.45226
0.75	10.61125	11.56821	12.60217	13.74771	14.93253	16.07729
0.80	11.08410	12.30813	13.35163	14.31296	15.29773	16.34951
0.85	11.14081	12.53845	13.87439	15.13166	16.29569	17.36492
0.90	11.41012	12.69611	13.98595	15.27241	16.54870	17.80976
0.95	12.29011	13.63758	14.92764	16.17285	17.38395	18.57040
0.99	12.48354	13.91571	15.30558	16.66232	17.99221	19.29977

2/3 of the cavity radius with almost no change in the eigenvalue of the system. As is to be expected, as R increases beyond this range, $k_{n1}^{(2)}a$ increases more rapidly with R. This rate of increase is amplified further with increasing n. Although this is quite similar to the behavior of the TE eigenvalues $k_{n1}^{(1)}(R{:}\varepsilon_r = 1/3)\,a$ as R becomes nearly unity, the two sets of trajectories display deviant behavior. Whereas the $k_{n1}^{(1)}a$ slow up abruptly for the upper range of R, the $k_{n1}^{(2)}a$ appear to continue smoothly and gradually.

Increasing p to 2, we obtain from equation (36) the TM eigenvalues $k_{n2}^{(2)}(R{:}\varepsilon_r = 1/3)\,a$, whose trajectories for each value of the index n are shown in figure 24, where n goes from $n = 1$ to $n = 9$. Corresponding numerical values are given in table 6(b). Comparison of the TM trajectories of figure 24 with those of the $k_{n1}^{(2)}a$ in figure 23 reveals that for p = 2 a dent appears in each curve. The dent appears in the midrange of R for n = 1. As n increases, the range of R decreases over which the dent is present. Furthermore, the dent moves to higher R values; that is, it is present for larger inner spheres, as n increases. Finally, we observe in figure 24, at the higher values of n, the dent in the trajectories $k_{n2}^{(2)}a$ seems to be washing out. Again comparing the eigenvalue trajectories in figure 24 with those in figure 23 we see that prior to the region of the dent, i.e., for lower R values, the curves are quite similar. However, the initial range of R, for which the $k_{n2}^{(2)}a$ values seem to change only very, very slowly with increasing R, decreases substantially compared to the corresponding range for the $k_{n1}^{(2)}a$ trajectories. At the upper end of the range of R, we note that the $k_{n2}^{(2)}(R{:}\varepsilon_r = 1/3)\,a$ trajectories increase slightly faster than the $k_{n1}^{(2)}(R{:}\varepsilon_r = 1/3)\,a$ curves.

Consider next the $p = 3$ TM eigenvalue trajectories, $k_{n3}^{(2)}(R{:}\varepsilon_r = 1/3)\,a$, for $n = 1$ to $n = 7$ shown in figure 25. Table 6(c) gives numerical values for the eigenvalues $k_{n3}^{(2)}(R{:}\varepsilon_r = 1/3)\,a$. A second indentation is now seen in each trajectory. For $n = 1$, the dents appear at about one-third and two-thirds of the range of R. As n increases, these dents move to higher R value, with the lower-lying one washing out rather rapidly as n increases. We also observe that the initial range of R, over which each trajectory displays a very slow increase with increasing R, shortens up as p increases. It is also of interest to compare the trajectories for $k_{n3}^{(2)}(R{:}\varepsilon_r = 1/3)\,a$ in figure 25 with the TE trajectories for $k_{n3}^{(1)}(R{:}\varepsilon_r = 1/3)\,a$ in figure 13. Both sets

have two indentations. Indeed, both sets are very similar in detail. Note that the TM eigenvalue trajectories tend to lose the sharpness of the indentation characteristic, compared to those in the TE trajectories of figure 13.

The final set of eigenvalue trajectories calculated from equation (36) that we consider is the curves plotted in figure 26 for $p = 4$, i.e., the TM trajectories $k_{n4}^{(2)}(R;\varepsilon_r = 1/3)\,a$ for $n = 1$ to $n = 6$. Numerical values for these eigenvalues are in table 6(d). Each eigenvalue trajectory now has three indentations, each successively shifted upward in R in quarterly intervals in R. Just as we saw for the lower values of the index p, the distinctness of these indentations in the trajectories fades out as n increases, with the lower ones fading faster for a given value of n. Again we observe that the initial slow increase with R for the early range of R has decreased as we increase p. We further see that increasing the index p results in predictable changes in the $k_{n4}^{(2)}a$ trajectories. Finally, we can compare the $k_{n4}^{(2)}(R;\varepsilon_r = 1/3\,)\,a$ trajectories of figure 26 with the TE $k_{n4}^{(1)}(R;\varepsilon_r = 1/3)\,a$ trajectories of figure 14. Clearly they look very much alike. Notice that the TE trajectories are shifted up in ka relative to the TM trajectories.

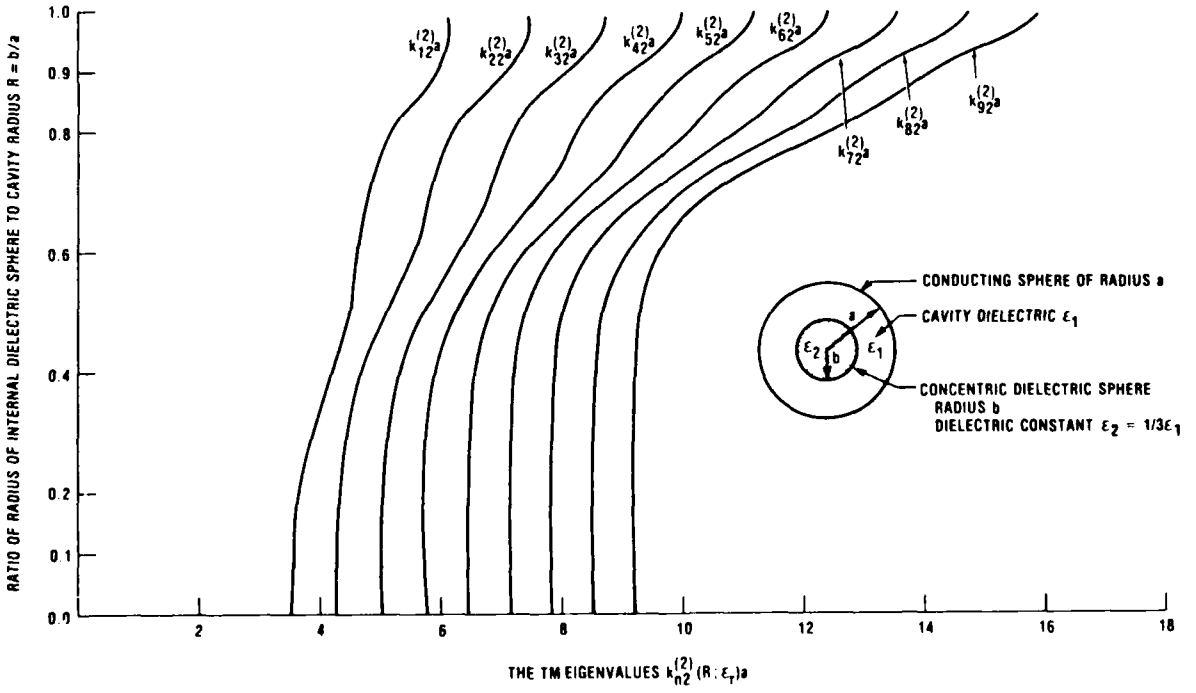

Figure 24. TM eigenvalues $k_{n2}^{(2)}(R;\varepsilon_r = 1/3)\,a$ for the spherical cavity of radius a filled with dielectric ε_1 internally loaded with a concentric dielectric sphere of radius b and strength $\varepsilon_2 = 1/3\varepsilon_1$.

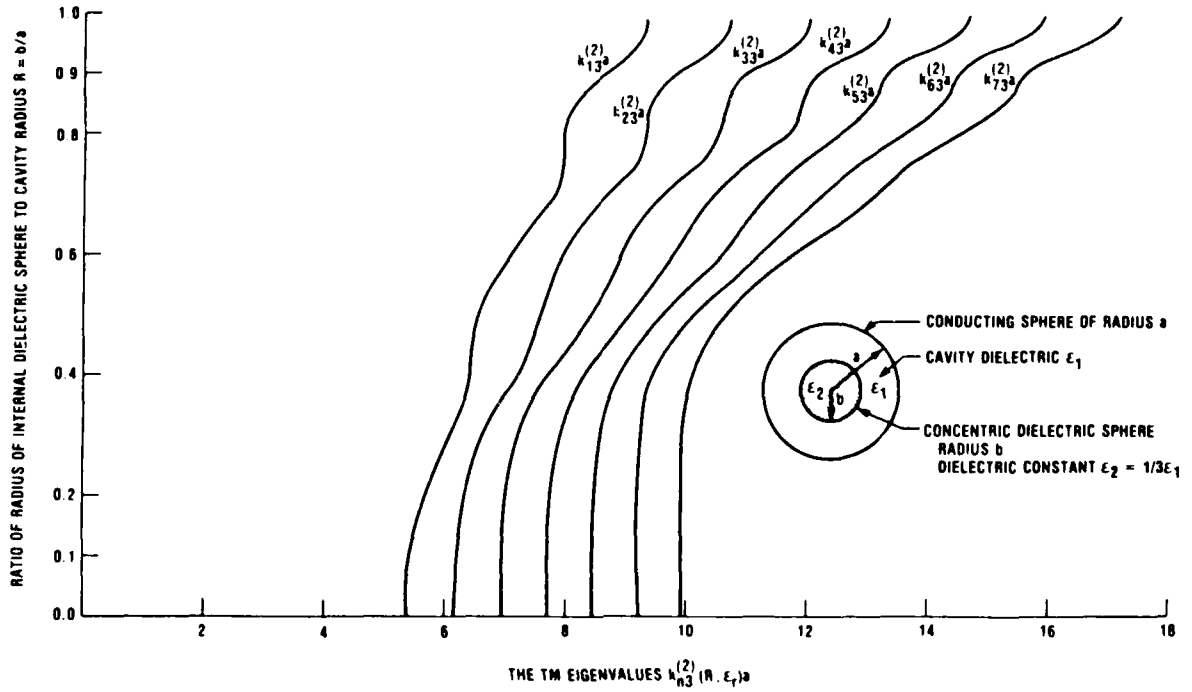

Figure 25. TM eigenvalues $k_{n3}^{(2)}(R;\varepsilon_r = 1/3)\,a$ for the spherical cavity of radius a filled with dielectric ε_1 internally loaded with a concentric dielectric sphere of radius b and strength $\varepsilon_2 = 1/3\varepsilon_1$.

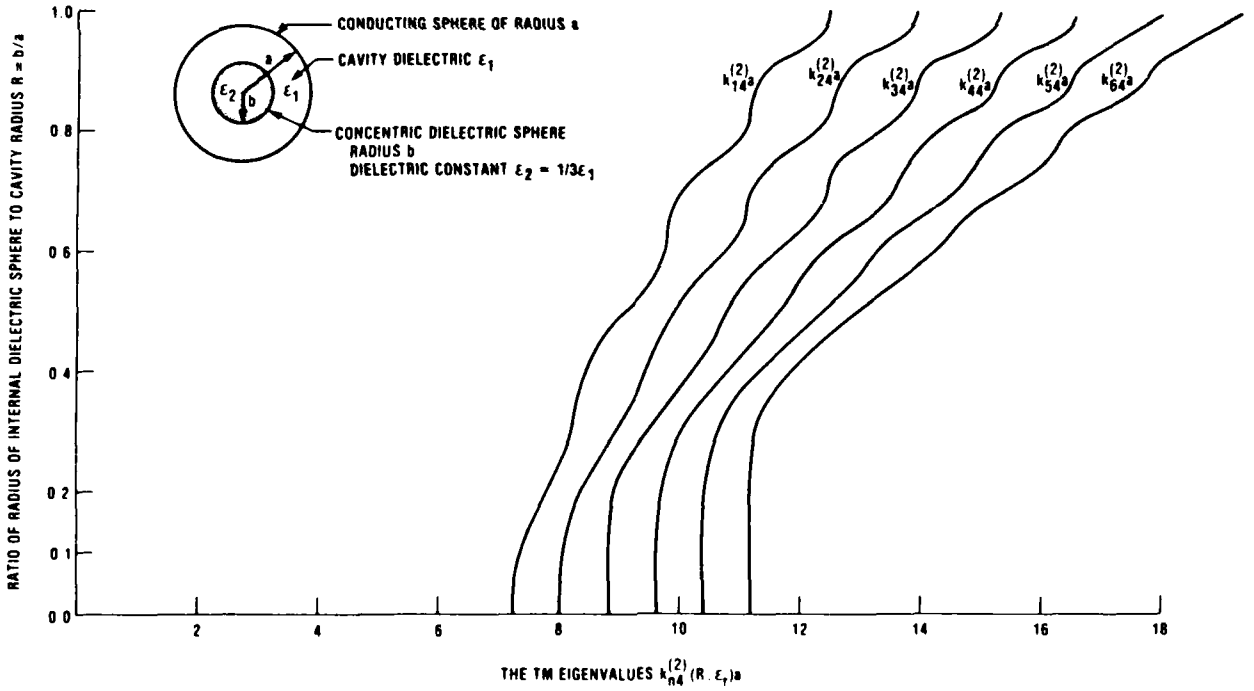

Figure 26. TM eigenvalues $k_{n4}^{(2)}(R;\varepsilon_r = 1/3)\,a$ for the spherical cavity of radius a filled with dielectric ε_1 internally loaded with a concentric dielectric sphere of radius b and strength $\varepsilon_2 = 1/3\varepsilon_1$.

Further increasing the index will add additional indentations to the trajectories. Otherwise, the trends already discerned will merely continue to manifest themselves. This will be the case if the dielectric system is the same. Changing the relative dielectric strengths with $\varepsilon_r < 1$ may introduce some new variations in the eigenvalue trajectories. Since we have not investigated this aspect of the eigenvalue problem for the generic system studies, we shall not go any further into this.

5. Summary and Discussion

5.1 General Summary

We have examined a very large number of eigenvalues calculated from equations (32) and (36). We shall now summarize briefly the general characteristics we have found for these eigenvalues. First, for $\varepsilon_r > 1$, all the eigenvalue trajectories are monotonically decreasing as R increases—i.e., as the inner load sphere increases in size. On the other hand, for relative dielectric strength $\varepsilon_r < 1$, the eigenvalue trajectories increase monotonically as the inner sphere grows. Increasing the index p by unity adds a knee to the TE as well as TM trajectories for $\varepsilon_r > 1$. Although for large ε_r the TM trajectories do not always show this knee, it is present for small enough n. For $\varepsilon_r < 1$, an identation is added instead.

Note that the knee and the indentation shift the trajectory toward lower ka values for TE and TM eigenvalues, but preserve the monotonicity of the trajectory.

We have seen that regardless of the size of the internal sphere loading the dielectric-filled spherical cavity, and for the chosen values of the dielectric strengths of the load sphere and the medium filling the cavity, the lowest-lying mode, or fundamental mode, of the system will be the TM eigenvalue $k_{11}^{(2)}(R;\varepsilon_r)\,a$.

Some quite remarkable behavior is manifested by the eigenvalues as the size of the inner dielectric sphere loading the cavity varies. We observed short and long ranges in the size of the inner dielectric sphere for which the eigenvalue exhibits virtually no significant change at all, as well as such ranges of R over which the eigenvalue changed at a very rapid rate. For many of the higher order eigenvalues several such regions of behavior have been seen following one after another. This is an unanticipated characteristic for the cavity system.

It is of interest to compare the rich variety of behavior seen for the eigenvalues of the dielectric loaded cavity with the homogeneously filled concentric conducting cavity eigenvalues [1]. Clearly for small values of R, as is to be expected, the two different cavity systems show the same kind of behavior. Except for lower order TM eigenvalues $k_{n1}^{(2)}a$ with $\varepsilon_r > 1$, the eigenvalues for the two cavity systems are markedly different in their dependence on R, the size of the inner interface radius.

Up to this point, we have constrained all our considerations to individual families of eigenvalue trajectories for the different ε_r values; i.e., we have fixed the index p and examined the set of curves for various ranges of the index n. One very clear feature of these sets is that the curves in each family of trajectories do not intersect. Unfortunately, this does not yet give a complete enough picture of the eigenvalue trajectory characteristics. We shall now proceed to consider the features of the eigenvalues and their variations as R and ε_r change by superimposing, for each given ε_r, first all the TE and then all the TM eigenvalues.

5.2 Overview of the TE and TM Eigenvalues for $\varepsilon_r = 3.00$

We have redrawn in figure 27 a superposition of the previously given 17 TE eigenvalue trajectories for the inner sphere of dielectric constant $\varepsilon_2 = 3\varepsilon_1$. It now is immediately evident that many of the trajectories do intersect one another. It is very important to emphasize that each point of intersection of any two eigenvalue trajectories represents a degenerate pair of eigenvalues. And this degeneracy occurs for the given values of ε_r at specific sizes, R, of the internal load sphere. Figure 27 shows explicitly only TE-TE intersections.

Let us begin a systematic examination of the patterns associated with the intersection points of the eigenvalue trajectories for the $k_{np}^{(1)}(R;\varepsilon_r = 3)a$. We first note that for $\varepsilon_r = 3$, $k_{11}^{(1)}a$ and $k_{21}^{(1)}a$ are not degenerate with any other TE eigenvalues. However, $k_{21}^{(1)}a$ and $k_{12}^{(1)}a$ approach each other at the single knee of $k_{21}^{(1)}a$, and the bottom of the second slow decrease with rising R in $k_{12}^{(1)}a$ with increasing R. In fact, we observe this as a general pattern with $k_{n1}^{(1)}a$ lying close to $k_{n-1,2}^{(1)}a$ in the corresponding region. As n increases, this separation decreases. Thus, at $n = 5$ the two trajectories almost intersect one another. Although it is not explicitly shown for $n > 5$, a pair of intersections will indeed occur in this corresponding region of R and, as n increases, the pair of intersections will move apart. This same

for the pairs $k_{np}^{(1)}a$ and $k_{n-1,p+1}^{(1)}a$ starting, for $\varepsilon_r = 3$, with $n = 2$ and for all p. A similar characteristic also occurs for the trajectories of $k_{22}^{(1)}a$ and $k_{13}^{(1)}a$ at the second knee and the region of R corresponding to the third slow decrease as R increases. This will be true in general for the pairs of trajectories $k_{np}^{(1)}a$ and $k_{n-1,p+1}^{(1)}a$ for $n \geq 2$. Clearly for the higher order trajectories this pattern of behavior will be repeated at larger R values corresponding to higher lying knees on $k_{np}^{(1)}a$ and higher lying, slowly varying regions of $k_{n-1,p+1}^{(1)}a$.

Next consider the eigenvalue trajectory pair of $k_{12}^{(1)}a$ and $k_{31}^{(1)}a$. It is plain to see in figure 27 that they are degenerate at two quite distinct values of R. What we are seeing is that there are two sizes for the inner dielectric sphere at which the system has $k_{12}^{(1)}a = k_{31}^{(1)}a$. One is at R just under 0.6 and the other is at R just under 0.7. After a little study of figure 27, we observe that, for n > 1, the trajectories for $k_{np}^{(1)}a$ and $k_{n+2,p-1}^{(1)}a$ are similarly degenerate at higher R values, in pairs of R. Clearly these eigenvalue trajectories are degenerate at two and only two R values.

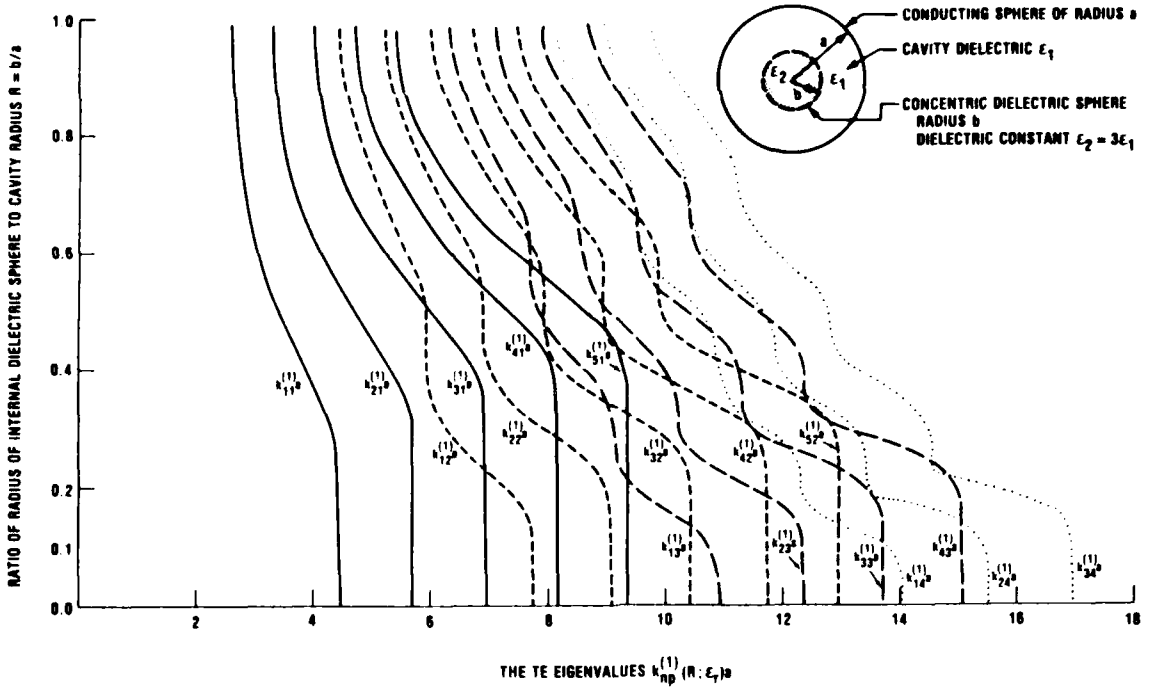

Figure 27. A composite of the TE eigenvalues $k_{np}^{(1)}(R;\varepsilon_r = 3)a$ for the spherical cavity of radius a filled with dielectric ε_1 internally loaded with a concentric dielectric sphere of radius b and strength $\varepsilon_2 = 3\varepsilon_1$.

It should be noted that the trajectories for $k_{12}^{(1)}a$ and $k_{31}^{(1)}a$ intersect at only the two points already indicated and the trajectories have no other degeneracies. The trajectories for $k_{22}^{(1)}a$ and $k_{41}^{(1)}a$ behave in the very same manner. From this point on, the trajectories of higher order radius will display a larger number of degeneracies. Thus the trajectory for $k_{51}^{(1)}a$ intersects that for $k_{32}^{(1)}a$ twice and that for $k_{13}^{(1)}a$ twice. The $k_{13}^{(1)}a$ trajectory also intersects the $k_{32}^{(1)}a$ trajectory four times. This degree of degeneracy becomes high rather rapidly. Thus for example, the trajectory for $k_{14}^{(1)}a$ is degenerate with the $k_{33}^{(1)}a$ trajectory for six different sizes of the inner dielectric load sphere. It should be evident that as ka exceeds about $ka \approx 8$ for mid-range values of R, the density of TE-TE degenerate modes can become rather large.

Before leaving the TE eigenvalues for $\varepsilon_r = 3$, we point out a very important feature. Although the characteristics of the eigenvalue trajectories may become quite interesting in detail for $0 < R < 1$, the sequence of eigenvalues at $R = 1$ is exactly the same as the sequence in which the eigenvalues occur at $R = 0$. In general there is a downward shift in the eigenvalues as R increases from zero up to unity.

Next let us examine the twenty-one TM eigenvalue trajectories which were expounded for $\varepsilon_r = 3$ in about the same detail. We first observe that the eigenvalue trajectories $k_{11}^{(2)}a$ and $k_{21}^{(2)}a$ exhibit no degeneracy whatever; $k_{31}^{(2)}a$ has only two degenerate values, both with $k_{12}^{(2)}a$. Note that $k_{41}^{(2)}a$ also has two degenerate values, both with $k_{12}^{(2)}a$. But $k_{41}^{(2)}a$ also has two degenerate values with $k_{22}^{(2)}a$ for a total of four degeneracies (at values of R of about 0.1, 0.4, 0.8, and 0.99). The trajectory for $k_{12}^{(2)}a$ exhibits four degeneracies and that for $k_{22}^{(2)}a$ also shows four sizes of internal sphere at which degenerate eigenvalues occur. As we go to higher order indices n,p the number of degeneracies rises rather rapidly. Thus $k_{51}^{(2)}a$ has two degeneracies with each of the trajectories for $k_{22}^{(2)}a$, $k_{13}^{(2)}a$, and $k_{32}^{(2)}a$ for a total of six degenerate sets.

Now we observe that for values of $ka \gtrsim 7$ the density of TM-TM degeneracies can become rather large. This holds for nearly the entire range of R. Again we note that the sequence of TM eigenvalues at $R = 0$ is preserved at $R = 1$ regardless of the behavior over intermediate R values. A general shift to lower ka values is evident for the eigenvalues as R increases.

We have thus far only separately considered TE-TE and TM-TM degeneracies. The complete picture requires taking into account TE-TM degeneracies for $\varepsilon_r = 3$. We now proceed to consider this aspect of the eigenvalue distribution. We will carry this out without attempting to show a superposition of all the TE and TM eigenvalues in one figure.

Now the only eigenvalue trajectory that does not have any degeneracies is that for the TM $k_{11}^{(2)}a$. The TE eigenvalue $k_{11}^{(1)}a$ and the TM eigenvalue $k_{21}^{(2)}a$ are both degenerate, intersecting at about $R = 0.45$ and at about $R = 0.8$. These are the only degeneracies for these eigenvalues. These two eigenvalue trajectories are the next lowest lying ones, with $k_{21}^{(2)}a$ lying below $k_{11}^{(1)}a$ for $0 < R \lesssim 0.45$ and $0.8 \lesssim R \leq 1$ and interchanging their order for the intermediate range of R. The trajectory for the TM eigenvalue $k_{31}^{(2)}a$ is not only doubly degenerate with the TM eigenvalue $k_{12}^{(2)}a$, but also intersects the TE eigenvalue trajectory $k_{21}^{(1)}a$ twice, first at about $R = 0.5$ and then at about $R = 0.85$. The order of occurrence of these eigenvalues at $R = 0$ is preserved at $R = 1$. In the intermediate range of R, examination of figures 27 and 28 shows that their order changes as R increases. Inspection of figures 27 and 28 shows that once we get beyond the TM eigenvalues $k_{11}^{(2)}a$ and $k_{21}^{(2)}a$ and the TE eigenvalue $k_{11}^{(1)}a$ a considerable amount of degeneracy appears, along with shifting around in sequence of the higher order eigenvalues. Furthermore, as ka increases into this region, there appears a rapid rise in the density of the combined TE and TM eigenvalues. Careful inspection of the figures reveals a considerable regularity in the occurrence of intersections of the set of combined trajectories. We will not elaborate any further on this subject.

Having seen the considerable complexity in the set of combined TE and TM eigenvalue trajectories for $\varepsilon_r = 3$, we next turn to considering the changes that result from varying the strength of the dielectric sphere loading the cavity.

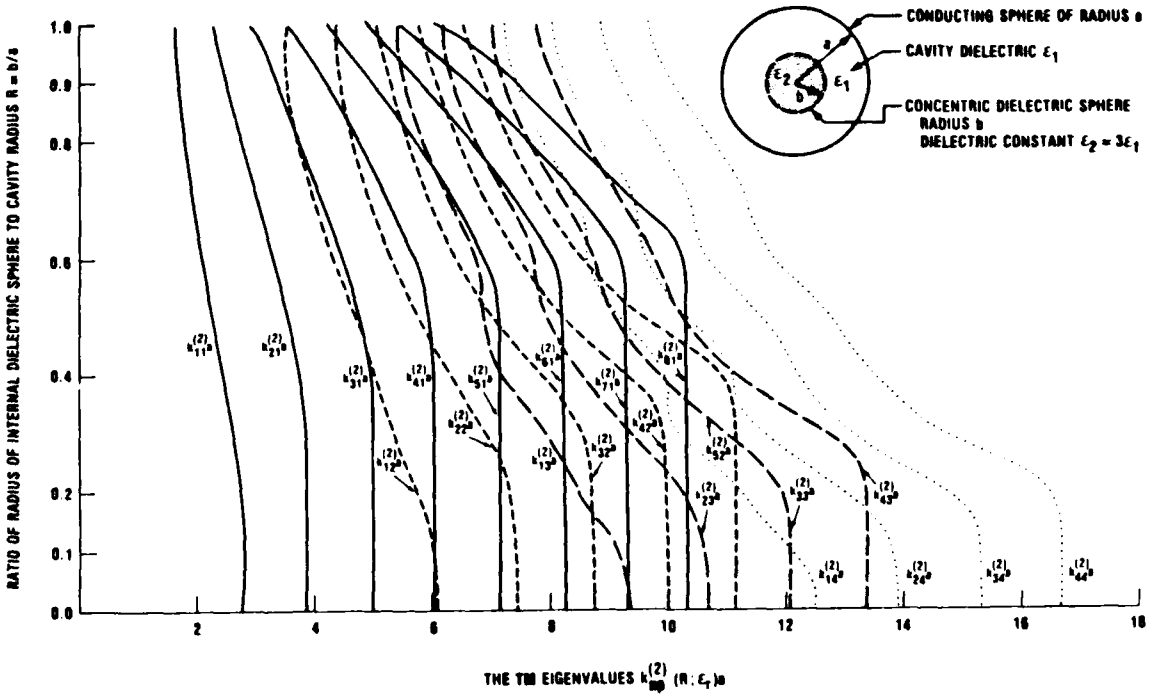

Figure 28. A composite of the TM eigenvalues $k_{np}^{(2)}(R;\varepsilon_r = 3)\,a$ for the spherical cavity of radius a filled with dielectric ε_1 internally loaded with a concentric dielectric sphere of radius b and strength $\varepsilon_2 = 3\varepsilon_1$.

5.3 Overview of the TE and TM Eigenvalues for $\varepsilon_r = 10.00$

Next we shall examine the superposition in figure 29 of the set of twenty-two TE eigenvalues, which we considered individually earlier. We now assume the inner dielectric sphere to be of strength $\varepsilon_2 = 10\varepsilon_1$. In figure 29 for $\varepsilon_r = 10$, we see that only the eigenvalue trajectory $k_{11}^{(1)}\,a$ has no intersections with any other TE trajectory. Recall that for $\varepsilon_r = 3$ there were two such eigenvalue trajectories.

The $k_{11}^{(1)}(R;\varepsilon_r = 10)\,a$ trajectory nearly coincides with the $k_{11}^{(1)}(R;\varepsilon_r = 3)\,a$ trajectory for the approximate range $0 < R \lesssim 0.15$. For higher R values, the $k_{11}^{(1)}(R;\varepsilon_r = 10)\,a$ trajectory lies lower. We also note that the eigenvalue trajectory for $k_{11}^{(1)}\,a$ at its knee lies near the eigenvalue trajectory for $k_{12}^{(1)}\,a$ just beyond its first knee and where it begins its slowly decreasing region with increasing R. This is true in the same R region in general for the eigenvalue pairs $k_{n1}^{(1)}\,a$ and $k_{n2}^{(1)}\,a$ for all $n \geq 1$. Although we have not explicitly shown it in figure 29, there will be a value of n where this set of trajectories intersects and continues to do so for all higher values of the index n. Many similar pairs of trajectories exhibit this same behavior, as can be seen by careful study of figure 29. We shall not go into this in any fur-

ther detail. We shall instead examine a further complexity in the degeneracy of the eigenvalues.

The TE eigenvalue trajectory $k_{21}^{(1)}a$ intersects the TE trajectory for $k_{12}^{(1)}a$ for two sizes of internal dielectric sphere load—at about $R = 0.15$ and at about $R = 0.25$. Note that $k_{21}^{(1)}a$ shows TE-TE degeneracy only at these two values. The eigenvalue trajectory for $k_{31}^{(1)}a$ has two points of degeneracy with the trajectory for $k_{12}^{(1)}a$—at about $R = 0.13$ and $R = 0.35$. It also has two points of degeneracy with the trajectory for $k_{22}^{(1)}a$—at about $R = 0.2$ and $R = 0.3$. Thus the eigenvalues $k_{31}^{(1)}a$ and $k_{12}^{(1)}a$ each have TE-TE degeneracy at four sizes of internal sphere load. Note that the points of degeneracy for these occur only for relatively small internal spheres. The situation really increases in complexity very rapidly as we go to higher order eigenvalues. Thus the eigenvalue $k_{41}^{(1)}a$ displays six TE-TE degenerate situations, and $k_{22}^{(1)}a$ also shows six such degeneracies. The eigenvalue $k_{51}^{(1)}a$ shows 10 TE-TE degeneracies. Clearly the number of TE-TE degeneracies is growing rapidly. We note that up to about $ka = 7$, the density of TE-TE degeneracies is rather substantial, but only for R values up to about 0.5. For higher ka values, this high density of TE-TE degeneracies spreads to much larger R values. What we are seeing is the general

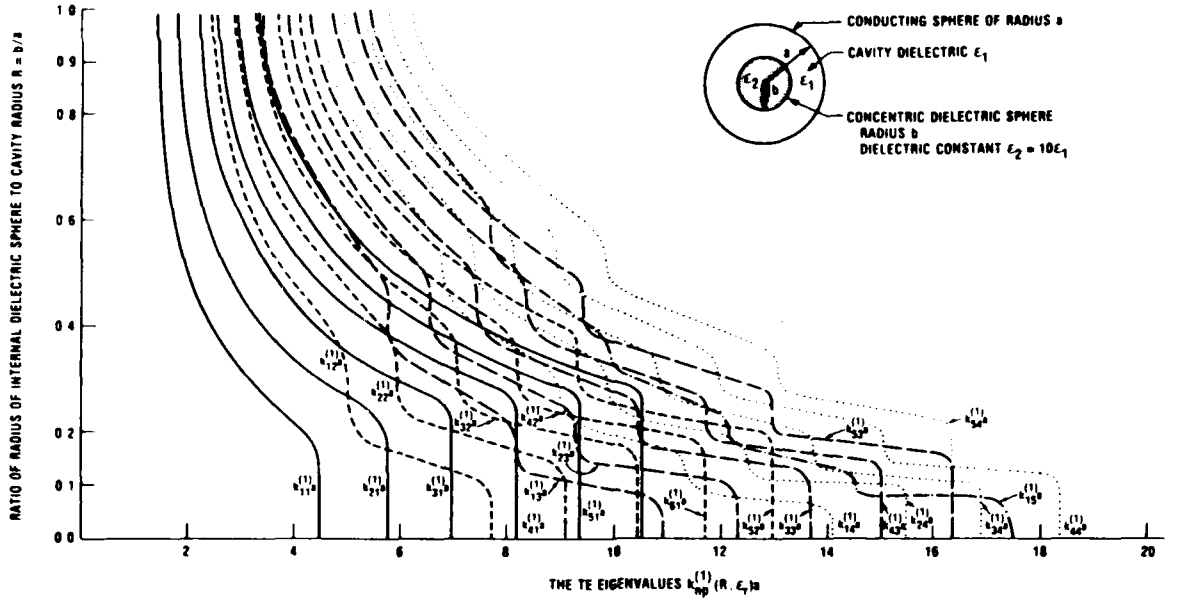

Figure 29. A composite of the TE eigenvalues $k_{np}^{(1)}(R;\varepsilon_r = 10)a$ for the spherical cavity of radius a filled with dielectric ε_1 internally loaded with a concentric dielectric sphere of radius b and strength $\varepsilon_2 = 10\varepsilon_1$.

tendency of the eigenvalues to move to lower ka as ϵ_r increases, with the higher order trajectories moving farther.

Figure 30 contains the superposition of all the twenty-three TM eigenvalue trajectories, $k_{np}^{(2)}(R{:}\epsilon_r = 10)\,a$, which we examined earlier in sets of eigenvalues for fixed index p. Let us examine figure 30 for TM-TM degeneracy. The first feature to note is that only one eigenvalue trajectory does not intersect any other, namely, the $k_{11}^{(2)}(R{:}\epsilon_r = 10)\,a$. Thus, in going from $\epsilon_r = 3$ to $\epsilon_r = 10$, the number of eigenvalues that have no trajectories with TM-TM degeneracy is reduced from two to only one. The eigenvalue curve $k_{21}^{(2)}a$, which exhibits no TM-TM degeneracy for $\epsilon_r = 3$, now has, for $\epsilon_r = 10$, degeneracy with $k_{12}^{(2)}(R{:}\epsilon_r = 10)\,a$ at about $R = 0.35$ and $R = 0.65$. These intersections are the only internal sphere radii at which $k_{12}^{(2)}a$ has TM-TM degeneracy. There are four TM-TM degeneracies for $k_{31}^{(2)}a$. Two are with $k_{12}^{(2)}a$ near $R = 0.25$ and $R = 0.95$, corresponding, respectively, to a small and a large load sphere in the interior, and two with $k_{22}^{(2)}a$ are at about $R = 0.30$ and $R = 0.55$, corresponding in both instances to intermediate-size inner dielectric spheres. Next we see that the trajectory of eigenvalues $k_{21}^{(2)}a$ has six points of intersection, with a total of three other TM eigenvalue trajectories. (There are two degeneracies with each of $k_{21}^{(2)}a$, $k_{31}^{(2)}a$, and $k_{41}^{(2)}a$.) Also, the degeneracies occur for inner load spheres whose sizes spread over almost the whole range of R. It is of interest also that for small inner spheres up to about $R = 0.10$, the eigenvalues $k_{41}^{(2)}a$ and $k_{12}^{(2)}a$ are very close to one another.

Going up in order, the eigenvalue $k_{41}^{(2)}a$ has a trajectory with eight intersections with other TM eigenvalue trajectories. It has two intersections with each of $k_{12}^{(2)}a$, $k_{13}^{(2)}a$, $k_{22}^{(2)}a$, and $k_{32}^{(2)}a$. Again, we can readily see that these degeneracies correspond to inner sphere radii almost over the whole range of R. From about $R = 0.60$ to about $R = 0.70$, $k_{41}^{(2)}a$ and $k_{13}^{(2)}a$ are very nearly equal. Thus we see the feature of two ranges in R for which the eigenvalue trajectory for $k_{41}^{(2)}a$ is close to degeneracy. If we continue to examine the higher order eigenvalue trajectories, e.g., $k_{51}^{(2)}a$, we find twelve TM-TM degeneracies of a large variety of characteristics. Clearly the TM-TM degeneracy picture is becoming considerably involved rather rapidly now.

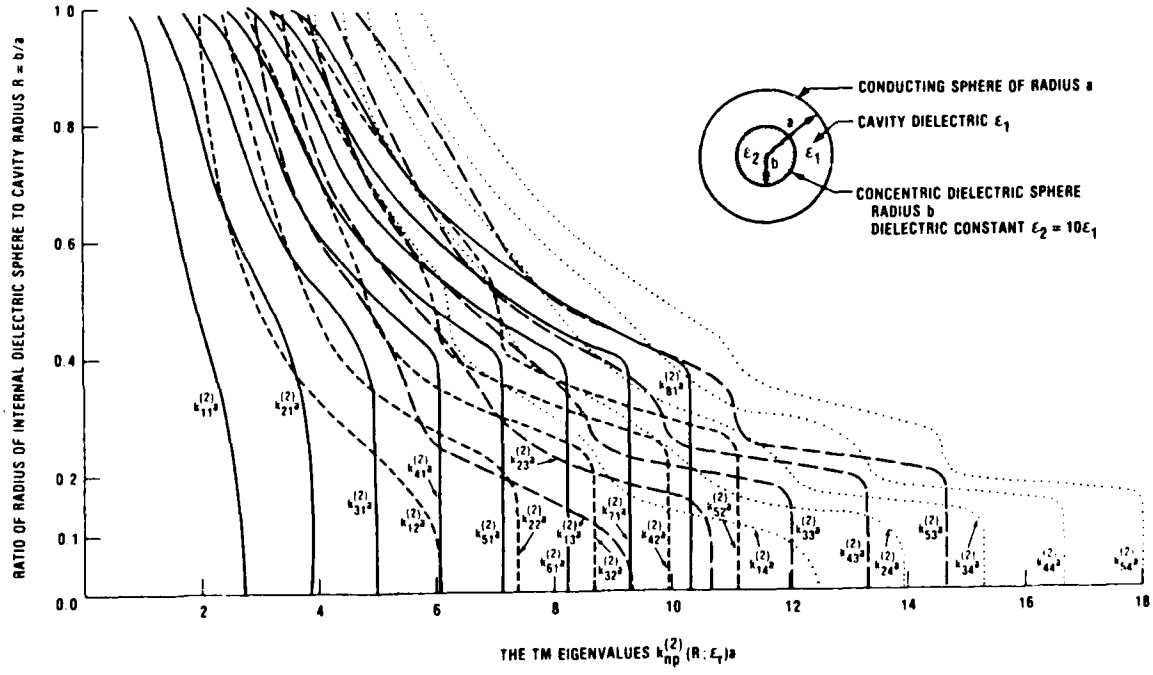

Figure 30. A composite of the TM eigenvalues $k_{np}^{(2)}(R;\varepsilon_r = 10)a$ for the spherical cavity of radius a filled with dielectric ε_1 internally loaded with a concentric dielectric sphere of radius b and strength $\varepsilon_2 = 10\varepsilon_1$.

Several novel features are apparent in figure 30. Degeneracy is rather common for inner dielectric spheres that nearly fill the entire cavity. It also occurs frequently for quite small inner spheres that load the c These features were already present for $\varepsilon_r = 3$, but are more empha for the higher ε_r case. There are substantial ranges of R for which nea TM-TM degeneracy occurs. The density of intersections of TM trajec tories becomes quite high rather soon. Many other regular features can be discerned in figure 30 which we shall not explicitly elaborate on. Finally, we again note that the order of the eigenvalues near $R = 0$ is preserved in the limit as R goes to unity. The general property of a downward shift of all trajectories to lower ka with increasing ε_r is evident at $R = 0$.

To get a much more thorough picture of the complicated situation that occurs at $\varepsilon_r = 10$ really requires that a single figure containing all forty-five TE and TM eigenvalue trajectories superimposed be available for a detailed analysis. Obviously such a picture would be a highly confused one, losing clarity and accuracy of detail rather quickly. What we shall use as an alternative mechanism to acquire the more complete overview of the whole TE and TM situation is simultaneous reference to both figure 29 for

the TE eigenvalues and figure 30 for the TM eigenvalues, for $\varepsilon_r = 10$. In this manner, we can study all TE-TE, TE-TM, and TM-TM degeneracies at once.

At the outset, we note one very striking characteristic. The TM eigenvalues of $k_{11}^{(2)}(R;\varepsilon_r = 10)\,a$, which are the lowest for all R, are the only ones not degenerate at any value of R with any other eigenvalue. This property is not new by any means. What does arise now is the feature that over the range of R from about $R = 0.43$ to about $R = 0.65$ the trajectory for $k_{11}^{(2)}a$ lies very close to the TE eigenvalue trajectory for $k_{11}^{(1)}a$. This raises an interesting and important question. Namely, if we take ε_2 sufficiently larger than ε_1, can we eventually attain degeneracy even for what so far has been the lowest eigenvalue, i.e., $k_{11}^{(2)}a$? Indeed, it can be demonstrated that for $\varepsilon_r = 100$, for example, the $k_{11}^{(1)}a$ curve intersects the $k_{11}^{(2)}a$ curve at two values of R (at approximately $R = 0.15$ and $R = 0.92$). Thus, for this case, all the modes are degenerate for some size of inner dielectric sphere that we load the cavity with. Furthermore, when $\varepsilon_r = 100$, the TM_{11} mode is the dominant mode only, for small and large values of $R = b/a$. In the intermediate range of R, which is bounded by the two TE_{11}-TM_{11} degeneracies, the TE_{11} mode surplants the TM_{11} as the dominant mode!

It can be further inferred that there exists a value of ε_r between 10 and 100, at which the $k_{11}^{(1)}a$ trajectory just grazes the $k_{11}^{(2)}a$ trajectory, thus producing only one value of degeneracy, and becoming the bounding ε_r below which only the TM_{11} mode can be the dominant mode, independent of R. If one wishes to generalize further, "grazing" values of ε_r should exist for the other degeneracy intersections as well. It would not be a difficult exercise to solve for these "grazing" values of ε_r, although we have not addressed that particular study for this report.

Continuing to investigate the situation for $\varepsilon_r = 10$ with regard to degeneracy as we have earlier, we find that the TE eigenvalue curve $k_{11}^{(1)}a$ is degenerate only with the TM curve $k_{21}^{(2)}a$ near $R = 0.2$ and near $R = 0.95$, i.e., for a small and for a quite large inner sphere. The TM eigenvalue curve $k_{21}^{(2)}a$ is degenerate with other modes for six distinct inner sphere sizes. In addition to the degeneracies with the TE mode $k_{11}^{(1)}a$, it is twice degenerate with the TE mode $k_{21}^{(1)}a$ and also with the TM mode $k_{12}^{(2)}a$. Note

that the lower R values (about $R = 0.35$) at which the $k_{21}^{(1)}a$ and $k_{12}^{(2)}a$ occur are nearly equal.

Proceeding to higher order, the TM eigenvalue curve $k_{31}^{(2)}a$ has degeneracies at 10 values of R. In addition the trajectory for $k_{31}^{(2)}a$ nearly coincides with several other eigenvalue trajectories for several ranges of R. Thus once we get beyond about $R = 0.1$, the density of degeneracies grows very rapidly. Further, as we go to higher order eigenvalues, this lower threshold in R decreases steadily. Clearly for $\varepsilon_r = 10$ we find a very dense distribution of degeneracies and a rich variety of near degeneracy as well. Again, the sequence of TE and TM eigenvalues near $R = 0$ remains invariant as R approaches the limit of unity, although many interesting variations in behavior occur in between these limits. Recall also that all the TE and TM eigenvalues decrease monotonically as R increases from zero to unity, where the inner sphere fills the entire cavity. The general downward shift to lower ka, for all the trajectories, which is larger for larger ε_r, tends to increase the density of degeneracies for $R > 0$.

We have now accumulated a considerable body of knowledge concerning the degeneracies in our system and the effect of increasing ε_r on them. Next we consider the corresponding situation, where we fill the cavity with a high dielectric medium and then load it in its interior with a concentric dielectric sphere of lower dielectric strength, i.e., $\varepsilon_r < 1$. We shall examine the results only in the single case of $\varepsilon_r = 1/3$.

5.4 Overview of the TE and TM Eigenvalues for $\varepsilon_r = 1/3$

We shall begin as before, by first examining the TE-TE degeneracy situation. Figure 31 contains in superposition all twenty of the TE eigenvalue trajectories we examined as single sets of curves for fixed values of the index p. Unlike what we observed in figures 27 and 29, we now see that the first three TE trajectories, $k_{11}^{(1)}a$, $k_{21}^{(1)}a$, and $k_{31}^{(1)}a$, are free of degeneracy for all R. Furthermore, these eigenvalues are well separated from all other TE eigenvalues for the entire range of R. The $k_{41}^{(1)}a$ curve shows the first degeneracy. Its trajectory intersects the $k_{12}^{(1)}a$ trajectory at about $R = 0.5$ and again at about $R = 0.85$. The eigenvalues of $k_{51}^{(1)}a$ are degenerate at four values of R—twice with $k_{12}^{(1)}a$ and twice with $k_{22}^{(1)}a$. All the TE-TE degeneracies cited thus far are well separated in R from each other. The trajectory for the eigenvalues $k_{12}^{(1)}a$ shows six sizes of inner sphere at which degeneracy occurs. There are two values of R for each of

$k_{41}^{(1)}a$, $k_{51}^{(1)}a$, and $k_{61}^{(1)}a$ at which these intersections lie. The $k_{22}^{(1)}a$ trajectory also has six degenerate values of R, two with each of the trajectories for $k_{51}^{(1)}a$ and $k_{61}^{(1)}a$, and although it is not explicitly shown, two more with $k_{71}^{(1)}a$. The $k_{51}^{(1)}a$ trajectory intersects $k_{22}^{(1)}a$ twice and $k_{12}^{(1)}a$ twice.

The $k_{61}^{(1)}a$ and $k_{32}^{(1)}a$ trajectories are nearly coincident for R, ranging all the way up to beyond $R = 0.3$. Similar behavior exists for $k_{71}^{(1)}a$ and $k_{42}^{(1)}a$. There are six degenerate R values for $k_{61}^{(1)}a$, two with each of $k_{12}^{(1)}a$, $k_{22}^{(1)}a$, and $k_{32}^{(1)}a$. The next trajectory, $k_{13}^{(1)}a$, has eight values of R at which degeneracy occurs. We can observe that the density of degenerate pairs of eigenvalues increases with increasing orders of n and p, but at a slower rate than we saw happen for $\varepsilon_r > 1$. Indeed, up to $ka \approx 6.5$, very little degeneracy can be found. Inspection of figure 31 reveals that as R increases the eigenvalues are shifted, in general, to higher values. Again we note that the sequence of eigenvalues at $R = 0$ is preserved at $R = 1$.

Next we examine the thirty-one TM eigenvalue trajectories for $\varepsilon_r = 1/3$ all superimposed in figure 32. We begin by noting that the four lowest order TM eigenvalues of $k_{11}^{(2)}a$, $k_{21}^{(2)}a$, $k_{31}^{(2)}a$, and $k_{41}^{(2)}a$ are not degenerate for any

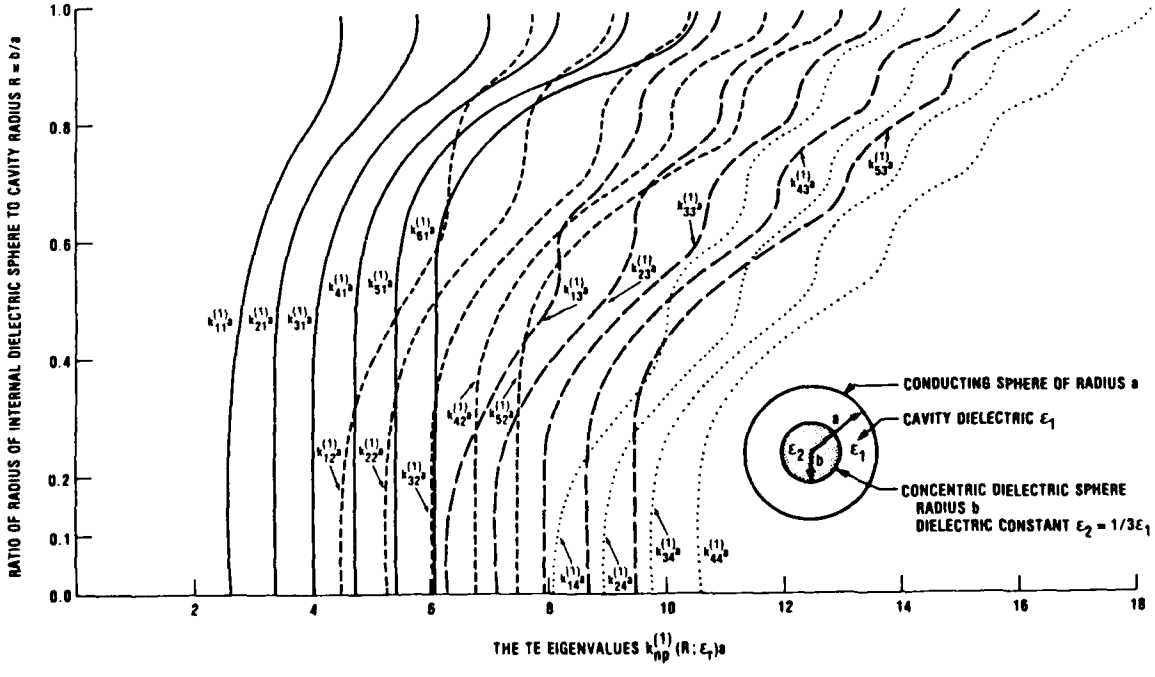

Figure 31. A composite of the TE eigenvalues $k_{np}^{(1)}(R;\varepsilon_r = 1/3)a$ for the spherical cavity of radius a filled with dielectric ε_1 internally loaded with a concentric dielectric sphere of radius b and strength $\varepsilon_2 = 1/3\varepsilon_1$.

values of R. Further, there is a clear separation of all these eigenvalues for all R values, with several exceptions. One exception is for R near unity, where $k_{41}^{(2)}a$ is very close in value to $k_{12}^{(2)}a$. The second exception is for the range of R up to about $R = 0.15$, where $k_{41}^{(2)}a$ and $k_{12}^{(2)}a$ nearly coincide in value. The TM eigenvalues $k_{51}^{(2)}a$ and $k_{12}^{(2)}a$ are degenerate with each other at two R values, the lower at about $R = 0.4$ and the upper just under $R = 0.9$. The eigenvalue trajectory for $k_{61}^{(2)}a$ also shows two inner sphere sizes where degeneracy occurs. These are at the values of R about $R = 0.45$ and at about $R = 0.95$. Both of these intersections are with the trajectory for the eigenvalue $k_{22}^{(2)}a$. In addition to these two degenerate R values with $k_{61}^{(2)}a$, the eigenvalues $k_{22}^{(2)}a$ have two degenerate values of R with $k_{71}^{(2)}a$. These latter R values are at about $R = 0.55$ and $R = 0.95$. The values at which the degeneracies occur for each eigenvalue are well separated in R.

The trajectory for $k_{71}^{(2)}a$ for six values of R is degenerate with other eigenvalues. These include two trajectory intersections with $k_{13}^{(2)}a$. One is at about $R = 0.05$ and the other very close to $R = 1.0$. Two more are with $k_{32}^{(2)}a$—one near $R = 0.4$ and the second near $R = 0.95$. The remaining two values are the degeneracies with $k_{22}^{(2)}a$ already indicated. The eigenvalue

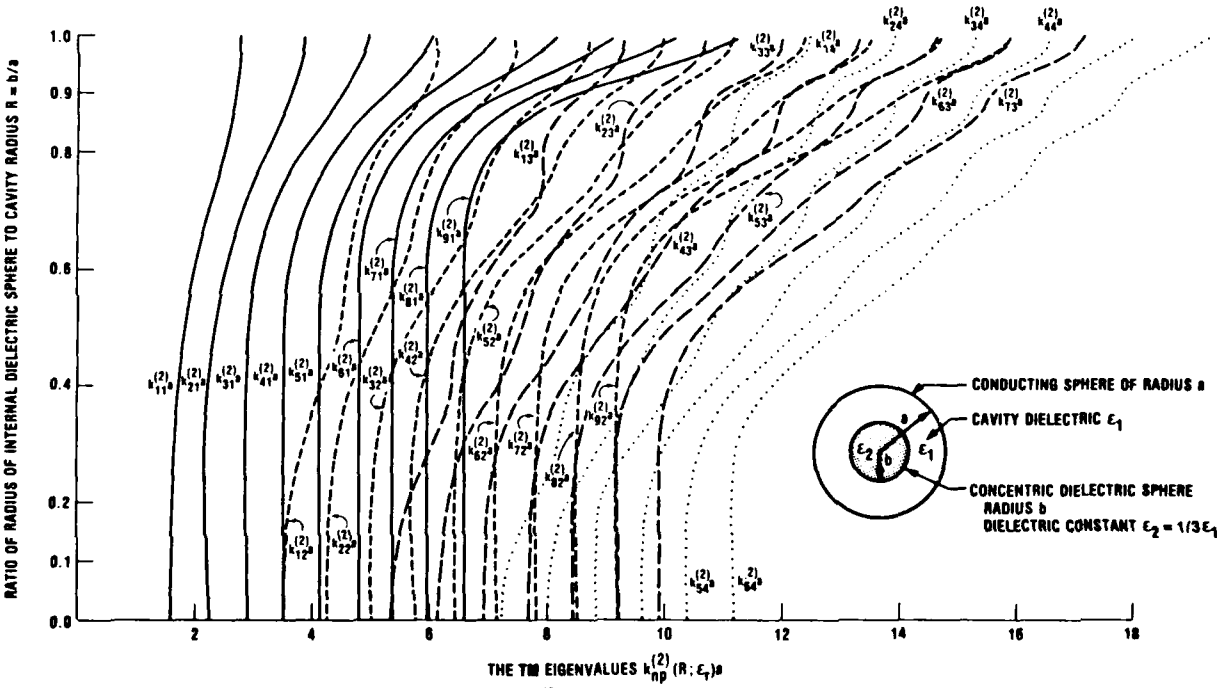

Figure 32. A composite of the TM eigenvalues $k_{np}^{(2)}(R;\varepsilon_r = 1/3)a$ for the spherical cavity of radius a filled with dielectric ε_1 internally loaded with a concentric dielectric sphere of radius b and strength $\varepsilon_2 = 1/3\varepsilon_1$.

trajectory $k_{32}^{(2)}a$ also has six sizes of inner sphere at which degeneracy exsists with other eigenvalues. Two with $k_{71}^{(2)}a$ have already been pointed out. Two more occur with each of two eigenvalues from $k_{81}^{(2)}a$ and $k_{91}^{(2)}a$. These are well spread out over R values from 0.5 up to 0.9. All higher order eigenvalue trajectories will show increasing numbers of R values at which degeneracy occurs with a larger number of other eigenvalues. Examination of figure 32 shows that above $ka = 6$ the density of degeneracies grows rather rapidly. Furthermore, we see in figure 32 the increase in frequency of occurrence of ranges of R over which many pairs of eigenvalues nearly coincide. These ranges are quite large in many cases.

As we expec', the order of the TM eigenvalues at $R = 0$ is preserved at $R = 1$. There is present a general upward shift in the eigenvalue trajectories for $R > 0$ for $\varepsilon_r < 1$. We recall that now all the eigenvalues are monotonically increasing as R increases. Many other interesting features are present in figure 32 showing all the TM trajectories for $\varepsilon_r = 1/3$. We shall not go any further into this subject, but shall instead go on to consider the composite of all fifty-one eigenvalue trajectories for $\varepsilon_r = 1/3$.

For obvious reasons, we do not include such a superposition plot of all the eigenvalues. We can analyze all the eigenvalue trajectories by simultaneously examining figures 31 and 32.

The very first observation to be made is that the TM trajectories $k_{11}^{(2)}a$ and $k_{21}^{(2)}a$ are nowhere degenerate with any other eigenvalues for any R value. For all R, the eigenvalues of $k_{11}^{(2)}a$ and $k_{21}^{(2)}a$ are well separated from all other eigenvalues. The TE eigenvalues of $k_{11}^{(1)}a$ and TM eigenvalues of $k_{31}^{(2)}a$, which respectively had no TE-TE and no TM-TM degeneracy, intersect. There is TE-TM degeneracy of these two curves at about $R = 0.55$ and at about $R = 0.9$. Now we note that the TE curve $k_{21}^{(1)}a$ has two values of R at which it is degenerate with the TM curve $k_{31}^{(2)}a$. These values near $R = 0.5$ and near $R = 0.97$ are the only degeneracies in $k_{21}^{(1)}a$. The TM eigenvalue $k_{41}^{(2)}a$ is also degenerate at only two values of R, near $R = 0.5$ and $R = 0.97$. Both degeneracies are with the TE eigenvalue curve $k_{21}^{(1)}a$. As we have already noted, $k_{41}^{(2)}a$ is nearly coincident with $k_{12}^{(2)}a$ for R up to about $R = 0.15$ and again near $R = 1$.

There are four R values at which the TM eigenvalues of $k_{12}^{(2)}a$ are degenerate. Two are with the TE eigenvalues of $k_{31}^{(1)}a$ at about $R = 0.35$

and also at about $R = 0.7$, and two are with the TM eigenvalues of $k_{41}^{(2)}a$ at about $R = 0.4$ and about $R = 0.9$. The $k_{31}^{(1)}a$ trajectory is degenerate at four R values, the two already referred to with $k_{12}^{(1)}a$ and two others with the eigenvalues of $k_{51}^{(2)}a$ at about $R = 0.5$ and $R = 0.98$. Four degeneracies exist for $k_{51}^{(2)}a$, the pair already mentioned with the TM curve $k_{12}^{(2)}a$ and the two with the TE curve $k_{31}^{(1)}a$. From this point on, the higher order eigenvalues show rapid increase in degeneracy. The density of degeneracy very quickly becomes high beyond $ka = 4$. In addition, many eigenvalue trajectories are nearly coincident with other eigenvalue trajectories for various ranges of R. Some ranges of R are quite extensive where this situation occurs. Thus, for example, the TE curve $k_{51}^{(1)}a$ and the TM curve $k_{71}^{(2)}a$ are nearly coincident for values of R from zero up to about $R = 0.5$.

All the $\varepsilon_r = 1/3$ trajectories increase monotonically with R. Finally, we state the expected condition that the sequence in which the eigenvalues are ordered at $R = 0$ remains invariant at $R = 1$. As usual, there are many interesting features present in the complete set of eigenvalue trajectories for $\varepsilon_r = 1/3$ which we shall not go into explicitly.

5.5 Final Summary and Discussion

We have analyzed the results of solving equations (32) and (36) for the TE and TM eigenvalue trajectories, for a dielectric-filled spherical cavity loaded with an inner concentric dielectric sphere.

By choosing the inner dielectric sphere of higher strength than that of the cavity dielectric for various values of $\varepsilon_r > 1$ and reversing the roles of the dielectrics and thus obtaining $\varepsilon_r < 1$, we studied the effects of eigenvalue trajectories. The specific values chosen for ε_r were 3.00, 10.00, and 1/3. These constitute a reasonably large range for ε_r. For values of $\varepsilon_r > 1$ all the eigenvalues decrease monotonically as the radius of the inner sphere increases. On the other hand, for $\varepsilon_r < 1$, all the eigenvalues increase monotonically as the radius of the inner sphere increases. In all cases of ε_r, although the eigenvalues display some very interesting behavior for inner sphere radii between $R = 0$ and $R = 1$, the eigenvalue sequence of $R = 0$ is preserved at $R = 1$. Comparing two cases of $\varepsilon_r > 1$, we find a general shift of the eigenvalues to lower values, for $R > 0$, for the higher ε_r case relative to the lower ε_r case. For two values of $\varepsilon_r < 1$, the reverse situation holds true. Varying ε_r induces a multitude of changes in which modes of the system are degenerate and for which values of radius of the inner

sphere the degeneracy occurs. Further varying ϵ_r affects the density of degeneracies among the eigenvalues.

A number of practical applications of the results of this study suggest themselves. For example, we see explicitly for the simple system studied that the characteristics of an empty cavity and a loaded cavity can be enormously different. We shall show in subsequent reports that the interior contents of a cavity can be sensed in the far field. The results reported on in this paper indicate that, if we appropriately add elements to the interior of the cavity, identification of the cavity and its interior components can be made very difficult. Thus we noted that adding a dielectric sphere of high strength inside shifts many high order modes to lower values. This gives rise to confusion in the array of resonances in the cavity rather than the simple response of only a few resonances. We also see analytic proof of the large number of resonances that enter into the cavity response when the cavity contains even a very simple element. The results of this study show that it can be very difficult to achieve and maintain EMC and EMI hardening of systems by introducing protective devices for selected frequencies because of the large number of frequencies that must be accounted for when even simple elements are in the interior of metallic shields. We have further shown that the well separated lower modes of systems can be shifted to higher frequencies if we coat the inner surface of the exterior metal boundary with high dielectric strength materials. We have by no means exhausted all possible application potentials of this study.

One final important area of application that suggests itself in this study is that of the difficult mode conversion problem. Using the work of Rowe and Warters [3] and that of Kindermann [4], Doane [5] showed how the degeneracy of the TE_{01} and the TM_{11} circular waveguide modes could be used to convert from the first to the second. The high degree of flexibility we have seen in controlling degeneracy among the many modes in the study we reported on presents us with an opportunity to develop an additional mode conversion capability.

We conclude the discussion by pointing out that one can achieve a deeper understanding of what we found in the study reported on here by studying the behavior of the spatial distribution of the field components in our system. This will be presented in a series of subsequent reports.

References

1. Louis F. Libelo and Morris M. Campi, *The Concentric Spherical Cavity TE and TM Eigenvalues*, Harry Diamond Laboratories, HDL-TR-2038 (July 1984).

2. R. F. Harrington, *Time-Harmonic Electromagnetic Fields*, McGraw-Hill Book Company, NY (1961), 270.

3. E. H. Rowe and W. D. Warters, *Transmission in Multimode Waveguide with Random Imperfections*, Bell System Technical Journal *41* (1962), 1031-1170.

4. H. P. Kindermann, *Optimierte Hoi-Krümmer Mit Dielektrischer Schicht*, A. E. U., *19* (1965), 699-701.

5. J. L. Doane, *Mode Converters for Generating the HE11 (Gaussian-Like) Mode from TE01 in a Circular Waveguide*, International Journal Electronics *53* (1982), 573-585.

DISTRIBUTION

ADMINISTRATOR
DEFENSE TECHNICAL INFORMATION CENTER
ATTN DTIC-DDA (12 COPIES)
CAMERON STATION
ALEXANDRIA, VA 22314

COMMANDER
US ARMY MATERIEL COMMAND
5001 EISENHOWER AVENUE
ALEXANDRIA, VA 22333-0001

DIRECTOR
US ARMY BALLISTIC RESEARCH LABORATORY
ATTN DRSAR-TSB-S (STINFO)
ABERDEEN PROVING GROUND, MD 21005

US ARMY ELECTRONICS TECHNOLOGY & DEVICES LABORATORY
ATTN DELET-DD
FT MONMOUTH, NJ 07703

MATERIALS TESTING DIRECTORATE
ARMY PULSE RADIATION DIV
ATTN CRAIG R. HEIMBACH
ABERDEEN PROVING GROUND, MD 21005

DIRECTOR
US ARMY MATERIEL SYSTEMS ANALYSIS ACTIVITY
ATTN DRXSY-MP
ABERDEEN PROVING GROUND, MD 21005

COMMANDER
US ARMY MISSILE & MUNITIONS CENTER & SCHOOL
ATTN ATSK-CTD-F
REDSTONE ARSENAL, AL 35809

US ARMY RESEARCH OFFICE
ATTN DR. JAMES MINK
PO BOX 12211
RESEARCH TRIANGLE, NC 27709

COMMANDER
US ARMY RSCH & STDY GP (EUR)
ATTN CHIEF, PHYSICS & MATH BRANCH
FPO, NY 09510

COMMANDER
U.S. ARMY WATERVLIET ARSENAL
AMCCOM
SOLID STATE RESEARCH LAB
ATTN MR. CLARK HOMAN
WATERVLIET, NY 12189

HQ, USAF
WASHINGTON, DC 20330

RADC/RBCT
ATTN DR. ROY F. STRATTON
GRIFFISS AFB, NY 13441

UNIVERSITY OF ARIZONA
ELECTRICAL ENGINEERING DEPT
ATTN PROF. CONSTANTINE BALANIS
ATTN PROF. DONALD DUDLEY
TUCSON, AZ 85721

CHAIRMAN ELECTRICAL ENGINEERING DEPT
PENN STATE UNIVERSITY
ATTN DR. KARL KUNZ
COLLEGE STATION, PA need zip code

ELECTRONICS RESEARCH LAB
COLLEGE OF ENGINEERING
UNIVERSITY OF CALIFORNIA
ATTN PROF. KEN MEI
BERKELEY, CA 94720

UNIV OF CALIFORNIA AT LOS ANGELES
ELECTRICAL ENGINEERING DEPT
ATTN PROF. CAVOUR YEH
LOS ANGELES, CA 90024

ENGINEERING SOCIETIES LIBRARY
ATTN ACQUISITIONS DEPT
345 EAST 47TH ST
NEW YORK, NY 10017

UNIVERSITY OF FLORIDA
PHYSICS DEPT
ATTN PROF. ALEX GREEN
GAINESVILLE, FL 32601

UNIV OF FLORIDA
SPACE ASTRONOMY LAB
ATTN RU T. WANG
GAINESVILLE, FL 32601

GENERAL RESEARCH CORP
ADVANCED TECHNOLOGIES DIVISION
ATTN DR. MICHAEL VON BLARICUM
5383 HOLLISTER AVENUE
SANTA BARBARA, CA 93111

CLEMSON UNIVERSITY
DEPT OF ELECTRICAL ENGINEERING
ATTN PROF. CHALMERS BUTLER
CLEMSON, SC need zip code

JAYCOR
ATTN DR. KENDALL CASEY
39510 PASCO PADRE PKWY
SUITE 300
FREMONT, CA 94538

DISTRIBUTION (cont'd)

MASSACHUSETTS INSTITUTE OF TECHNOLOGY
DEPT OF ELECTRICAL ENGINEERING &
COMPUTER SCIENCE
ATTN PROF. J. A. KONG
CAMBRIDGE, MA 02139

UNIVERSITY OF MASSACHUSETTS
DEPT OF ELECTRICAL & COMPUTER
ENGINEERING
ATTN PROF. DANIEL SCHAUBERT
AMHERST, MA 01003

UNIVERSITY OF MICHIGAN
DEPT OF ELECTRICAL & COMPUTER
ENGINEERING
ATTN PROF. VAL LIEPA
ANN ARBOR, MI 48109

McDONNELL DOUGLAS CORP
ATTN DR. W. PEARSON
ST LOUIS, MO 63166

PANAMETRICS INC
ATTN DR. NORMAN PEDERSEN
221 CRESCENT STREET
WALTHAM, MA 02254

SANDIA NATIONAL LABORATORIES
ATTN DR. MARVIN E. MORRIS
PO BOX 5800
ALBUQUERQUE, NM 87185

SYRACUSE UNIVERSITY
ELECTRICAL ENGINEERING DEPT
ATTN PROF. ROGER HARRINGTON
SYRACUSE, NY 13210

LAWRENCE LIVERMORE LABORATORY
ATTN RICHARD ZIOLKOWSKI, L-156
PO BOX 808
LIVERMORE, CA 94550

US ARMY LABORATORY COMMAND
ATTN TECHNICAL DIRECTOR,
AMSLC-CT

INSTALLATION SUPPORT ACTIVITY
ATTN LEGAL OFFICE, SLCIS-CC

USAISC
ATTN RECORD COPY, ASNC-LAB-TS
ATTN TECHNICAL REPORTS BRANCH,
ASNC-LAB-TR (3 COPIES)

HARRY DIAMOND LABORATORIES
ATTN D/DIVISION DIRECTORS
ATTN LIBRARY, SLCHD-TL (3 COPIES)
ATTN HDL LIBRARY, SLCHD-TL (WOODBRIDGE)
ATTN ZABLUDOWSKI, B., SLCHD-IT-EB
ATTN JOHNSON, T., SLCHD-ST
ATTN PISANE, G., SLCHD-ST-AB (20 COPIES)
ATTN RUTH, B., SLCHD-NW-RI
ATTN LIBELO, L., SLCHD-NW-RI (30 COPIES)

END
DATE
FILMED
7-88
DTIC